Delft University of Technology

Control of the key phenomena in continuous and batch crystallization processes
Novel process and equipment design

Anisi, Fatemeh

DOI
10.4233/uuid:0c094cf9-ba07-4442-8008-7a216f63b1f3

Publication date
2019

Document Version
Final published version

Citation (APA)
Anisi, F. (2019). *Control of the key phenomena in continuous and batch crystallization processes: Novel process and equipment design*. [Dissertation (TU Delft), Delft University of Technology]. https://doi.org/10.4233/uuid:0c094cf9-ba07-4442-8008-7a216f63b1f3

Important note
To cite this publication, please use the final published version (if applicable).
Please check the document version above.

Copyright
Other than for strictly personal use, it is not permitted to download, forward or distribute the text or part of it, without the consent of the author(s) and/or copyright holder(s), unless the work is under an open content license such as Creative Commons.

Takedown policy
Please contact us and provide details if you believe this document breaches copyrights.
We will remove access to the work immediately and investigate your claim.

This work is downloaded from Delft University of Technology.
For technical reasons the number of authors shown on this cover page is limited to a maximum of 10.

Control of the key phenomena in continuous and batch crystallization processes;
Novel process and equipment design

Fatemeh ANISI

Layout and printed by: Optima Grafische Communicatie (www.ogc.nl)
ISBN 978-94-6361-229-6
Copyright © 2018 by Fatemeh Anisi
Email: anisi.fatima@gmail.com

Control of the key phenomena in continuous and batch crystallization processes;
Novel process and equipment design

Proefschrift

ter verkrijging van de graad van doctor
aan de Technische Universiteit Delft,
op gezag van de Rector Magnificus Prof. dr. ir. T.H.J.J. van der Hagen;
voorzitter van het College voor Promoties,
in het openbaar te verdedigen op
donderdag 28 februari 2019 om 15:00 uur

door

Fatemeh ANISI
PDEng in Bioprocess Engineering,
Delft University of Technology, the Netherlands
geboren te Kerman, Iran

Dit proefschrift is goedgekeurd door de:
Promotor: Prof. dr. ir. A. Stankiewicz
Copromotor: Dr. ir. H.J.M. Kramer

Samenstelling promotiecommissie:

Rector Magnificus,	voorzitter
Prof. dr. ir. A. Stankiewicz	Technische Universiteit Delft, promotor
Dr. ir. H.J.M. Kramer	Technische Universiteit Delft, copromotor

Onafhankelijke leden:

Prof. dr. A.E.D.M. van der Heijden	Technische Universiteit Delft
Prof. dr. ir. J. Ter Horst	University of Stratclyde, Glasgow
Prof. dr.-ing G. Schembecker	Technische Universiteit Dortmund
Prof. dr. ir. A. de Haan	Technische Universiteit Delft
Dr. ir. P. Vonk	Royal DSM

To my self-devoted mom,
who always wanted to see this day and finally could not,
To my beloved dad,
& to love of my life, Erfan
تقدیم به مادرم که این روز را ندید و رفت
تقدیم به پدرم که همواره مثل کوه ایستاده است
تقدیم به همسرم که عشق و امید این روزهای من است

SUMMARY

Crystallization is one of the essential downstream steps of the manufacturing of chemical and pharmaceutical compounds when it comes to separation, purification, and final product formation. Although it has been years since it is widely applied in the aforementioned industries, it is known as one of the complex processes where continuous optimization is increasingly necessary. Insufficient understanding of crystallization phenomena and their interactions from one side, and demanding requirements for product specifications in such industries from the other side, form the basis of challenges within this unit operation.

Solution to these challenges might be realized by improvement of the methods to manipulate and control the crystallization phenomena, which requires improvements in the design of both the crystallizer and the crystallization process in order to overcome the limitations of current equipment and facilitate the widening of the window of operation. Moving from batch to continuous processes is, for example, a large step toward better product quality and stability; however sufficient knowledge and understanding about the operation of a continuous crystallization process properly is still immature, giving the chance to the researchers to develop novel ideas and explore the field freely.

One of the main challenges of crystallization is the unavoidable entanglement of the different crystallization phenomena. For example there is a strong interaction between secondary nucleation and crystal growth, which are both dependent on the supersaturation and the turbulence level, induced by the stirring device or pumps in the crystallizer. As nucleation and growth have a total different effect on the quality of the end product, optimization of product quality is difficult to achieve in the traditional crystallization processes and often results in bimodal and varying crystal size distribution.

Task-based design is a novel design approach to separate the entangled crystallization phenomena or tasks in separate equipment or parts of the equipment, using these crystallization tasks as individual building blocks of the crystallization process. Realizing this idea, however, requires the design of equipment to be done in a way that one of the phenomena is dominant, while the others are suppressed. An airlift crystallizer is designed based on the idea to eliminate the main source of secondary nucleation caused by collisions of the crystals. Due to the absence of an impeller it exhibits a different hydrodynamics with low shear forces, which results in a growth dominated crystallizer. Results of cooling seeded batch crystallization experiments in airlift crystallizer have confirmed qualitatively that secondary nucleation is suppressed for a broad range of supersaturation and that the growth is the dominant phenomena in such a crystallizer.

In chapter 2, a quantitative analysis of the kinetics in this crystallizer is presented and compared to that of a 5 L draft tube stirred crystallizer to investigate whether the available models in literature are able to describe the kinetics in the airlift crystallizer adequately.

A modelling framework has been developed consisting of the population, mass and energy balances in which a number of models for crystal growth and secondary nucleation were implemented. Application of dynamic parameter estimation techniques on the data of a large number of batch experiments in the forementioned two crystallizers enabled us to identify and verify the relevant kinetic models. The results confirm that attrition by crystal-impeller and crystal-crystal collisions in the airlift crystallizer can be completely neglected, while in the draft tube crystallizer, this process could only be described adequately when a combined model including both a surface nucleation model and an attrition model is used. The results confirm the strong suppression of the secondary nucleation in the airlift crystallizer due to the absence of attrition but also as a result of the lower values of the rate constants for the surface nucleation model. The proposed surface nucleation model perfectly describes the nucleation observed in the airlift crystallizer at higher and intermediate supersaturation levels. The requirement to use an activated nucleation model to get an acceptable description of the secondary nucleation in the draft tube crystallizer is one of the important results of this study and explains the often observed, early nucleation events in batch crystallization.

Although cooling crystallization in the growth oriented airlift crystallizer led to excellent results, the design of the process itself can be also improved. One of the most important limits in the design of such a process is the method through which supersaturation is generated. Cooling and evaporation are the two common ways of generating supersaturation for a crystallization process but application of membranes for the generation of supersaturation offers an interesting opportunity to improve on their drawbacks, such as scaling on the cooling surfaces or the limitation of the yield or of the rate of supersaturation generation by the surface area for boiling. The use of membranes is preferred due to the low energy consumption compared to evaporation. Use of a membrane contactor to assist the crystallization process showed interesting results which lead to (1) improved performance of the crystallizer with an extended yield which is only constrained by the impurities in the system and (2) additional features for the crystallization process, such as more flexibility, added sustainability and better controllability.

Membrane distillation and reverse osmosis are the two alternatives to be integrated with a crystallization process. Despite higher energy usage, membrane distillation is, for compounds with high osmotic pressure such as L-ascorbic acid, a better choice than reverse osmosis. In order to benefit from membrane distillation the module should be characterized and optimized and finally simulated and validated, because every module has its own unique properties and operational method and configuration which impose several adjustments to the existing models.

In chapter 3 a Liqui-Cel® Extra flow membrane module was used to concentrate a solution of L-ascorbic acid in water with the aim of supersaturation generation for crystallization processes. Characterization of this membrane module was done altering the process conditions; feed flow rate, temperature, concentration and air flow rate. A model coupling mass and heat transfer was developed to predict the membrane flux and to investigate the temperature and concentration polarization. Feed temperature and air flow rate have been found as controlling parameters. Air flow rate has been found as the best parameter for this manipulation since it influences the flux promptly. Since the predicted membrane flux by the developed model is in accordance with the results from the experiments, the model can be used for further membrane-assisted crystallization investigations.

Since every aspect of a batch process is transient, batch to batch variation is a common issue and therefore precise monitoring and control is very essential, though complex. On the other side, a continuous crystallization process is, in general, operated in a steady state meaning that the conditions inside the crystallizer are more or less constant and are thus easier to control. Although a continuous process is inflexible and cannot be easily adapted to realize different product specifications, a more consistent product quality and production rate, a lower footprint and more stable product are possible when optimized for a single product.

In chapter 4 the continuous cooling and membrane-assisted crystallization experiments are discussed. Continuous cooling crystallization experiments have been performed in the airlift crystallizer applying different process conditions. Supersaturation was selected low enough to ensure that no secondary nucleation was expected. In the model crystal growth was only active while secondary nucleation was completely suppressed. The kinetic model developed and validated for batch cooling crystallization experiments has been tested for continuous cooling crystallization and resulted in acceptable outcome. Continuous membrane-assisted crystallization experiments in an airlift crystallizer have been performed for the first time and the results confirm the possibility to use this model for design purposes. The developed model is used to design the experiments based on optimized process conditions for different objectives such as large median size or high yield. In addition it can be used also for the design of a new process and equipment and further it can be used to optimize the process conditions as well.

Up to now the enhancement of growth and supersaturation generation and suppression of secondary nucleation as the important crystallization phenomena in seeded crystallization have been taken into consideration. However, seed generation from a solution (primary nucleation) is another important crystallization phenomenon.

Seed generation from existing product crystals, for example using a ball mill, is an elaborate process but it has been always stated that making seed crystals in a reproducible way is difficult.

Use of alternate energies such as electric field, ultrasound, or microwave is being investigated as one of the ways for influencing and controlling nucleation. This is especially true in the application of ultrasound which has been demonstrated to positively affect the primary nucleation. It has been found that ultrasonic waves decrease the supersaturation limits and induction time, which means they increase the rate of crystallization and crystal productivity. Decreasing the supersaturation limits means the nucleation occurs at lower levels of supersaturation and that means the width of the metastable zone is reduced.

In chapter 5 it is observed that the application of ultrasound enhances the nucleation rate by 6 to 9 orders of magnitude. Two modes of ultrasound application, pulsed and continuous, have been exercised. Despite of achieving similar results in terms of nucleation rate, pulsed ultrasound is continued to be used due to lower energy consumption.

Firstly, a supersaturation regime at which primary nucleation can be induced by application of ultrasound is determined. Nucleation at low supersaturations, well within the metastable zone width, is targeted to avoid excessive nucleation leading to fines formation and hence poor size distribution. Two different ultrasound configurations were tested; one for batch application in which the ultrasound horn was inserted directly in a batch crystallizer, and one for continuous seed generation in which the ultrasound was applied in a flow-through-cell.

From the current experiments we know that the ultrasound increases the nucleation rate and the size and volume density is somehow controllable. The developed model validated for kinetics of L-ascorbic acid in chapter 2 was able to produce the same results as seen in the experiments.

Finally, the ultrasound generated seeds have been applied to an airlift crystallizer which provides controlled growth conditions. FBRM has been used where possible to characterize the crystallization phase in the process. A narrow crystal size distribution has been achieved for the cooling batch experiments in the airlift crystallizer with larger number of counts of seed crystals. The lower number of counts meaning also smaller seed crystals resulted in broader crystal size distribution which suggests that the secondary nucleation has started later in the process.

SAMENVATTING

Kristallisatie is een van de essentiële stappen in de downstream behandelingen van de productie van chemische en farmaceutische verbindingen waar de scheiding, zuivering en productvorming plaatsvinden. Hoewel kristallisatie al jaren in de voornoemde industrieën wordt toegepast, staat het bekend als een van de ingewikkeldste processen waarin blijvende optimalisering noodzakelijk is. Ontoereikende kennis van kristallisatie verschijnselen en hun interacties aan de ene kant, en de steeds hogere eisen met betrekking tot de product-specificaties in deze industrieën aan de andere kant, vormen de basis van de uitdagingen binnen deze unit operation.

Een oplossing voor deze uitdagingen kan worden gerealiseerd door een verbetering van de methode waarmee de belangrijkste kristallisatie verschijnselen gemanipuleerd en beheerst kunnen worden. Verbeteringen in het ontwerp van zowel de kristallisator als het kristallisatieproces zijn nodig om de beperkingen van de huidige apparaten te overwinnen en om het operatie gebied voor deze processen te verbreden. De overgang van batch naar continu processen is bijvoorbeeld een grote stap naar een betere en stabielere productkwaliteit. De kennis en het begrip over de adequate bedrijfsvoering van een continu kristallisatieproces is echter nog ontoereikend. Dit geeft onderzoekers de gelegenheid om innovatieve ideeën te ontwikkelen en het gebied vrij te exploreren.

Een van de belangrijkste uitdagingen voor batch kristallisatie is de onvermijdelijke verstrengeling van de belangrijkste kristallisatieverschijnselen. Zo is er bijvoorbeeld een sterke interactie tussen secondaire kiemvorming en kristalgroei, die beide afhankelijk zijn van de oververzadiging en de turbulentie, opgewekt door de roerwerk of pompen, in de kristallisator wordt. Doordat beide nucleatie en kristalgroei een totaal verschillend effect hebben op de uiteindelijke productkwaliteit, is de productoptimalisatie van een traditioneel kristallisatieprocess vaak erg moeilijk te realiseren en wordt vaak een bimodaal kristalgrootteverdeling verkregen.

Task-based Design is een innovatief ontwerpidee om de verstrengelde kristallisatie verschijnselen, aangeduidt als kristallisatie taken, te scheiden in aparte apparaten of gedeeltes van apparaten of waarbij deze kristallisatie taken gebruikt worden als individuele bouwstenen. Om dit idee te realiseren moet het ontwerpen van equipment worden uitgevoerd op basis van een dominant verschijnsel waarbij de andere kristallisatie taken worden onderdrukt. Een airlift kristallisator is ontworpen om de hoofdoorzaak van secondaire kiemvorming, het reorwerk impeller, te vermijden. Vanwege de afwezigheid van een impeller vertoont de airlift kristallisator een andere hydrodynamica met een lage shear forces wat leidt tot een kristalgroei gedomineerde kristallisator. Het resultaat van seeded batch koelkristallisatie experimenten in de airlift kristallisator bevestigt kwalitatief dat secundaire kiemvorming onderdrukt wordt voor een wijder bereik van supersaturation en dat de kristalgroei het dominante verschijnsel is in zo’n kristallisator.

In hoofdstuk 2 wordt een kwantitatieve analyse van de kinetiek in deze kristallisator gepresenteerd en vergeleken met de experimenten in 5 L draft tube kristallisator om na te gaan of de beschikbare modellen in de literatuur in staat zijn om de kinetiek in de airlift kristallisator voldoende te beschrijven. Een modelvormingsraamwerk is ontwikkeld dat bestaat uit populatie-, massa- en energiebalansen waarin meerdere kristalgroei en het secundaire nucleatie modellen zijn geïmplementeerd. Toepassing van dynamische parameterschatting op de data van een groot aantal van de voornoemdeexperimenten stelde ons in staat om de relevante kinetiek modellen te verifieren en identificeren. Het resultaat bevestigt dat in een airlift kristallisator attritie ten gevolge van kristal-impeller en kristal-kristal botsingen verwaarloosd kan worden; terwijl het proces in de draft tube kristallisator alleen met behulp van een gecombineerd model adequaat beschreven kan worden als daarin zowel oppervlakte nucleatie model als het attritie model opgenomen worden. Het resultaat bevestigt de sterke onderdrukking van secundaire kiemvorming in de airlift kristallisator door de afwezigheid van de attritie maar ook door lagere waardes voor snelheidsconstante voor het oppervlakte nucleatie model. Het voorgestelde oppervlakte nucleatie model kan de kiemvorming in de airlift kristallisator op een adequate manier beschrijven bij hoge en middelhoge niveaus van supersaturation. De noodzaak om een geactiveerd nucleatie model te gebruiken om een aanvaardbare beschrijving voor de secundaire kiemvorming in de geroerde draft tube kristallisator te verkrijgen is ook een belangrijk resultaat van deze studie omdat het de vaak waargenomen vroege kiemvorming in de batch kristallisatie kan verklaren.

Hoewel de koelkristallisatie in de voor kristalgroei ontworpen airlift kristallisator tot zeer goede resultaten leidde, kan het ontwerp nog verbeterd worden. Een belangrijke beperking tijdens het ontwerp van zo’n proces is de methode waarmee de oververzadiging gegenereerd wordt. Koeling en verdamping zijn twee gebruikte methoden om oververzadiging voor het kristallisatieproces te genereren, terwijl applicatie van membranen een interessante mogelijkheid biedt om de nadelen van die twee, namelijk de aankorsting op het koeloppervlak of beperkingen van het rendement of van de snelheid waarmee de oververzadiging kan worden opgewekt, te verbeteren. Het gebruik van membranen voor het opwekken van oververzadiging krijgt steeds meer aandacht, vooral vanwege de lage energieconsumptie in vergelijking tot verdamping. Het gebruik van een membraan contactor om kristallisatie te bevorderen geeft een interessant resultaat dat leidt tot (1) een verbeterd prestatie van de kristallisator met een verbeterde opbrengst die alleen door onzuiverheden wordt beperkt en (2) extra functionaliteit voor het kristallisatieproces zoals een hogere flexibiliteit, een hogere duurzaamheid en een betere beheersbaarheid.

Membraandestillatie en reverse osmosis zijn twee alternatieven om in het kristallisatieproces geïntegreerd te worden. Ondanks hoger energieconsumptie is membraandistallatie, in het geval van verbindingen met hoge osmotische druk zoals L-ascorbic acid, een betere keuze dan reverse osmosis. Om van membraandistallatie te profiteren moest de module gekarakteriseerd en geoptimaliseerd, en uiteindelijk gesimuleerd en gevalideerd worden, omdat elk module eigen specificaties en operationele methoden en configuraties heeft die verschillende aanpassingen van bestaande modellen vereisen.

In hoofdstuk 3 is een Liqui-Cel Extra flow membraan module gebruikt om een oplossing van L-ascorbic acid in water te concentreren met als doel de opwekking van oververzadiging voor kristallisatieprocessen. Om dit membraan module te karakteriseren werden de procescondities zoals het debiet, temperatuur en samenstelling van de voedingsstroom en het debiet van de luchttoevoer, veranderd. Een model is ontwikkeld waarin massa- en energieoverdracht gekoppeld zijn om de flux van membraan te voorspellen en om de temperatuur- en concentratiepolarisatie te analyseren. Uit de analyse zijn de temperatuur van de voeding en het debiet van de lucht als de belangrijkste stuurparameters naar voren gekomen. Het debiet van de luchttoevoer beïnvloedt de flux van het membraan het meest, en is daarom de beste parameter voor de manipulatie van de oververzadiging. Omdat de gesimuleerde flux goed overeenkomt met die van de experimenten, kan het model voor verdere onderzoek naar membraan-geassisteerde kristallisatie gebuikt worden.

Omdat elk aspect van een batch proces dynamisch is, is de variatie in de productkwaliteit tussen verschillende batches een veel voorkomend probleem waardoor procesbewaking en regeling zeer essentieel maar ingewikkeld zijn. Aan de andere kant worden continue processen, in het algemeen in de steady-state geopereerd, waardoor de procescondities binnen de kristallisator min of meer constant zijn. Daarom is het proces makkelijker om te regelen. Hoewel een continuproces inflexibel is en niet makkelijk aan te passen om een andere pruductspecificatie te realiseren is het mogelijk om continu een meer consistente productkwaliteit, een hogere productiesnelheid, een lagere footprint en stabielere product te verkrijgen als het voor een enkel product geoptimaliseerd wordt.

In hoofdstuk 4 worden de continue koel- en membraan kristallisatie experimenten besproken. Continue koelkristallisatie experimenten zijn in de airlift kristallisator uitgevoerd waar verschillende procescondities zijn aangepast. De oververzadiging is laag genoeg gehouden om te verzekeren dat geen secundaire nucleatie kan werd verwacht. In het ontwikkelde model is bij deze oververzadiging alleen kristalgroei actief en de secundaire nucleatie is helemaal onderdrukt. Het ontwikkelde model voor batch koelkristallisatie is getest voor continue koelkristallisatie experimenten en leidde tot aanvaardbare resultaten voor verschillende procescondities. Continu membraan-geassisteerde kristallisatie in de airlift kristallisator zijn voor het eerste uitgevoerd en het resultaat bevestigt de mogelijkheden van het model voor ontwerp doeleinden. Het door ons ontwikkelde model is gebruikt om de experimenten te ontwerpen op basis van geoptimaliseerde procesconditie voor verschillende doelen zoals grote mediaan maat of hoge yield. Daarnaast kan het ook gebruikt worden voor nieuwe processen en equipment te ontwerpen en de procescondities verder te optimaliseren.

Tot nu toe hebben wij rekening gehouden met versterking van kristalgroei en onderdrukking van secundaire nucleatie als belangrijke kristallisatie verschijnselen in seeded batch kristallisatie. Kiemvorming uit een oplossing (primaire nucleatie) is echter een ander belangrijke kristallisatie verschijnsel.

Het aanmaken van kiemkristallen uit bestaande product kristallen door bijvoorbeeld in een kogelmolen is een niet eenvoudig om hiermee een consitente kwaliteit van de kiemkristallen te verkrijgen.

Het toepassen van alternatieve energie bronnen zoals electrisch velden, ultrasound of microgolven om nucleatie te beïnvloeden en te beheersen worden momenteel onderzocht. Dit is vooral het geval voor de toepassing van ultrasound wat een positief effect vertoont op het kristallisatieproces. Uit onderzoek blijkt dat ultrasonic waves de oververzadiging limieten en de inductietijd verlagen voor primare kiemvorming wat betekent dat ze de kristallisatiesnelheid de productiviteit verhogen. Verlagen van oververzadiging limieten betekent dat de nucleatie bij een lagere oververzadiging optreedt en dat betekent dat breedte van de metastable zone is verlaagd.

In hoofdstuk 5 worden de effecten van het toepassen van ultrasound op de kiemvorming besproken. Zo wordt de kiemvormingssnelheid verhoogd met een factor rond 6 tot 9. Het Ultrasound is op twee manieren toegepast, continu en gepulst. Vanwege de vergelijkbare resultaten is de pulserende manier geselecteerd vanwege de lagere energieconsumptie.

Als eerste, is een oververzadiging regime bepaald waarbij primaire nucleatie kan worden geïnduceerd door de applicatie van ultrasound. Nucleatie is gericht op lage supersaturatie maar binnen de bereik van metastabiele zone om buitensporige nucleatie te voorkomen wat zou leiden tot vorming van fijne kristallen en daardoor slechte grootte distributie. Er zijn twee verschillende ultrasound configuraties die getoetst zijn: één voor batch applicatie waarbij de ultrasound hoorn direct in een batch kristallisator is gestoken, en één voor continu kiemvorming waarbij de ultrasound in een flow cel in een circulatiestroom werd toegepast.

Uit de resultaten van deze experimenten blijkt dat ultrasound de rate van nucleatie verhoogt en daardoor de maat en volume dichtheid beheersbaar zijn. Het door ons ontwikkelde model dat voor de kinetica van L-ascorbic acid in hoofdstuk 2 is gevalideerd kon gelijksoortige resultaten reproduceren.

Ten slotte zijn de door US gegeneerde kiemen toegevoegd aan de airlift kristallisator waar condities voor beheerbare kristalgroei gerealiseerd werden. Een FBRM is gebruikt om de kristallisatie fases in het proces te karakteriseren. Een smalle kristal grootte verdeling werd verkregen tijdens de batch koelkristallisatie experimenten in de airlift kristallisator met een groter aantal kiemen vergeleken met een normale seeded batch. Het lagere aantal tellingen van seeds leidt tot bredere kristal grootte distributie wat suggereert dat secundaire nucleatie later in het proces begint.

TABLE OF CONTENTS

Chapter 1 Introduction 23

Abstract 24

1.1 Crystallization methods and driving force 25

1.1.1 Background 25

1.1.2 Crystallization phenomena 26

1.2 Current prospects in crystallization process research 29

1.3 Scope, objectives and outline of thIS thesis 32

1.4 Acknowledgement 34

1.5 References 35

Chapter 2 Crystallization Kinetics in an Airlift and a Stirred Draft Tube Crystallizer; Secondary Nucleation Models Revisited 39

Abstract 40

2.1 Introduction 41

2.2 Materials and Methods 43

2.2.1 Model Development 43

2.2.2 Experiments 50

2.2.3 Calculation: Parameter estimation 51

2.3 Results 53

2.3.1 Initial distributions 53

2.3.2 Structure of the model 53

2.4 Discussion 55

2.5 Conclusions 60

2.6 References 61

Chapter 3 Membrane-assisted Crystallization: Membrane Characterization, Modelling and Experiments 65

Abstract 66

3.1 Introduction 67

3.2 Materials and Method 68

3.2.1 Materials 68

3.2.2 Experimental Setup 69

3.3 Process Model 71

3.3.1 Heat Transfer 71

3.3.2 Mass transfer 73

3.3.3 Coupling of Mass and Heat Transfer 74

3.3.4 Calculation Algorithm: Segmentation 75

3.4 Experimental Procedure 78
3.4.1 Characterization of the Membrane Performance 78
3.4.2 Membrane-assisted crystallization 78
3.5 Results and discussion 79
3.5.1 Sweeping Gas Membrane Distillation 79
3.5.2 Model Accuracy 83
3.6 Conclusions 83
3.7 References 85

Chapter 4 Continuous Crystallization of L-ascorbic acid using Airlift crystallizer and Membrane Distillation 91
Abstract 92
4.1 Introduction 93
4.1.1 Chapter outline 95
4.2 Materials and Methods 96
4.2.1 Model development 96
4.2.2 Seeding 97
4.2.3 CSD representation 97
4.2.4 Seeding procedure 98
4.2.5 Experimental setup 98
4.2.6 Continuous cooling crystallization (CCC) of L-ascorbic acid 98
4.2.7 Continuous membrane-assisted crystallization (CMaC) experiments with L-ascorbic acid 100
4.3 Results and Discussions 102
4.3.1 Seeding 102
4.3.2 Continuous cooling crystallization 102
4.3.3 Continuous membrane-assisted crystallization (CMaC) of L-ascorbic acid 106
4.4 Conclusions and Further Recommendations 111
4.5 References 112

Chapter 5 Ultrasound-Assisted Seed Generation for Continuous Processes 117
Abstract 118
5.1 Introduction 119
5.2 Overview of application of ULTRASOUND in the crystallization processes 121
5.3 Materials and Methods 124

5.3.1 Metastable zone width (MSZW) determination without US 124
5.3.2 US device and setup 125
5.4 Results and Discussion 126
5.4.1 Determination of the process conditions for US application 126
5.4.2 Effect of US on nucleation in batch operation 126
5.4.3 Applicability of flow cell for seed generation 128
5.5 US-assisted seed generation for an airlift crystallizer 132
5.6 Conclusions and recommendations 136
5.7 References 138

Chapter 6 Conclusions & Recommendations 143

List of Publications 149
Portfolio 151
(Inter)national conferences 151
About the Author 153
Acknowledgment 155

TABLE OF FIGURES

Figure 1-1 Schematic view of airlift crystallizer used in this study 30

Figure 2-1 Seed size distribution fitting (marker and line indicating experimental and modelling results respectively) 54
Figure 2-2 The 90% (smallest), 95%, and 99% confidence ellipsoids for estimation for airlift experiments 56
Figure 2-3 The supersaturation profile and quantiles (L_{10}, L_{20}, L_{30}, L_{40}, L_{50} and L_{90}) for ALC experiment #09 (purple) and #14 (blue) and DTC experiment #03 (red) and #04 (orange). Markers represent the experimental value and lines are the modelling results. The same colours apply to the right figure. A relative 5% error bar for relative supersaturation and a constant 50μm error bar for quantiles are used and demonstrated. (markers and lines indicating experimental and modelling results respectively) 57
Figure 2-4 Simulation results for total secondary nucleation (lines) and the particular contribution of attrition in the total secondary nucleation (dashed lines) for experiments #03 (red), #04 (orange) in DTC and experiments #09 (purple) and #14 (blue) in ALC. *57*
Figure 2-5 Simulation results for the median size evolution (lines) and the experimental results for final product L_{50} (median size) values (markers). A constant 50 μm error bar for the median size is used and demonstrated. (Experiment #03 (red), #04 (orange) in DTC and experiments #09 (purple) and #14 (blue) in ALC) 58

Figure 3-1 Overview of Liqui-cel® Extra Flow module 69
Figure 3-2 Schematic representation of MaC setup 70
Figure 3-3 Heat fluxes and heat transfer resistances in SGMD (redrawn from [6]) 72
Figure 3-4 Resistances to transmembrane mass transport of water vapor in SGMD. (based on drawing from [13]) 73
Figure 3-5 Schematic representation of applying free surface model, a) for a fiber, and b) for a module with free surface (redrawn from 76
Figure 3-6 Effect of feed temperature on membrane flux for two different air flow rates. The feed flow rate was a) 276 L/hr and b) 552 L/hr (markers represent the experimental value and lines are the modelling results) 80
Figure 3-7 Effect of air flow rate on membrane flux in different feed temperatures and feed flow rate of 552 L/hr (markers represent the experimental value and lines are the modelling results) 81
Figure 3-8 Effect of concentration on membrane flux in different air flow rates (markers represent the experimental value and lines are the modelling results) 81

Figure 3-9 Generation of supersaturation in a crystallization process (markers represent the experimental value and lines are the modelling results) 83
Figure 3-10 Comparison of predicted and experimental membrane fluxes (markers represent the experimental value and line are the modelling results) 83

Figure 4-1 Schematic view of the continuous cooling crystallization process 100
Figure 4-2 Schematic view of the continuous membrane-assisted crystallization process a) configuration 1, b) configuration 2 101
Figure 4-3 Seeds size distribution; Markers displaying the experimental results and lines displaying the model fit, purple and green presenting seeds of 173 and 245 µm. 102
Figure 4-4 Simulation (lines) and experimental (markers) results for (a) Relative supersaturation, (b) quantiles (L_{10}(○), L_{20}(Δ), L_{30}(+), L_{40}(□), L_{50}(◊), L_{90}(χ)) at the end of experiments and (c) CSD of initial seeds (green) and the products of experiments #1C (blue) and #2C (red) 103
Figure 4-5 Simulation (lines) and experimental (markers) results for effect of amounts of seeds on (a) Relative supersaturation during the whole experiments (b) quantiles from the product (L_{10}(○), L_{20}(Δ), L_{30}(+), L_{40}(□), L_{50}(◊), L_{90}(χ)) and (c) experimental CSD of the seeds (dark green) and product in the last hour for experiments #3C (orange) and #4C (light green) 105
Figure 4-6 Simulation (lines) and experimental (markers) results for (a) Relative supersaturation, (b) comparison of simulation and experimental quantiles (L_{10}(○), L_{20}(Δ), L_{30}(+), L_{40}(□), L_{50}(◊), L_{90}(χ)) at the end of experiments and (c) CSD of initial seeds (dark purple) and the products of experiments #5C (light purple), #6C (light blue) and #7C (black) *106*
Figure 4-7 Level of relative supersaturation of L-ascorbic acid in the buffer vessel for experiments #1 to #7. 107
Figure 4-8 Simulation (lines) and experimental (markers) results for (a) Supersaturation level, (b) quantiles (L_{10}(○), L_{20}(Δ), L_{30}(+), L_{40}(□), L_{50}(◊), L_{90}(χ)) and (c) CSD of seeds (dark purple) and product after 4 hours for experiments #1 (pink) and #2 (blue) *108*
Figure 4-9 Simulation (Lines) and experimental (markers) results for (a) Relative supersaturation, (b) quantiles (right) comparison of simulation and experimental quantiles (L_{10}(○), L_{20}(Δ), L_{30}(+), L_{40}(□), L_{50}(◊), L_{90}(χ)) at the end of experiments #3 (orange), #4 (green), #5 (grey), #6 (light purple) and #7 (red) and (c) the CSD of seeds (dark purple) and experiments as indicated 109
Figure 4-10 Effect of membrane flow on supersaturation profile and median size (M=0.05 (purple), M=0.1 (green), M=0.3 (red), M=0.45 (blue)) 110

Figure 4-11 Influence of crystallizer residence time on supersaturation profile and product median size (RT=1 (blue), RT=2 (red)) 110
Figure 4-12 Influence of membrane flow rate and crystallizer residence time on product median size 110
Figure 4-13 Offline and inline image of the product crystals from one of the CMaC experiments 111

Figure 5-1 Configurations of the setups used: a) without US for determination of MSZW, b) with direct application of US into the solution c) with US horn attached to and immersed in the flow through cell connected to a feed vessel either for recirculation or continuous flow 126
Figure 5-2 Reduction in induction time observed upon application of US at various fixed intial supersaturation under batch operation (500 ml) using configuration ‘b’ for Melamine in various supersaturations, well within the MSZ 127
Figure 5-3 Effect of US on nucleation kinetics of AA in batch operation a) blank experiment with initial supersaturation of 1.33, b) experiment with US at initial supersaturation of 1.33. The blue dashed lines indicating the slope of increase of counts before the outburst starts and red dashed lines show the outburst of crystals when the number of counts starts rising very sharply. 129
Figure 5-4 US experiments with lower initial supersaturation of 1.18 129
Figure 5-5 Normalized particle size density distribution (volume based) of sample taken from US-assisted and blank process (S=1.33) at batch times of 60 min and 120 min corressponding to FBRM counts of 2000. (measured offline with laser diffraction device) 130
Figure 5-6 FBRM chord length distribution of seeds generated with US (presented by markers) fitted with a volume density distribution equation in the model (presented by lines). Blue and red indicate the experiments with 2000 and 1000 counts of seeds respectively. 131
Figure 5-7 Expected supersaturation level for seeds with counts of 2000 (experiment #1, blue) and 1000 (experiment #2, red) 132
Figure 5-8 Process flow diagram of the ALC setup for the cooling batch experiments 133
Figure 5-9 Relative supersaturation profile and final CSD for experiments #1 and #2 in the ALC. Blue and red colors indicate the results for experiments #1 and #2 respectively. *134*
Figure 5-10 Relative supersaturation profile and final CSD for experiment #9 from [2]. Orange and green indicate the results for seeds and experiment #9. *135*
Figure 5-11 Comparison of microscopic and in-line images of conventional and US generated seeds and product of ALC using these seeds 136

TABLE OF TABLES

Table 2-1 Description of experiments in the 5 L DTC used in the model. 51
Table 2-2 Description of experiments in the 18 L ALC used in the model. 51
Table 2-3 Model parameters for kinetic parameter estimation 52
Table 2-4 Fitting parameters of seeding population 54
Table 2-5 Values for kinetic parameters, their 95 % confidence intervals, and their standard deviations estimated using the seeded batch experiments described in Lakerveld, et al. [4], for the ALC (columns 2-4) and for the DTC (columns 5-7) 55
Table 2-6 Values for kinetic parameters, their 95 % confidence intervals, and their standard deviations estimated using the seeded batch experiment #4 described in Lakerveld, et al [4] 56

Table 3-1 Membrane specifications 69
Table S1 Overview of membrane characterization experiments (process conditions and experimental results) 88
Table S2 Overview of membrane characterization experiments with solution of AA/water (process conditions and experimental results) 89
Table 3S Overview of membrane-assisted crystallization experiments (process conditions and experimental results) 89

Table 4-1 Process conditions for continuous cooling experiments. Residence time for all experiments is 2 hours and seeds are added every 30 minutes. 99
Table 4-2 Process conditions for CMaC experiments. Residence time for all experiments is 2 hours and 33gr seeds of 173 µm is added every 30 minutes. 102
Table 4-3 Fitted parameters for equation 4-5 for two seed sizes used in the experiments 102
Table 4-4 Crystal fraction for CMaC experiments 107

Table 5-1 Overview of the studied compounds with their corresponding process conditions. The nucleation has been detected visually. MSZW is derived as the difference between saturation and nucleation temperature at the given conditions. 126
Table 5-2 Fitting parameters of seeding population 131

Chapter 1

Introduction

ABSTRACT

Crystallization is one of the important steps in separation, purification, and product formation. In such a process, a solid product with predefined properties occurs from a solution, from the melt or via deposition of material from the gas phase. Due to several advantages of this separation process, namely mild operating conditions, low energy consumption, resulting in a stable particulate product and a high attainable product purity in one separation step, crystallization is widely applied in chemical and pharmaceutical industries. Yet insufficient understanding of crystallization phenomena and their interactions from one side, and rigorous product specifications requirements in chemical and pharmaceutical industries from the other side, challenge the application of crystallization processes. Improvement in design, in general, is needed to allow a better manipulation and control of the crystallization process and of quality of the produced crystals in particular. Moving from batch to continuous processes is also considered as one of the improvements in the area of process control and product manipulation for crystallization processes. However, more knowledge and understanding is still needed in order to design, operate and control such processes.

In this thesis an attempt is made to improve industrial crystallization processes by focusing on the design of the process and equipment. First of all, a membrane-assisted crystallization process is developed, enhancing both the sustainability and the robustness of the process by a better control of supersaturation generation during the crystallization. Secondly, the development and optimization of an airlift crystallizer is described as an alternative crystallizer design in which a better control of secondary nucleation can be achieved. In our opinion the application of those improvements can solve a number of crystallization problems and will introduce new windows of operation in where conventional designs are unable to operate.

This chapter discusses the crystallization fundamentals and a more detailed analysis of the current problems encountered in crystallization processes with the help of an overview of relevant literature. The objective and scope of this thesis is then formulated followed by the approach which is taken through this research.

1.1 CRYSTALLIZATION METHODS AND DRIVING FORCE

1.1.1 Background

Crystallization can be operated in different methods such as crystallization from a solution such as cooling crystallization, precipitation, anti-solvent crystallization, and evaporative crystallization or crystallization from melt. In crystallization the driving force is the difference in chemical potential of the crystallization compound in the solution and that of the crystalline phase at the same temperature and pressure. In solution crystallization, this driving force, often referred to as the supersaturation, can mostly be simplified as the difference between the actual value of the solute concentration and the equilibrium concentration. Supersaturation is the driving force for both formation of a new solid phase, nucleation and consecutive growth of these nuclei, both of which cannot occur under saturated or undersaturated conditions.

A solubility diagram derived at constant pressure is mostly used in cooling and evaporative crystallization showing the solubility of the compound as a function of temperature. A solution with a concentration higher or lower than the solubility at the current temperature is called supersaturated or undersaturated respectively [1-4].

There are several methods to generate the supersaturation in a crystallization process: decreasing the temperature (cooling), evaporating the solvent (evaporative), adding another solvent to reduce the solubility (anti-solvent), or cooling the melt below its melting point (melt crystallization). The method is principally selected based on the thermodynamics of the solid-liquid equilibrium of the product and the required product quality. The product quality includes crystal morphology, habit, size, and purity together with crystal size distribution (CSD) as the important specifications to meet the requirements. The performance of the crystallization processes is usually assessed by yield and product quality which are determined by the size distribution (average size, mono-dispersity and width of distribution), the shape and morphology of the produced crystals [5]. For batch operated crystallization processes batch-to-batch reproducibility often forms a problem especially at large scale. This latter issue is also one of the reasons for the recent interest in transitioning from batch to continuous manufacturing. Moving to continuous processing has the potential for huge increases in efficiency, flexibility and product quality [6-8]. Continuous processing offers, on the one hand, the advantages of enhanced reproducibility of results with the material crystallizing under uniform conditions whereas in batch operation conditions change with time, resulting in crystal characteristics which are difficult to control and inconsistent from batch to batch. On the other hand, several factors such as cost reduction, improved process efficiency, optimal use of equipment, flexibility in production capacity, etc. are inspiring the pharmaceutical and chemical industries to investigate in continuous processes. Thus, there is a need to develop robust continuous crystallization processes which produce crystals with high yield and purity [9-12].

1.1.2 Crystallization phenomena

Crystallization is a complicated process in which several phenomena occur simultaneously or sequentially such as primary nucleation, growth, secondary nucleation, supersaturation generation, mixing, etc. Here only the most important phenomena will be discussed. A more complete discussion of these phenomena and their influence on the crystallization process can be found in one of the crystallization handbooks [1-3].

1.1.2.1 Primary nucleation

Primary nucleation is the formation of a new solid phase from a liquid or vapour when no solute crystals are present. Depending on the conditions there are two mechanisms possible: homogeneous and heterogeneous nucleation. In homogeneous nucleation no solid particles or surfaces are involved. In heterogeneous nucleation solid particles of foreign substances can act as a template for the nuclei which cause an increase in the rate of nucleation that would otherwise not occur. Primary nucleation can occur only if the solution is in the supersaturated region which forms the dominant driving force for primary nucleation.

1.1.2.2 Secondary nucleation

Secondary nucleation is the formation of new crystal phase in the presence of crystals from the same solute induced by a high supersaturation level (surface nucleation) or attrition due to the interaction of the existing crystals with the liquid (fluid shear), the hardware (baffles, stirrer, pumps) or each other (crystal-crystal collisions). In industrial crystallizers, attrition (which refers to the process by which fines are removed from the surface of parent crystals) is recognized as a major cause of secondary nucleation [3-5]. Breakage is another sort of secondary nucleation and it is different from attrition since breakage involves the fracture of a particle into two or more pieces, but in attrition it breaks into one slightly smaller particle and many much smaller ones.

It is favourable to minimize or suppress the secondary nucleation to increase the process controllability and product quality consistency. Control of secondary nucleation in impeller-mixed crystallizers is difficult and the current models considering operating conditions and the crystallizer geometry often fail to accurately predict the secondary nucleation [5, 6].

1.1.2.3 Growth and dissolution

Crystal growth is the deposition of solute molecules from a supersaturated solution onto the crystal lattice. The pattern resembles the rings of an onion. Crystal growth creates molecular thin layers of solute molecules on the surface of a growing crystal slowly increasing its size, surface area and mass. The rate of deposition is determined by the mass transfer and surface integration of the solute molecules on the one hand and heat transfer to remove the heat of fusion from the crystal surface on the other hand [3]. Diffusion of growth units (molecules, atoms or ions) to the crystal surface, the surface diffusion, orientation, and the incorporation into the lattice occur in the growth phase. If the saturation level falls below the equilibrium concentration, due to a change in temperature or concentration, dissolution may happen. Dissolution is limited by mass transfer only; therefore the rate of dissolution is in general higher than that of growth [3, 7].

1.1.2.4 Supersaturation generation

The solution needs a driving force such as supersaturation to trigger the aforementioned physical phenomena. Crystals can only nucleate and grow in a supersaturated solution which can be generated by cooling the solution (depending on temperature dependence of solubility), evaporating the solvent (decreasing the solvent concentration), or by pressure increase.

Supersaturation in the crystallizer is typically generated at the mixing points and the cooling and evaporating surfaces. Mixing points are where feed solution and/or an added reagent such as an anti-solvent is introduced in the crystallizer and mixed with the bulk suspension. Despite the high turbulence in industrial crystallizers a local increase of the supersaturation around these points is inevitable. In addition, at the cooling surface of the internal or external heat exchanger the local temperature is lower than the bulk temperature, and the solute concentration in the boiling surface of an evaporative crystallizer is elevated compared to the bulk concentration, giving rise to a local zone of higher supersaturation compared to the supersaturation in the bulk of the crystallizer.

Generating substantial local supersaturation at these points can result in encrustation, high nucleation rates and small crystals. Controlling the fouling is the important factor in improving the economic performance of the crystallizers [8]. Whether fouling or encrustation occur depends firstly on the solubility characteristics of the fouling component. The location in the crystalliser where fouling occurs depends on the method of supersaturation generation e.g. on heat exchange surfaces in cooling crystallisers and on the walls and agitator shaft at the vapour release surface in evaporative crystallisers.

A number of other issues are also identified for evaporative and cooling crystallization. For example, the rate at which supersaturation can be generated is limited by the available surface area for evaporation [9-11]. The vapour velocity cannot exceed certain limits in order to avoid entrainment of liquid droplets into the condenser. Furthermore, due to mixing limitations, significant supersaturation gradients can occur, exhibiting zones without any substantial supersaturation, which reduce the efficiency of the crystallizers [12]. In addition, the elevated supersaturation which exists in the boiling zone can have a distinct influence on the dynamic behaviour of crystallizers [13]. Finally, thermal labile compounds cannot be produced by evaporative crystallization as investment costs are, in general, too high to evaporate at low temperatures.

Membranes are potentially capable of making a step improvement in this regard. Membranes offer a good possibility to play a role as an energy-efficient and more flexible alternative to evaporation and cooling in assisting crystallization processes.

Combination of membranes and crystallization is a high potential concept receiving many attentions over the past decade. The main focus is usually on two modes of operation, namely membrane-assisted crystallization (MaC) using reverse osmosis (MaC-RO) and membrane distillation (MaC-MD). MD is generally less affected by polarization than RO and is not limited by the osmotic pressure. Less energy consumption and more process flexibility are also mentioned when compared to the conventional methods of supersaturation generation [14, 15]. In section 1.2 it will be more discussed in details.

1.1.2.5 Mixing and suspension

Crystals as solids generally have higher density than their surrounding liquid which needs compensation to let the solids stay suspended. That is why crystallizers are equipped with a stirrer of any kind to induce mixing. Although mixing improves the transport phenomena and sufficient turbulence is required to prevent settling, a high turbulence causes shear damages to the crystals [1, 2, 16]. The agitation rate should be sufficient to keep all the crystals suspended and in motion preventing settling but should not be too high to cause significant secondary nucleation. On the large scale, gradients in supersaturation are influenced by the intensity of macromixing. Macromixing refers to the main convective flow in a processing compartment. Mass and heat transfer processes which have a distinct influence on the execution rate of crystallization tasks are influenced by mixing on a smaller scale (micromixing). Beside transport processes, mixing on a smaller scale also influences the shear rates acting on a crystal surface, which can induce undesired secondary nucleation resulting in broad CSDs [2].

To optimize crystal growth without compromising on the width of the CSD, air-mixed devices are developed in which sufficient mixing is provided and shear forces acting on particles are minimized, and therefore undesired secondary nucleation is reduced. Such a ‘growth’ oriented compartment will be more discussed in chapter 2 and 4.

Some crystallizer designs consciously segregate product crystals based on particle size. In such a classified product removal or elutriation method crystals settle against an up flow which is set such that only crystals matching or exceeding a critical size and settling rate can leave the crystallizer. Another design strategy is 'fines destruction' in which fine particles caused by excessive secondary nucleation are removed using a settling zone in a recycle stream where they can be re-dissolved and returned to the crystallizer in the feed solution [17, 18].

1.2 CURRENT PROSPECTS IN CRYSTALLIZATION PROCESS RESEARCH

Over the past 30 years many developments paved the way towards better understanding of crystallization from the evolutionary introduction of population balances by Randolph and Larson in 1988 to presentation of a systematic design procedure for crystallization processes by Bermingham et al. in 2000 [19, 20]. According to Rawlings et al. in 1993 and Braatz in 2002, optimization procedures and process modelling are necessary to generate optimal process conditions [21, 22]. Ma et al. in 2002 and Mazzotti et al. in 2004 carried out model-based optimization studies aiming at single objective optimization [23, 24]. Sakar et al. later in 2006 demonstrated the potential for multi-objective optimization of crystallization processes [25, 26]. Model-based optimization efforts have been and are made to handle the conflicting entanglement of several crystallization phenomena (supersaturation generation, nucleation and growth) due to their occurrence in one piece of equipment. Although problems regarding crystallization operation are covered systematically in such studies and it allows the design to combine with optimization, Braatz and Nagy concluded that despite applying these techniques in the field of crystallization the manipulation of the product properties is still difficult to achieve in the current crystallizer designs and the strong non-linear behaviour of crystallization process complicates the dynamic response of actuation.

To overcome this limitation, process stability and flexibility in the design phase must be enhanced. Nagy et al. in 2008 and 2009 and Mesbah et al. in 2011 tried to achieve effective strategies to control supersaturation via design and automated control [27, 28]. But it is still a complex, ongoing problem that leads to limited flexibility and off spec and varying product quality. Nagy in 2013 used a plug flow crystallizer consisted of multiple segments with the temperature of the segments as decision variables. In situ fines removal by temperature cycling allowed to successfully manipulate the CSD in a size-dependent kinetics system at the expense of a prolonged batch time [29]. In systems with a large flow at a high temperature and concentration, the use of multistage crystallization equipment permitted certain economics in operation, and examples of 5 to 12 stages crystallization were successfully operated according to Myerson in 2015 [30]. Nagy demonstrated a 2 stage crystallization equipped with an automated direct nucleation control in MSMPR systems to manipulate and control the nucleation phenomenon [31, 32]. Optimization is again needed to manipulate final product quality.

“Is optimization of current crystallization equipment the only solution?” Design and optimization based on equipment could be replaced with phenomenon-based approach. Task-based design (TBD) is the idea in which crystallization phenomena are used as individual building blocks. Crystallization functions are separated to form a multi-stage crystallization process. Further development of the design procedure followed by optimizing superstructures showed that the ones formed based on crystallization tasks rather than a sequence of unit operation are more flexible and less complex, which helps in manipulating the product properties. However, strategic information is missing regarding behaviour of different crystallization tasks under relevant process conditions in batch and continuous processes. Accurate models and frameworks are needed to allow for superstructure development and optimization; this will lead to next generation industrial crystallizers. This is an optimal goal that firstly needs a solid foundation to allow for TBD.

This idea shifts the thinking to design equipment on the basis of one dominant phenomenon and suppression of the other ones [33-38]. Menon in 2006 and Lakerveld in 2010 tried to apply TBD methodology to focus on the important phenomena as starting points for design rather than the equipment itself. They have applied a multi-scale and task-based decomposition strategy for the design procedure to develop novel processing units. Therefore, they applied a complementary strategy to reduce secondary nucleation by achieving the flexibility and simplicity of a stirred vessel in absence of moving parts. They have investigated the control feasibility over several key crystallization tasks in novel processing units, including ultrasound (US) for improved control over nucleation, membrane-assisted crystallization for improved control over supersaturation generation, and air-mixed devices (bubble column and airlift column) to provide mixing with low shear forces for improved control over crystal growth [9, 36].

An airlift crystallizer (ALC shown schematically in Figure 1-1) is an interesting alternative for conventional suspension crystallizers due to suppression of secondary nucleation [39]. Due to its different hydrodynamics (absence of impeller) it exhibits low shear forces while sufficient mixing, which leads to isolation of crystal growth. An airlift system consists of a riser and a downcomer, which are in open connection. A difference in density between the content of the riser and downcomer is induced due to higher gas hold-up in the riser, resulting from selective gas injection. This density difference is the driving force for a circulation flow between riser and downcomer. R. Lakerveld and A. Soare performed several cooling batch crystallization experiments in this ALC applying various process conditions. Their results confirm

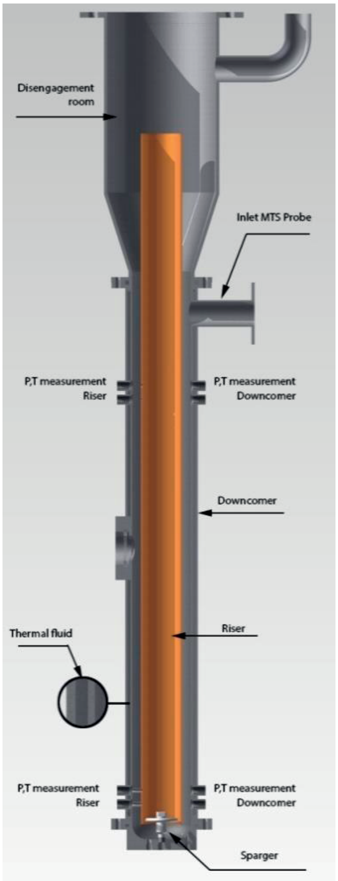

Figure 1-1 *Schematic view of airlift crystallizer used in this study*

qualitatively that secondary nucleation is suppressed for a broad range of supersaturation and that the growth is the dominant phenomenon in such a crystallizer [35, 39]. However, secondary nucleation at high supersaturation levels is inevitable. To understand the kinetic mechanism inside ALC more work is needed as for the further development and design of this type of crystallizer a proper understanding of the relevant kinetic phenomena is required. There is a need to:

- **clarify if the current growth and nucleation kinetic models are capable of describing the kinetic mechanism in such a crystallizer.**

Application of membranes offers an interesting opportunity to improve on the drawbacks for cooling and evaporative crystallization processes, namely scaling on the cooling surfaces or the limitation on the yield or of the rate of supersaturation generation by the surface area for boiling. The use of membranes is preferred due to the low energy consumption compared to evaporation. Investigations to examine the use of membrane technology to assist the crystallization or precipitation processes started in the 1980s and were mainly focused on the heterogeneous nucleation of crystals with extremely low soluble biomolecules. Later it was realised that membrane-assisted crystallization (MaC) is also useful for well soluble compounds applying either reverse osmosis (RO) or membrane distillation (MD). MaC has attracted a lot of attention from the previous decade, which has led to a large amount of academic research papers on this subject. Drioli et al. in 2011 and 2012, as well as Chabanon et al. and Pramanik et al. in 2016 have published review papers giving an overview on the different aspects of MaC and its design and show the potential to combine the membrane and the crystallization technology into a hybrid process [40-43]. Drioli and coworkers gave an excellent overview over the historical timeline of the use of different membrane systems to assist industrial crystallization processes.

They have shown that the use of a membrane contactor to assist the crystallization process can lead to (1) improved performance of the crystallizer with an extended yield which is only constrained by the impurities in the system and (2) additional features for the crystallization process, such as more flexibility, added sustainability and better controllability.

In 2009, Kuhn et al. showed the feasibility of MaC-RO using a hybrid setup in which the membrane separation occurs in a shell and tube RO module equipped with polyamide membranes. In an attempt to generalise the applicability of MaC-RO, the authors concluded that for systems with moderate to low solubility in terms of molar concentrations, energy savings in the order of 10 can be obtained. Evaporative crystallization is only favourable if: the solubility curve is very flat which requires a very high membrane temperature to avoid crystallization on the membrane surface or the system has a high solubility at the crystallizer temperature in which the osmotic pressure is too high [14].

For compounds with high osmotic pressure, however, MD is a promising alternative to RO technology. Gryta et al. in 1998 and Souhaimi in 2011 applied direct contact and sweeping gas membrane distillation (DCMD and SGMD) to crystallization processes

[44-46]. Although various models have been developed, every module has its own unique properties and operational method and configuration which imposes several adjustments to the existing models [15, 46, 47]. Therefore, there is a need to:

- **Investigate membrane technology and its feasibility to be integrated with airlift crystallizer in a crystallization process.**

It is important to note that characterization of the ALC is only done for batch-wise operation [35, 48]. In light of the before mentioned interest on especially the pharmaceutical industry to shift away from the traditional batch operated crystallization processes, which in general perform suboptimal in terms of costs, footprint, quality control and safety compared to continuous operation [30, 49], the performance of this novel type of growth oriented crystallizer for continuous operation would be of interest. Therefore, the question is:

- **Can we extend the operation of airlift crystallizer to be used in a continuous cooling process and further to be integrated with membrane distillation unit?**

Heretofore the enhancement of growth and supersaturation generation and suppression of secondary nucleation as the important crystallization phenomena in seeded crystallization have been taken into consideration. However, seed generation from a solution (primary nucleation) is another important crystallization phenomenon which helps the full task-based crystallization setup develops even further. Use of alternate energies such as electric field, US or microwave is being investigated as one of the ways for influencing and controlling nucleation. This is especially true in the application of US, which has been demonstrated to positively affect the primary nucleation. It has been found that US waves decrease the supersaturation limits and induction time, which means they increase the rate of crystallization and crystal productivity. Induction time is defined as the time elapsed between the creation of supersaturation and the appearance of the crystals. Decreasing the supersaturation limits means the nucleation occurs at lower levels of supersaturation and that means the metastable zone is reduced [50-52]. Therefore, there is a need to:

- **Investigate the potential of ultrasound technique to assist the crystallization process.**

These above-mentioned new processing units are needed to target certain tasks and to enable estimation of crystallization kinetics in a more stable and solid way, helping to improve overall process behaviour.

1.3 SCOPE, OBJECTIVES AND OUTLINE OF THIS THESIS

The feasibility of the task-based design approach and the development of new equipment to isolate certain tasks are accomplished and confirmed by R. Lakerveld in TU Delft. The scope of this thesis is to investigate the three developed unit operations (ultrasound, airlift crystallizer and membrane distillation unit) and to study the isolation of three important crystallization phenomena (primary nucleation, growth, and supersaturation generation). It is indeed necessary to develop a modelling framework in which task-based crystallization processes can be designed and simulated to facilitate further optimization and to enhance predictability. Such a modelling framework requires experimental validation, which is also within the scope of this thesis. The overall objective of the thesis is summarised as:

Investigation and optimization of newly developed airlift crystallizer and its integration with ultrasonic seed generation and a membrane unit to achieve assisted crystallization capabilities through

- 1: Modelling and design of the membrane-assisted crystallization
- 2: Description of the crystallization kinetics in airlift crystallizers
- 3: Continuous operation of the airlift crystallizer and the membrane-assisted crystallization process in this crystallizer
- 4: US based seed generation

The research questions addressed in this thesis include:

1. How can we describe the *growth*-dominated airlift crystallizer?
2. How is it beneficial to use membrane distillation as an alternative to evaporation or cooling methods to assist the crystallization process in generation of supersaturation?
3. What are the optimal process conditions for continuous operation of a crystallization process using an airlift crystallizer combined with a membrane distillation unit?
4. How do we control and optimize *primary nucleation* using an alternative driving force, ultrasound?

Experiments were done using an ultrasound system, airlift crystallizer and membrane distillation unit separately to optimize the process conditions and to observe and control the desired tasks of primary nucleation, growth and supersaturation generation. The chapters are classified accordingly.

Chapter 2 which covers research question 1, focuses on the development of the modelling framework for TBD crystallization processes and implementation of various kinetic models in this framework. Kinetic parameter estimation is performed in order to validate the model with the data from batch seeded cooling crystallization experiments, which are performed in the ALC. The results are analysed and compared with the one from conventional draft tube stirred crystallizer in pursuance of confirming the suppression of the secondary nucleation in the ALC quantitatively.

Chapter 3, which covers research question 2, shows the mechanism of sweeping gas membrane distillation and its potential to be integrated in a crystallization process. Membrane characterization experiments are performed and a model is developed and validated based on the experiments.

Chapter 4, which covers research question 3, concentrates on continuous crystallization experiments. Membrane-assisted crystallization experiments are performed, and the process potential and the product quality in terms of mainly supersaturation profile and CSD are analyzed and discussed. The developed model has been modified to be used for a continuous crystallization process.

Chapter 5, which covers research question 4, focuses on operability of US in facilitating and accelerating the primary nucleation. In the designed experiments, continuously- and pulsed-applied US have been used to investigate the effect on induction time and the product quality. The nucleation rate has been calculated using existing models. The enhanced ultrasound triggering primary nucleation rate and induction time is then analysed and compared with the ones when primary nucleation happens naturally in a supersaturated solution above the metastable zone. The US generated seeds are then applied to the ALC in order to grow to a larger size and the results are analyzed and discussed.

Finally, chapter 6 summarizes the results along with suggestions concerning follow-up research questions.

1.4 ACKNOWLEDGEMENT

This research was funded by the European Commission in the framework of the FP7, research project called “OPTICO” which aimed at the intensification of crystallization processes for pharmaceutical products.

1.5 REFERENCES

1. Lewis, A., et al., *Industrial Crystallization: Fundamentals and Applications*. 2015: Cambridge University Press.
2. Myerson, A., *Handbook of industrial crystallization*. 2002: Butterworth-Heinemann.
3. Mersmann, A., *Crystallization technology handbook*. 2001: CRC Press.
4. Gahn, C. and A. Mersmann, *Brittle fracture in crystallization processes Part A. Attrition and abrasion of brittle solids.* Chemical Engineering Science, 1999. **54**(9): p. 1273-1282.
5. Evans, T., G. Margolis, and A. Sarofim, *Mechanisms of secondary nucleation in agitated crystallizers.* AIChE Journal, 1974. **20**(5): p. 950-958.
6. Botsaris, G.D., *Secondary nucleation—a review*, in *Industrial crystallization*. 1976, Springer. p. 3-22.
7. Chen, J., et al., *Pharmaceutical crystallization.* Crystal Growth & Design, 2011. **11**(4): p. 887-895.
8. Kramer, H.J., S.K. Bermingham, and G.M. Van Rosmalen, *Design of industrial crystallisers for a given product quality.* Journal of crystal growth, 1999. **198**: p. 729-737.
9. Lakerveld, R., et al., *The application of a task-based concept for the design of innovative industrial crystallizers.* Computers & Chemical Engineering, 2009. **33**(10): p. 1692-1700.
10. Kuhn, J., et al., *Characterization and Dynamic Optimization of Membrane-Assisted Crystallization of Adipic Acid.* Industrial & Engineering Chemistry Research, 2009. **48**(11): p. 5360-5369.
11. Lakerveld, R., et al., *Membrane assisted crystallization using reverse osmosis: Influence of solubility characteristics on experimental application and energy saving potential.* Chemical Engineering Science, 2010. **65**(9): p. 2689-2699.
12. Bermingham, S.K., P.J.T. Verheijen, and H.J.M. Kramer, *Optimal design of solution crystallization processes with rigorous models.* Chemical Engineering Research & Design, 2003. **81**(A8): p. 893-903.
13. Menon, A.R., et al., *A task-based synthesis approach toward the design of industrial crystallization process units.* Industrial & Engineering Chemistry Research, 2007. **46**(12): p. 3979-3996.
14. Kuhn, J., et al., *Characterization and dynamic optimization of membrane-assisted crystallization of adipic acid.* Industrial & engineering chemistry research, 2009. **48**(11): p. 5360-5369.
15. Kramer, H.J., et al., *4.1 Membrane Crystallization Technology and Process Intensification.* 2017.
16. Mersmann, A., *Crystallization technology handbook.* Drying Technology, 1995. **13**(4): p. 1037-1038.
17. Price, C.J., *Continuous Pharmaceutical Crystallization from Solution*, in *Engineering Crystallography: From Molecule to Crystal to Functional Form*. 2017, Springer. p. 315-329.
18. Acevedo, D., et al., *A continuous multi-stage mixed-suspension mixed-product-removal crystallization system with fines dissolution.* Chemical Engineering Research and Design, 2018.
19. Randolph, A. and M. Larson, *Theory of Particulate Processes, Acad.* Press, New York, 1988.
20. Bermingham, S.K., et al., *A design procedure and predictive models for solution crystallisation processes.* 2000.
21. Rawlings, J.B., S.M. Miller, and W.R. Witkowski, *Model identification and control of solution crystallization processes: a review.* Industrial & Engineering Chemistry Research, 1993. **32**(7): p. 1275-1296.
22. Braatz, R.D., *Advanced control of crystallization processes.* Annual reviews in control, 2002. **26**(1): p. 87-99.
23. Ma, D.L., D.K. Tafti, and R.D. Braatz, *Optimal control and simulation of multidimensional crystallization processes.* Computers & Chemical Engineering, 2002. **26**(7): p. 1103-1116.

24. Worlitschek, J. and M. Mazzotti, *Model-based optimization of particle size distribution in batch-cooling crystallization of paracetamol.* Crystal Growth & Design, 2004. **4**(5): p. 891-903.
25. Sarkar, D., S. Rohani, and A. Jutan, *Multi-objective optimization of seeded batch crystallization processes.* Chemical Engineering Science, 2006. **61**(16): p. 5282-5295.
26. Kalbasenka, A., A. Huesman, and H. Kramer, *Modeling batch crystallization processes: Assumption verification and improvement of the parameter estimation quality through empirical experiment design.* Chemical engineering science, 2011. **66**(20): p. 4867-4877.
27. Nagy, Z.K., et al., *Comparative performance of concentration and temperature controlled batch crystallizations.* Journal of Process Control, 2008. **18**(3): p. 399-407.
28. Mesbah, A., et al., *A comparison of nonlinear observers for output feedback model-based control of seeded batch crystallization processes.* Journal of Process Control, 2011. **21**(4): p. 652-666.
29. Majumder, A. and Z.K. Nagy, *Fines removal in a continuous plug flow crystallizer by optimal spatial temperature profiles with controlled dissolution.* AIChE Journal, 2013. **59**(12): p. 4582-4594.
30. Alvarez, A.J., A. Singh, and A.S. Myerson, *Crystallization of cyclosporine in a multistage continuous MSMPR crystallizer.* Crystal Growth & Design, 2011. **11**(10): p. 4392-4400.
31. Yang, Y., L. Song, and Z.K. Nagy, *Automated Direct Nucleation Control in Continuous Mixed Suspension Mixed Product Removal Cooling Crystallization.* Crystal Growth & Design, 2015. **15**(12): p. 5839-5848.
32. Nagy, Z.K. and R.D. Braatz, *Advances and new directions in crystallization control.* Annual review of chemical and biomolecular engineering, 2012. **3**: p. 55-75.
33. Kramer, H., G. Van Rosmalen, and J. Ter Horst, *Basic process design for crystallization processes.* Delft University of Technology, Delft, The Netherlands, 2003.
34. Menon, A.R., *A task based design procedure and modelling approached for industrial crystallization processes*. 2006: TU Delft, Delft University of Technology.
35. Lakerveld, R., *Development of a task-based design approach for solution crystallization processes*. 2010: TU Delft, Delft University of Technology.
36. Lakerveld, R., et al., *Application of generic principles of process intensification to solution crystallization enabled by a task-based design approach.* Chemical Engineering and Processing: Process Intensification, 2010. **49**(9): p. 979-991.
37. Kramer, H.J. and P.J. Jansens, *Tools for design and control of industrial crystallizers–state of art and future needs.* Chemical engineering & technology, 2003. **26**(3): p. 247-255.
38. Kramer, H., et al., *Modelling of industrial crystallizers, a compartmental approach using a dynamic flow-sheeting tool.* Journal of crystal growth, 1996. **166**(1): p. 1084-1088.
39. Soare, A., et al., *Minimization of Attrition and Breakage in an Airlift Crystallizer.* Industrial & Engineering Chemistry Research, 2012. **51**(33): p. 10895-10909.
40. Drioli, E., A.I. Stankiewicz, and F. Macedonio, *Membrane engineering in process intensification—An overview.* Journal of Membrane Science, 2011. **380**(1): p. 1-8.
41. Drioli, E., G. Di Profio, and E. Curcio, *Progress in membrane crystallization.* Current opinion in chemical engineering, 2012. **1**(2): p. 178-182.
42. Chabanon, E., D. Mangin, and C. Charcosset, *Membranes and crystallization processes: State of the art and prospects.* Journal of Membrane Science, 2016. **509**: p. 57-67.
43. Pramanik, B.K., et al., *A critical review of membrane crystallization for the purification of water and recovery of minerals.* Reviews in Environmental Science and Bio/Technology, 2016. **15**(3): p. 411-439.
44. Gryta, M. and M. Tomaszewska, *Heat transport in the membrane distillation process.* Journal of membrane science, 1998. **144**(1): p. 211-222.

45. Souhaimi, M.K. and T. Matsuura, *Membrane distillation: principles and applications*. 2011: Elsevier.
46. Khayet, M., *Membranes and theoretical modeling of membrane distillation: A review.* Advances in colloid and interface science, 2011. **164**(1): p. 56-88.
47. Karanikola, V., et al., *Sweeping gas membrane distillation: numerical simulation of mass and heat transfer in a hollow fiber membrane module.* Journal of Membrane Science, 2015. **483**: p. 15-24.
48. Lakerveld, R., J.J. Van Krochten, and H.J. Kramer, *An air-lift crystallizer can suppress secondary nucleation at a higher supersaturation compared to a stirred crystallizer.* Crystal growth & design, 2014. **14**(7): p. 3264-3275.
49. Zhang, H., et al., *Development of continuous anti-solvent/cooling crystallization process using cascaded mixed suspension, mixed product removal crystallizers.* Organic Process Research & Development, 2012. **16**(5): p. 915-924.
50. Louhi-Kultanen, M., et al., *Crystallization of glycine with ultrasound.* International journal of pharmaceutics, 2006. **320**(1): p. 23-29.
51. Zhang, Z., et al., *Enhancement of Crystallization Processes by Power Ultrasound: Current State-of-the-Art and Research Advances.* Comprehensive Reviews in Food Science and Food Safety, 2015. **14**(4): p. 303-316.
52. Cains, P.W., P.D. Martin, and C.J. Price, *The use of ultrasound in industrial chemical synthesis and crystallization. 1. Applications to synthetic chemistry.* Organic process research & development, 1998. **2**(1): p. 34-48.

This chapter is based on the published article:

Anisi F, Kramer. H.J.M. Crystallization Kinetics in an Airlift and a Stirred Draft Tube Crystallizer; Secondary Nucleation Models Revisited, Chemical Engineering Research and Design 138 (2018) 200-211

Chapter 2

Crystallization Kinetics in an Airlift and a Stirred Draft Tube Crystallizer; Secondary Nucleation Models Revisited

ABSTRACT

In this research, a process model has been developed for an airlift crystallizer and compared with that of a draft tube stirred crystallizer to clarify the crystallization kinetics in this novel type of crystallizer. Recently it has been shown that although secondary nucleation is strongly suppressed in this crystallizer, it is not completely absent and further development and scale up requires a more quantitative prediction of the kinetics in this type of crystallizer.

A number of growth and nucleation models were examined in a parameter estimation study in which a dataset of a number of seeded batch experiments has been used to estimate the kinetics in both an airlift and a draft tube stirred crystallizer.

It is shown that a kinetic model, consisting of a two-step growth model and two additive nucleation mechanisms, i.e. an attrition based and a surface nucleation mechanism, gives an excellent and statistically acceptable description of all studied experiments with one parameter set each for both type of crystallizers. The main difference in the two types of crystallizers was found to be that the attrition terms by crystal-impeller and crystal-crystal collisions in the airlift crystallizer can be completely neglected.

Keywords: Crystallization, Parameter estimation, Kinetics, growth, Secondary nucleation

2.1 INTRODUCTION

Crystallization processes are one of the most important purification processes where achieving the desired crystal size distribution is critical for efficient downstream processing. Accurate kinetic modelling is a prerequisite to the optimal control of crystallization processes. However, the estimation of the kinetics of a crystallization process where key phenomena, nucleation and growth, occur at the same time, with different but considerable rates and degrees of nonlinearity, is challenging. In a seeded crystallization process where the supersaturation is kept within the metastable zone to avoid primary nucleation, the main source of nuclei is believed to be secondary in nature. Secondary nucleation mechanisms are often believed to be related to the high impact crystal collisions induced by the presence of an impeller or a pump, but can be induced as well by surface nucleation in case of relative high supersaturation levels [1, 2].

Airlift crystallizers (ALCs) have been recently proposed as an interesting alternative for conventional stirred crystallizers in which secondary nucleation can be suppressed to achieve a more growth-dominated crystallization process [3, 4]. An airlift system consists of a riser, where air is released, and a downcomer, which is in open connection. The density difference between the suspension/air mixture in the riser and the suspension in the downcomer, in which hardly any air is present, forms the driving force for a circulation flow between riser and downcomer. Low mechanical forces on the crystals and sufficient mixing in this crystallizer let the crystal growth to become the dominant kinetic mechanism. For these reasons airlift columns are frequently encountered in biotechnology when cells and fragile components must be kept in suspension [5, 6]. Recently it has been shown that the secondary nucleation rate in an airlift crystallizer compared to a draft tube stirred crystallizer (DTC) can be strongly but not completely suppressed [4]. Although these results, obtained at mini pilot plant scale (18 L), confirm the potential of the ALC, further development and also the design and optimization of this type of crystallizer, requires more insight in the secondary nucleation mechanism and thus a kinetic model of the system.

The most used models to describe the crystallization phenomena are formulated in the form of power law models. These classical models contain a number of fitting parameters that can be experimentally estimated to provide rather acceptable steady states values of relevant process variables but they suffer from a limited predictive capability. The application of such simplified models is restricted to experimental conditions close to the ones used for the estimation of the parameters [7-9]. They often fail to describe the dynamics in a crystallization process under slightly different process conditions or crystallizer geometries due to lumped parameter approach which do not consider mechanical properties of the crystalline substance nor the geometry and hydrodynamics of the crystallizer [10-13].

More sophisticated, physical-based models take into account the influence of the crystal size, the impeller properties and hydrodynamics of the crystallizer on the kinetics as well.

These process parameters are the identifiers which differentiate the crystallizers with different mixing strategies such as ALC from DTC and must therefore be taken into account to get a more predictive description of the crystallization kinetics in different crystallizer types.

The Mersmann model to describe the growth rate (the so-called two-step model), has a predictive character taking both integration in the crystal lattice and the diffusion from the bulk to the crystal surface of the solute molecules into account [9].

The Evans model is known as one of the most accurate predictive models for description of secondary nucleation in different crystallizers' hydrodynamics [10, 12-16]. In addition the model takes crystal-crystal and crystal-impeller collisions due to gravity and turbulence into account to describe the secondary nucleation, which is especially useful for application in an ALC in which no impeller is present. Using this model it is possible to evaluate the contribution of each mechanism and the influence of attributable parameters to these mechanisms.

At high levels of supersaturation, besides attrition, another secondary nucleation mechanism, surface nucleation, might play a role. Removal of growth units from the surface of growing crystals undergoing rough or dendritic growth can have a considerable impact on the crystallization process at elevated supersaturation levels and must be considered separately from the attrition due to the dominant dependency on the supersaturation [1].

In previous studies, an 18 L ALC equipped with a gas disengagement zone on the top (to maintain high liquid velocities in the central tube and to minimize the entrainment of bubbles in the downcomer) has been characterized and optimized with various model compounds [3, 4]. The authors have qualitatively drawn the conclusion from the seeded batch experiments of L-ascorbic acid (AA) that ideal growth (i.e. growth of crystals without any nucleation) can be achieved up to levels of supersaturation where in an impeller-mixed crystallizer a clear contribution of secondary nucleation is visible. At higher levels of supersaturation, however, the presence of some sort of secondary nucleation is inevitable [3, 4].

In the light of these results it is essential to develop a model that can adequately describe the kinetics in the ALC in order to design and optimize crystallization experiments in such a crystallizer. Especially needing attention is the description of the observed secondary nucleation at the higher supersaturation levels in the ALC, in which attrition of crystals by high energetic collisions with the impeller and baffles are not likely to occur. Can the secondary nucleation in this crystallizer be described with the commonly used attrition-based nucleation models, or do we need another type of model to get an adequate description of the kinetics in the crystallizer? The surface nucleation model described by Mersmann [1], which predict a supersaturation induced secondary nucleation beyond a certain supersaturation threshold could be a promising candidate. Therefore, a combined model has been developed in which contribution of both an attrition-based model and a surface nucleation model have been combined. The model was tested using data set of experiments performed under comparable condition in both DTC and ALC and allows the comparison of the crystallization kinetics in both types of crystallizers.

In this contribution the modelling results of the crystallization process in an ALC and a DTC are discussed. Specific attention is given on which kinetic models give the best representation for the crystallization behaviour of the two crystallizers. The process model consists of a component mass balance, an energy balance and a full population balance together with kinetic models for growth and secondary nucleation. Dynamic parameter estimation is used to estimate and verify the kinetics of the system based on a set of batch crystallization experiments from the work of Lakerveld, et al. [4]. The data comprises the profile of concentration, temperature and CSD at the end of the batch for a number of experiments in an 18 L ALC and a 5 L DTC, covering a broad range of process conditions. These data are used to develop and validate the kinetic model for the ALC in order to be further used in the development and design of this novel crystallizer. In addition the results shed light on the differences in the kinetics between these two types of crystallizers and the importance of the different secondary nucleation mechanisms [2].

The crystallization process modelling framework is implemented in gCRYSTAL (Process Systems Enterprise Ltd., 2015), a commercial general purpose modelling tool containing formal, mathematical-based optimization methods.

2.2 MATERIALS AND METHODS

2.2.1 Model Development

In this study a 1-D crystallization process with growth and nucleation phenomena is considered. The model is based on a population balance equation (PBE), which is coupled with the kinetic expressions for AA.

The assumptions considered for the PBE equation are as follows:

- No agglomeration and breakage
- The crystallizer volume is well-mixed, meaning no spatial variations in temperature, solute concentration and crystal size distribution.
- Single-solute single-solvent system
- The solid phase only contains a single pure solute.
- The vapour flow contains only solvent (water) and the feed flow is crystal free.
- Nucleation occurs at the size boundary and the mass of the nuclei is neglected.

The population balance is in fact a distributed mass balance for the solid or dispersed phase and is linked to the liquid or the continuous phase via the crystallization kinetics. This can be seen in the formulation of the other conservation relations. The so-called moments of a distribution can be related to lumped properties of the entire crystal population; for example, growth moment, representing an interphase mass flux between the liquid and solid phase which couples the PBE with the conservation equation.

Growth and nucleation are highly interconnected in a crystallization process. As primary nucleation only occurs at relatively high supersaturations, it can be neglected in seeded crystallization experiments as long as the level of supersaturation remains in the metastable region. Below, an overview of the applied kinetic models for growth and secondary nucleation is presented:

2.2.1.1 Growth

Assuming that the volume-diffusion of solute from the bulk solution to the solution-crystal interface and the surface integration of solute into the crystal lattice are the two steps in which the crystal growth process may be simplified [8, 17]; one of these steps can be dominant depending on the supersaturation level.

For surface integration-controlled growth at low levels of supersaturation where growth tends to be smooth and steps are present, the parabolic spiral model dominates, but at higher supersaturation the exponential birth and spread model takes over and at still higher supersaturation linear rough growth dominates [7].

Volume diffusion-controlled growth is dominant when the crystallizing compound has a high solubility and the integration of the solute molecules is easy. For this growth model, Fick's law can be used.

Mersmann, et al. gave an equation for a combined diffusion integration mechanism, the so called two-step model [1, 7, 9, 18, 19]:

$$\frac{G(L)}{2k_d(L)} = \frac{\Delta C}{C_s} + \frac{k_d(L)}{2k_r C_s}\left(\frac{C_{sat}}{C_s}\right)^2 - \sqrt{\left(\frac{k_d(L)}{2k_r}\right)^2 \left(\frac{C_{sat}}{C_s}\right)^4 + \frac{k_d(L)}{k_r}\left(\frac{C_{sat}}{C_s}\right)^2 \frac{\Delta C}{C_s}} \qquad \textit{(2-1)}$$

Where C_s is molar density in solid phase and C_{sat} is molar saturation concentration. k_r is the coefficient for surface integration and can be determined as:

$$k_r = f_g \frac{D_{AB}}{d_m} \frac{\left(\frac{C_{sat}}{C_s}\right)^{4/3}}{ln \frac{C_s}{C_{sat}}} \qquad \textit{(2-2)}$$

Where f_g is a constant to be estimated, D_{AB} is binary diffusion coefficient between solute and solvent, and d_m is molecular diameter which can be calculated as follows [1]:

$$d_m = \left(\frac{M_w}{n_{avo}\rho_c}\right)^{\frac{1}{3}} \qquad \textit{(2-3)}$$

Where M_w and ρ_c are the molecular weight and density of AA respectively, μ is the viscosity, and n_{avo} and k_b are Avogadro and Boltzmann constants respectively. For the applied temperature and supersaturation the value of D_{AB} is in the order of 5×10^{-6} cm^2/s, which is in line with measured values for AA [20, 21].

k_d is mass transfer coefficient, which can be estimated from the hydrodynamic conditions in the crystallizer using a Sherwood correlation as:

$$k_d(L) = \frac{D_{AB}}{L}\left[2 + 0.8\left(\frac{\varepsilon_{cr}L^4}{\nu_L^3}\right)^{\frac{1}{5}}\left(\frac{\nu_L}{D_{AB}}\right)^{\frac{1}{3}}\right] \tag{2-4}$$

Where ε_{cr} is the dissipated power by the impeller per unit mass of suspension and is defined as:

$$\varepsilon_{cr} = \frac{P_0 N_{imp}{}^3 D_{imp}{}^5}{V} \tag{2-5}$$

Where, ν_L is kinematic viscosity of the liquid; P_0, N_{imp} and D_{imp} are power number, impeller frequency and diameter; and V is the size of control volume.

Since the impeller is absent in the ALC, ε_{cr} can be defined with the help of the specific power input given by the gas per unit of liquid volume, P, which is due to gas isothermal expansion along the riser height in the ALC. $P_{airlift}$ can be defined as [3]:

$$P_{airlift} = \frac{Q_g R T}{V}\, ln\left(1 + \left(\frac{\rho_l g Z}{P_a}\right)\right) \tag{2-6}$$

Where Q_g is the molar gas flow rate, R is the ideal gas constant, T is the gas temperature, g is the gravitational acceleration, Z is the fluid height, and P_a is the pressure at top of the liquid. To use equation 2-1, $\varepsilon_{airlift}$ can be defined for ALC as:

$$\varepsilon_{airlift} = \frac{P_{airlift}}{\rho_l V} \tag{2-7}$$

2.2.1.2 Secondary Nucleation

Contrary to the relatively high supersaturations required for primary nucleation, secondary nucleation already occurs at low to moderate supersaturation levels either due to cluster detachment, sheer stress, fracture, attrition or needle breaking, or by surface breeding; the removal of growth units (irregularities) on the surface of growing crystals and their displacement into the bulk by a removal mechanism [1, 11, 22].

There are several models available in the literature trying to describe these mechanisms [7, 11, 13, 14, 18, 22, 23]. In this paper are discussed: the general simple power law model, which describes the secondary nucleation with a power law function from the supersaturation, the crystal mass fraction, and the turbulence in the crystallizer; the surface nucleation model, which depends on the supersaturation and the surface area of the crystals; and finally the model of Evans, which correlates the secondary nucleation to the probability on collisions of the crystals with each other and with the impeller, the energy of these collisions, and the tendency of the crystalline material to form fragments. A combined model consisting of two secondary nucleation models has been used in this study and is introduced at the end of section 2.2.1.2.

2.2.1.2.1 The power law model for secondary nucleation

The most used power law models consider attrition as the dominant mechanism for secondary nucleation and contain terms for the supersaturation, the amount of crystal mass, and a term describing the level of turbulence in the suspension. The advantage of the use of these simple models is that they are able to describe the development of the crystal size distribution reasonably well. The obvious disadvantage is the lack of predictive capabilities, which is needed for design purposes.

In general, the secondary nucleation rate in power law models is assumed to be the result of energy transfer to the crystals by collisions, the efficiency of contacts, and the survival of formed fines [2, 23-28]. It is described as:

$$B_{0\,(power\ law)} = K_{SN}\sigma^{n1}\varepsilon^{a}\varphi_T \qquad (2\text{-}8)$$

Equation 2-8 is an example of power law secondary nucleation model in where supersaturation and hydrodynamics are considered together to describe the total secondary nucleation. ε is the dissipated power defined in equations 2-5 and 2-7, and φ_T is the volumetric holdup defined as:

$$\varphi_T = \frac{m_T}{\rho_c} \qquad (2\text{-}9)$$

Where m_T is the suspension density and ρ_c is the solid density. K_{SN}, n_1, and a are the fitting parameters for equation 2-8.

2.2.1.2.2 Surface nucleation

With increasing supersaturation in seeded batch crystallizers the probability of surface nucleation rises. There is evidence in the literature that under certain conditions, mostly at higher supersaturation, secondary nuclei are not only formed as attrition fragments but also are chipped off from the edges of the mother crystals due to the mechanical impact or fluid shear. Under higher supersaturation conditions, secondary nuclei are rather formed as pre-ordered species or clusters in the immediate solution vicinity of the crystal surface or on the crystal surface induced by growth roughening or dendritic growth. These latter mechanisms can lead to the formation of nuclei and/or the detachment of small dendrites from the crystal surface without the need for high fluid or mechanical shear. Surface nuclei are formed when the relative supersaturation exceeds a certain critical value of S_{min} [1, 29, 30]. The model describing surface nucleation is as follows:

$$B_{0(SN)} = K_{SN1} m_2 \frac{D_{AB}}{d_m^4} e^{(-\pi \frac{KSN2}{lnS})} \qquad (2\text{-}10)$$

Where S is the relative supersaturation, m_2 is the second moment, and K_{SN1} and K_{SN2} are the parameters to be estimated within the model. Assuming d_m and D_{AB} as constant, we can define the following parameters which need to be estimated as $K'_{SN1} = K_{SN1}.D_{AB}/d_m^4$ and $K'_{SN2} = K_{SN2}.\pi$.

2.2.1.2.3 Attrition (Evans model)

Attrition can be subdivided into crystal-crystal, crystal-vessel wall and/or crystal-impeller collisions, which chip off small crystalline fragments from the mother crystals. All these mechanisms have in common the fact that a minimal collision energy is needed to chip off fragments from the mother crystals [1].

The driving force for attrition is determined by the probability that a crystal in the crystallizer collides with the impeller or other crystals, the energy of those collisions and the hardness of the crystal (i.e. the tendency of the crystal to produce fragments upon an impact). The relative kinetic energy of a collision is determined by the size and relative velocity of the particle, which in its turn is a function of the slurry motion, viscosity and particle size. The rate coefficient or resistance for attrition is a function of the shape, surface roughness and mechanical properties of the colliding crystal. The rate coefficient is also indirectly influenced by the supersaturation, which determines factors such as surface roughness and healing of corners and surfaces damaged due to previous collisions.

The high energetic crystal-impeller collision is a strong function of the stirrer speed determining the circulated volumetric flow of the suspension. However, crystal-crystal collision is proportional to the square of the volumetric holdup is much less energetic and result in fewer nuclei per unit area than in a corresponding crystal-impeller contact.

Collisions of crystals with the vessel wall occur preferentially at places where the suspension flowing from the impeller has to change direction. After a collision with the wall the crystal participates again in the circulation pattern of the suspension in the vessel. In fact, this situation is comparable with that of crystal-impeller collisions. The velocity of the solution near the wall is, however, low compared to the tip speed of the impeller. The impact energy will be less and, consequently, the nucleation rate for crystal-wall collisions. Depending on the level of supersaturation and system hydrodynamics these mechanisms can act differently.

The two major types of attrition mechanisms—collisions with the crystallizer (wall or impeller) driven by the bulk flow and by the turbulence, and collisions of crystals with each other by gravity and turbulence—can act independent from level of supersaturation [10].

Investigations of Evans, et al. mechanistically consider the dependence of the nucleation rate purely on design parameters such as agitation rate and scale of equipment as well as experimental parameters such as crystal size and solution properties. This model includes (1) collisions of crystals with an impeller as the crystals swept by the impeller in steady flow, (2) collision between crystals in a turbulent flow field and various surfaces in the crystallization, (3) collision between crystals as a consequence of differences in their terminal velocities and (4) collision between crystals driven by turbulent eddy motion [14, 15, 31]:

$$B_{0(attrition)} = \Omega \left[K_{c\text{-}i} \left(\frac{N_{imp}}{P_0} \right) \varepsilon_{cr} K_v \rho_c m_3' + K_{c\text{-}c} \rho_{sl} x \varepsilon_{cr}^{5/4} \bar{L}^4 m_0' \right] \tag{2-11}$$

Where

$$m'_3(t) \left[\frac{m^3}{m^3} \right] = \int_{L_{c\text{-}i}}^{\infty} n(L,t) L^3 dL, \text{ and } m'_0(t) \left[\frac{m^0}{m^3} \right] = \int_{L_{c\text{-}c}}^{\infty} n(L,t) L^0 dL \tag{2-12}$$

$$x = \frac{K_v \rho_c \pi \bar{L}^3 m_0'}{6 \rho_{sl}} \tag{2-13}$$

Where $L_{c\text{-}i}$ and $L_{c\text{-}c}$ are minimum crystal sizes from which this equation is valid to account for the fact that in order for a collision to occur the particles need to have a minimal mass, otherwise the collision will not be powerful enough to break fragments from the crystal or the crystals will just follow the streamlines of the flow. The first term on the right side of equation 2-12 describes the crystal-impeller collisions and the second term describes the crystal-crystal collisions. Ω [#/J] is the number of nuclei generated per unit collision energy and ε_{cr} [W/kg] is defined according to equation 2-5 for DTC and equation 2-7 for ALC. Considering $\Omega=1$, $K_{c\text{-}i}$ and $K_{c\text{-}c}$ are the proportionality constants for crystal-impeller and crystal-crystal collisions which can be estimated.

Independent of the type of impeller it is shown that 70-80% of the fines are produced by crystal-impeller collisions in a DTC. Therefore, the contribution of crystal-crystal collision is usually neglected in the literature [14, 15, 27]. The model of Ottens and the one from Gahn and Mersmann try to describe formation of fragments and their subsequent growth in two parts, brittle fracture model for attrition and abrasion of brittle solids and a growth model for growth of these fragments [1, 12, 13, 32, 33]. Since they assume the highest velocities of particles in a crystallizer when they collide with the impeller, crystal-crystal collision is always assumed to be negligible.

However, the energy dissipation occurring in the bulk associated to the presence of bubbles in the ALC can be defined as the summation of the dissipation associated to the wall friction and the one associated to the bulk flow in the riser and the downcomer. According to the experimental data in literature the dissipation associated to the wall friction is very small and in practice negligible, but the dissipation associated to the bulk flow depends highly on the applied gas flow rate [34].

The model of Evans is applied in this contribution in order to enable us to evaluate the contribution of different attrition mechanisms when comparing kinetics in DTC and ALC.

For ALC the first term on the right side of equation 2-11 is not applicable due to absence of moving objects. Therefore, $K_{c\text{-}c}$ is the parameter to be estimated for ALC.

2.2.1.2.4 Combined model

In slow growing systems such as the AA/water system conditions can arise that secondary nucleation by both attrition and surface nucleation can occur simultaneously. For those cases we have implemented both models (equations 2-10 and 2-11) as follows:

$$B_0 = B_{0(SN)} + B_{0(attrition)} \tag{2-14}$$

In this way we hope to achieve an acceptable description of the crystallization kinetics with a single model in both types of crystallizers.

2.2.1.3 Seeding

Since all of the experiments considered are seeded batch experiments and the size of the final product is dictated by the initial size distribution, it is necessary to do the parameter estimation from a similar initial point. A mathematical expression for the initial distribution is obtained by fitting two additive log normal distributions to the volume density distribution. The five parameters, $L_{g,1}$, $L_{g,2}$, σ_1, σ_2 and F_1, in equation 2-15 are used as fitting parameters. $L_{g,i}$ is the geometric mean (location parameter), σ_i the geometric standard deviation (spread parameter), and F_1 gives the relative weighting of the two log-normal distributions:

$$\tilde{v}_0(L) = \frac{F_1}{L}\,\frac{1}{ln\sigma_1\sqrt{2\pi}}\,exp\left(-\frac{ln^2\left(\frac{L}{L_{g,1}}\right)}{2ln^2\sigma_1}\right) + \frac{1-F_1}{L}\,\frac{1}{ln\sigma_2\sqrt{2\pi}}\,exp\left(-\frac{ln^2\left(\frac{L}{L_{g,2}}\right)}{2ln^2\sigma_2}\right) \tag{2-15}$$

And it is transformed to the initial number density with:

$$n_{seeds}\left[\frac{\#}{m^3 m}\right] = \frac{\tilde{v}_0(L)}{k_V L^3}\,\frac{\rho_{seeds}}{\rho_c} \tag{2-16}$$

In where ρ_{seeds} denotes the initial concentration of seeds.

2.2.1.4 CSD representation

The quantile, symbolically denoted as L_q, is defined as the crystal size for which q% of the observed volume density distribution has a size smaller than or equal to this value:

$$\frac{q}{100} = \bar{V}(L_q) \tag{2-17}$$

Where

$$\bar{V}(L) = \frac{\int_{Lmin}^{L} n(L)\, k_v L^3 dL}{\int_{Lmin}^{Lmax} n(L)\, k_v L^3 dL} \tag{2-18}$$

The CSD width is expressed as L_{90}/L_{10} and the median size is L_{50}.

To follow the previous studies two main ideas must be taken into account: (1) multiple (in both terms of measured parameters and measurement frequency) experimental data are essential to estimate the kinetics of crystallization process and (2) quantification of CSD or quantiles for appropriate estimation of kinetic phenomena [35]. In this contribution all of the experiments categorized in [4] have been used including the experimental data for relative supersaturation and the final product quantiles (L_{10}, L_{20}, L_{30}, L_{40}, L_{50} and L_{90}) for the kinetic parameters estimation.

2.2.2 Experiments

2.2.2.1 Seeded batch crystallization experiments

Seeded batch crystallization of AA in water has been done in an 18 L ALC and a 5 L DTC with similar process conditions. The experiments and the process conditions are described in Lakerveld, et al. [4]. The actual concentration of AA in water was measured in the beginning and during the experiments. To avoid primary nucleation during the experiments the supersaturation level was kept within the metastable zone. The CSDs of the final product were measured in triplicate using a laser diffraction instrument (Microtrac, S3500). Experiments 3 to 6 for DTC and 7 to 14 for ALC fully described in [4] are considered in this study. A summary of process conditions for these experiments is given in Table 2-1 and Table 2-2. Saturation temperature is 40 ºC for all experiments. The seed load (C_s) is defined as the ratio of the seed mass (M_s) over the theoretical mass of the final product based on solubility and the measured initial concentration [4].

The experiments for ALC can be generally categorized as 'high temperature seeding' and 'low temperature seeding' experiments. In high temperature seeding experiments the seeds are introduced early in the process when the level of the supersaturation is low compared to the low temperature seeding experiments where the seeds are introduced later in the process when the level of supersaturation is high. It has been tried to widen the window of operation with introduction of these two types of experiments for ALC. Whether similar kinetics (set of parameters) apply for both categories show the level of flexibility in the ALC.

Table 2-1 *Description of experiments in the 5 L DTC used in the model*

#	Time [h]	M_s [g]	C_s [wt%]	T_s [ºC]	T_f [ºC]
3	6	14.4	1.9	31.6	25
4	6	9	1.9	37.0	31
5	8	9	2.1	37.0	31
6	8	9	2.0	37.0	31

Table 2-2 *Description of experiments in the 18 L ALC used in the model*

#	Time [h]	M_s [g]	C_s [wt%]	T_s [ºC]	T_f [ºC]
7	6	52	2.0	31.6	25.0
8	6	11.6	0.6	31.6	31.0
9	6	11.6	0.6	31.6	31.0
10	6	11.6	0.6	31.6	31.0
11	6	3.5	0.2	31.6	31.0
12	6	0	0	31.6	31.0
13	6	32.5	1.6	37.0	31.0
14	8	32.5	1.8	37.0	31.0

2.2.3 Calculations: Parameter estimation

The experiments are modelled from the seeding point when the third-order temperature profile starts. The control variables are mass of seeds, initial and final temperature, crystallizer volume, initial concentration and time of operation, which are assigned for every experiment accordingly. The measured data, supersaturation at every time step, and the final quantiles (L_{10}, L_{20}, L_{30}, L_{40}, L_{50} and L_{90}) are given to the model. The model tries to dynamically estimate the optimal parameters for kinetic equations by fitting the relative supersaturation profile and the final crystal size distribution (quantiles). gCRYSTAL has a built-in parameter estimation module which attempts to determine values for the unknown parameters in order to maximize the probability that the mathematical model will predict the values obtained from the experiments. Assuming independent, normally distributed measurement errors with zero means and standard deviations, σ_{ijk}, the maximum likelihood goal can be captured through the following objective function:

$$\phi = \frac{N}{2}\, ln(2\pi) + \frac{1}{2}\, min_{\theta}\{\sum_{i=1}^{NE}\sum_{j=1}^{NVi}\sum_{k=1}^{NMij}[ln(\sigma_{ijk}^{2})] + \frac{(\tilde{Z}_{ijk} - Z_{ijk})^{2}}{\sigma_{ijk}^{2}}\} \qquad (2\text{-}19)$$

Where the symbols have the following definitions:

N: total number of measurements taken during the experiments

θ: set of model parameters to be estimated

NE: number of experiments performed

NVi: number of variables measured in the ith experiment

NMij: number of measurements of the jih variable in the ith experiment

σ^2_{ijk}: variance of the kth measurement of variable in the ith experiment

$\tilde{Z}_{ijk}$: k^{th} measured value of variable j in experiment i

Z_{ijk}: k^{th} (model-)predicted value of variable j in experiment i

The maximum likelihood objective function (equation 2-19) gives the flexibility for several types of variance models to be specified by the user. A constant relative variance model for relative supersaturation data is chosen because the experimental error is assumed to be proportional to response. For the quantiles data a constant variance model is chosen since it is presumed that all data points are of equal importance. A value of ω=0.05 and 50 has been chosen for supersaturation and quantile data based on the maximum errors from measurement systems (density meter for supersaturation measurements and laser diffraction machine for CSD measurements).

The model consists of the population, enthalpy and material balances, together with kinetic relations for growth and secondary nucleation. The growth kinetics is described by equations 2-1 and 2-5 for the DTC and equation 2-1 and 2-7 for the ALC. The secondary nucleation is either described by the power law model using equation 2-8 or the combined model using equation 2-14 for both the DTC and the ALC. Note that the contribution of the crystal-impeller and the crystal-crystal collisions in the ALC to the attrition model of Evans were neglected in the final results as discussed in section 2.2.1.2.3.

The relevant parameters to be estimated for each model are listed in Table 2-3.

Table 2-3 *Model parameters for kinetic parameter estimation*

Model Parameters	Symbol
Two-step growth model (equation 2-1)	F_g
Surface nucleation model (equation 2-10)	K'_{SN1}, K'_{SN2}
Power law attrition model (equation 2-8)	K_{SN}, n_1, a
Evans attrition model (equation 2-11)	K_{cc}, K_{ci}

Due to random errors in the measurements, the estimated parameters are stochastic variables with probability distributions. Equation 2-20 is a distribution that can be used to estimate the hyperellipsoidal confidence region that quantifies the accuracy of the parameters:

$$E_P \equiv \{P : (P - \hat{P})^T M (P - \hat{P}) \leq \chi^2_{NP}(\alpha)\} \tag{2-20}$$

Where α is the confidence level, N_p is the number of parameters, χ^2_{Np} is the chi-squared distribution with N_p degrees of freedom, and M is equal to the inverse of the variance-covariance matrix computed via linearization or Monte Carlo simulations. Comparing E_P with χ^2_{Np} is a goodness-of-fit analysis for which a smaller E_p means a good fit.

To show the percentage accuracy of the estimated parameters with respect to the 95% confidence intervals, the t-value is introduced. The associated t-values, t_i, are compared with the reference 95% t-value, $t(0.95, N - N_p)$, which is again calculated using internal statistical functions as:

$$t_i = \frac{\hat{P}_i}{X_i(0.95)} \text{ Where } X_i(\alpha) = t\left(\frac{1+\alpha}{2}, N\text{-}N_p\right).\sqrt{V_{ii}} \qquad (2\text{-}21)$$

Where p_i are the parameters and v_{ii} is the square root of each diagonal element and approximated standard deviation of the respective estimated parameter.

Moreover the confidence ellipsoid is bounded by the box of $\hat{P}_i$ - X_i (α) and $\hat{P}_i$ + X_i and can be visualized.

A t-value larger than the reference t-value indicates that the corresponding parameter has been accurately estimated (the standard deviation and the confidence interval are small compared to the value of the estimated parameter); a smaller value indicates a poor estimate of the corresponding parameter.

During all parameter estimation attempts the initial values of the parameters are changed to confirm the optimum found is global.

2.3 RESULTS

2.3.1 Initial distributions

Figure 2-1 shows the fit of the seed distribution, which forms the initial distribution of the process model. The model is described by equation 2-15 and 2-16. Table 2-4 provides the fitting parameters required for equation 2-15. The perfect fit of initial distribution is necessary as a starting point to enable us to compare the final product distribution accordingly.

2.3.2 Structure of the model

The parameter estimation study was performed using the population balance-based model described in section 2.2.1. The two-step growth model (equation 2-1) was implemented to describe the growth of the crystals while for secondary nucleation both the Evans attrition (equation 2-11) and the surface nucleation (equation 2-10) model were implemented. In the parameter estimations, the following particular settings were used:

- In growth equation 2-1, the specific power input is estimated using equation 2-5 for the DTC and equation 2-7 for the ALC.
- In the surface nucleation model the nucleation rate is assumed to be zero below a certain supersaturation threshold. In our model the supersaturation threshold, $S_{min,}$ in equation 2-10 was estimated to be 1.13 which is in accordance with Mersmann's studies [1].

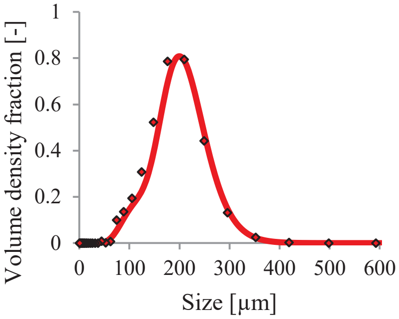

Figure 2-1 *Seed size distribution fitting (marker and line indicating experimental and modelling results respectively)*

Table 2-4 *Fitting parameters of seeding population*

Parameter	Fitted amount for 212µm
$L_{g,1}$	212×10^{-6}
$L_{g,2}$	140×10^{-6}
σ_1	1.23
σ_2	1.4
F_1	0.80

- The value of lower integration limits will differ for the different kinds of collisions, and should be determined for crystal-crystal collisions and crystal-impeller collisions separately. These bounds indicate that crystals with a size smaller than this lower bound are excluded from the distribution [10]. Since crystal-impeller collisions is dominating in DTC the value of lower integration have been found to be 300 µm while crystal-crystal collisions are of less importance and therefore rate of attrition was found to be independent of a lower integration limit for this type of collision.
- Despite the fact that the applied gas flow rate and the associated energy dissipation due to the bulk flow in the ALC is very small compared to the ones applied in literature, the attrition model for the crystal- crystal collisions was implemented and tested in the model. The results confirmed that the contribution of the crystal-crystal collisions was very low, which made the estimation of the rate constant very difficult and resulted in large standard deviations and uncertainty in the model parameters. Therefore the Evans model was removed from the final estimation runs of the ALC.
- Similarly, for the experiments of DTC the contribution to the nucleation rate of crystal-crystal collisions was found to be orders of magnitude lower than that of crystal-impeller collisions. As an example, in experiment #4 of the DTC, the maximal nucleation rate by crystal-impeller and crystal-crystal collisions were estimated to be 1.3×10^6 and 1 [#/m^3s] respectively). The estimated parameter, K_{cc}, resulted in a large standard deviation while the crystal-crystal collisions rate hardly contributed in the total attrition rate. Therefore the contribution of the crystal-crystal collisions to the secondary nucleation were removed from the final parameter estimation runs.

For comparison, parameter estimation has also been performed for the DTC replacing the Evans and the surface nucleation model with equation 2-8 (power law model), which correlates the supersaturation and dissipated energy in one equation.

2.4 DISCUSSION

Dynamic parameter estimation was performed using the supersaturation profile and the quantiles at the end of the batch of all experiments in the ALC and the DTC described in the work of Lakerveld, et al. [4] yielding one parameter set for both crystallizers. The parameter estimation results based on the data of the mentioned experiments are presented in the form of values of the optimal parameters, their standard deviations and the 95% confidence interval (Table 2-5) and a graphical comparison between the experimental data and simulations for both ALC and DTC experiments. Ellipsoids plots between f_g and K_{sn2} with different levels of confidence for ALC experiments as an example of degree of correlation are shown in Figure 2-2.

The results of the parameter estimation using the power law equation for the secondary nucleation, equation 2-8, are presented in Table 2-6.

Table 2-5 *Values for kinetic parameters, their 95 % confidence intervals, and their standard deviations estimated using the seeded batch experiments described in Lakerveld, et al. [4], for the ALC (columns 2-4) and for the DTC (columns 5-7)*

Exp	All batch seeded crystallization in ALC			All batch seeded crystallization in DTC		
Par	Amount estimated	95% confidence interval	Standard deviation	Amount estimated	95% confidence interval	Standard deviation
f_g	2.39×10^{-6}	2.87×10^{-7}	1.45×10^{-7}	3.07×10^{-6}	2.56×10^{-7}	1.27×10^{-7}
K_{cc}	-	-	-	-	-	-
K_{ci}	-	-	-	7.59×10^{5}	2.81×10^{5}	1.4×10^{5}
K'_{SN1}	1.29×10^{5}	2.34×10^{4}	1.18×10^{-4}	1.80×10^{6}	9.33×10^{5}	4.65×10^{5}
K'_{SN2}	4.12×10^{-1}	2.22×10^{-2}	1×10^{-2}	5.13×10^{-1}	6.75×10^{-1}	3.36×10^{-1}

Table 2-6 *Values for kinetic parameters, their 95 % confidence intervals, and their standard deviations estimated using the seeded batch experiment #4 described in Lakerveld, et al [4]*

Exp	Experiment #4 of DTC		
Par	Amount estimated	95% confidence interval	Standard deviation
f_g	3.07×10^{-6}	2.56×10^{-7}	1.27×10^{-7}
K_{SN}	5.00×10^{10}	3.91×10^{12}	1.97×10^{12}
A	4.26	1.71	0.85
n_1	0.64	27.60	13.75

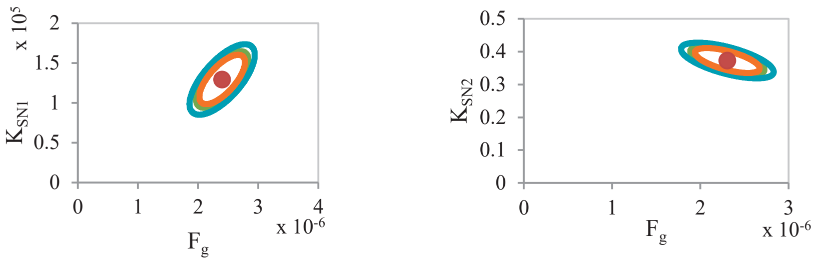

Figure 2-2 *The 90% (smallest), 95%, and 99% confidence ellipsoids for estimation for airlift experiments*

The optimal values of parameters for DTC experiments compared to the ones from ALC show a larger standard deviation and thus larger confidence ellipsoids. However, a goodness-of-fit analysis based on the 95% χ^2 criterion computed from equation 2-20 shows weighted residual of always lower than χ^2 , meaning the fit is optimal. Moreover the 95% t-value is always larger than reference 95% t-value, which is another means to trust the good quality of the parameter estimation.

The supersaturation profile and quantiles of both the experiments and the modelling results for two examples from ALC experiments and two similar ones from DTC experiments are shown in Figure 2-3. Experiment #3 for DTC and #9 for ALC are the representatives for low temperature seeding and experiments #4 for DTC and #14 for ALC are the ones for high temperature seeding. These examples are representatives of rest of experiments.

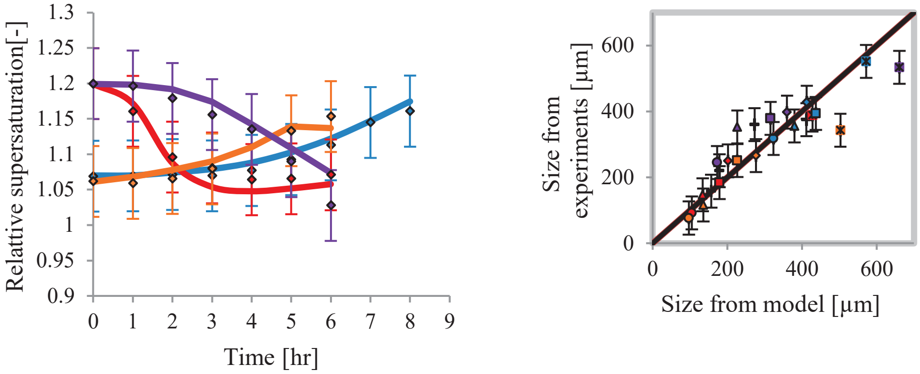

Figure 2-3 *The supersaturation profile and quantiles (L_{10}, L_{20}, L_{30}, L_{40}, L_{50} and L_{90}) for ALC experiment #09 (purple) and #14 (blue) and DTC experiment #03 (red) and #04 (orange). Markers represent the experimental value and lines are the modelling results. The same colours apply to the right figure. A relative 5% error bar for relative supersaturation and a constant 50 µm error bar for quantiles are used and demonstrated. (markers and lines indicating experimental and modelling results respectively)*

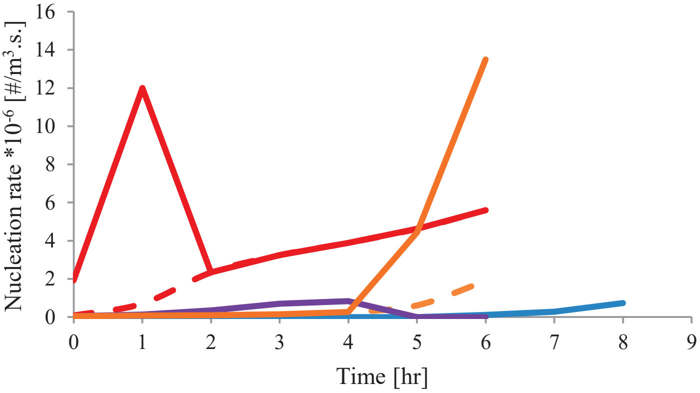

Figure 2-4 Simulation results for total secondary nucleation (lines) and the particular contribution of attrition in the total secondary nucleation (dashed lines) for experiments #03 (red), #04 (orange) in DTC and experiments #09 (purple) and #14 (blue) in ALC.

Figure 2-3 (left) shows the fits of the supersaturation level in experiments #04 of DTC and #14 of ALC, both starting from a low supersaturation. The model clearly reproduces the gradual increase, with different slopes, of the supersaturation. The larger median size found in the ALC (Figure 2-3 [right]) shows the competition between the growth and the secondary nucleation in the two crystallizers. Figure 2-4 gives the trend in the secondary nucleation in both crystallizers and clearly shows the large suppression of the nucleation in the ALC.

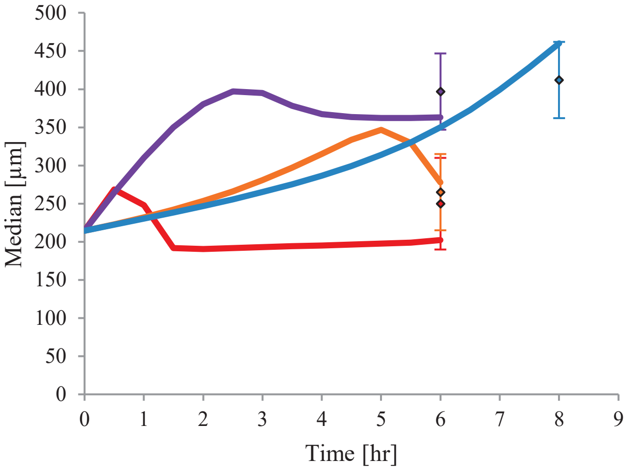

Figure 2-5 Simulation results for the median size evolution (lines) and the experimental results for final product L_{50} (median size) values (markers). A constant 50 µm error bar for the median size is used and demonstrated. (Experiment #03 (red), #04 (orange) in DTC and experiments #09 (purple) and #14 (blue) in ALC)

Figure 2-3 also shows the rapid depletion of the high initial supersaturation in experiment #03 (DTC) compared to that in experiment #09 (ALC) which can be explained by the strong increased secondary nucleation rate after one hour (Figure 2-4) causing a decrease in the median size and the creation of additional surface area of the crystals leading to the drop in the supersaturation. Figure 2-4 also shows the contribution of the attrition to the secondary nucleation rate and shows that the first peak for low temperature seeding experiments can almost be entirely attributed to surface nucleation. After about two to three hours the contribution of the attrition rises and becomes almost completely dominant due to the increase in the size and the mass of the crystals and the decrease in the supersaturation. The difference in the slope of the supersaturation decrease in the two experiments is clearly explained by the difference in the nucleation rate in the two crystallizers.

The results of simulation for evolution of median values for experiments in the DTC and ALC are shown in Figure 2-5. During the course of the experiments in DTC growth of large seed crystals is followed by a pronounced secondary nucleation and the outgrowth of these nuclei in this crystallizer (Figure 2-4). This is also reported for almost every impeller-equipped crystallizer [32]. It confirms the competition for growth between the seed crystals and the produced nuclei in the DTC while the same initial growth in ALC is not limited by attrition and results in a product with a larger median size.

According to Lakerveld, et al. a larger median size in case of ALC may mean a higher growth rate than the one in the DTC [4]. Mersmann discusses the growth mechanism as when the diffusive/convective transport of units takes place rapidly (i.e., mass transfer coefficient $k_d \rightarrow \infty$ or the integration reaction takes place very slowly $k_r \rightarrow 0$), crystal growth is determined by the integration occurring on the crystal surface. For all of the experiments, both in ALC and DTC, the growth rate is found to be similar. k_d is estimated to be three orders of magnitude larger than k_r which means that the integration reaction is rate determining. The calculated growth rate for both crystallizers confirms the crystal size dependency of the growth mechanism. Although similar growth rates in both crystallizers is estimated, the total nucleation rate for experiments of DTC is much higher and the produced secondary nuclei compete with the growth of the seed crystals which also explains the wide and bimodal final CSD of the products from these experiments.

The parameter estimation results for all the DTC experiments using the power law model (equation 2-8) in which the supersaturation, the crystal mass and hydrodynamic dependencies are taken into account are given in Table 2-6. The results were statistically not sufficient. The standard deviation and the confidence interval were for most of the parameters larger than the optimal values. Although acceptable parameter estimation results for individual experiments could be obtained, the power law model in combination with the two-step growth model was not capable to describe the series of batch experiments in this crystallizer. This indicates that the parameters in this secondary nucleation model are strongly dependent on the process conditions, which makes the applicability for process design and development questionable and are therefore not discussed further here.

The most striking result of the parameter estimation study is that the kinetics of the ALC can be described adequately over a fairly broad range of process conditions by the surface nucleation model and the two-step growth model only. Despite the small number of parameters, good fits were obtained with small standard deviations. The results confirm the earlier reported suggestion that attrition-based secondary nucleation can be neglected in this type of crystallizer. On the other hand, the results indicate that supersaturation control remains essential in this crystallizer to avoid the surface nucleation.

For the DTC the parameter estimation results were more of a surprise. It was expected that an attrition-based model should be able to describe the secondary nucleation in this type of crystallizer adequately. However, a reasonable description of the experiments could only be obtained using both the Evans model and the surface nucleation model. Our simulation results indicate that two completely different secondary nucleation models play a role in the batch operated cooling crystallization of AA in the DTC. Looking at the parameter values, the rate constant K'_{SN2} is even an order higher than the value found in the ALC. This could be due to the more efficient removal of the nuclei from the surface of the crystals in the higher turbulence around the impeller.

The entanglement of different kinetic phenomena in DTC could explain why the optimal estimated parameters for the experiments in DTC show larger confidence intervals. Large confidence ellipsoids are an indication of insufficient quality of experimental data and/or a violation of the model assumption. As can be seen in Figure 2-3, the quantiles (L_{10}, L_{20}, L_{30}, L_{40}, L_{50} and L_{90}) of the experiments in which secondary nucleation is relatively high have a less satisfactory fit than the others. Among the possible explanations are varying values of the strain content of the crystal lattice and the volumetric shape factor as well as the changing state of the crystal surface [32].

2.5 CONCLUSIONS

A dynamic parameter estimation study has been performed to describe and compare the crystallization kinetics in an ALC and a DTC in a series of seeded cooling experiments of AA/water system in both crystallizers described by Lakerveld, et al., 2014 [4].

The crystallization kinetics in both types of crystallizers could be adequately described using a population balance based process model with a unified model structure for secondary nucleation consisting of contributions of both surface nucleation and attrition; ssuming that the contribution of the latter kinetics was zero for ALC due to the absence of an impeller. The results confirm that the attrition terms by crystal-impeller and crystal-crystal collisions in the ALC can be completely neglected, while in the DTC, this process could only be described adequately when both the surface nucleation model and the attrition model of Evans were taken into account.

The reliability and precision of the estimates in this study are confirmed using a goodness-of-fit analysis based on the 95% confidence intervals and standard deviations. The statistical tests of the estimation results showed an acceptable precision in the estimated parameters.

The results confirm the strong suppression of the secondary nucleation in the ALC compared to the DTC due to the absence of attrition but also as a result of the lower values of the rate constants for the surface nucleation model. The proposed surface nucleation model perfectly describes the nucleation observed in the ALC at higher and intermediate supersaturation levels. The requirement of an activated nucleation model to get an acceptable description of the secondary nucleation in the DTC is one of the important results of this study and explains the often observed, early nucleation events in batch crystallization.

2.6 REFERENCES

1. Mersmann, A., *Crystallization technology handbook*. 2001: CRC Press.
2. Farrell, R.J. and Y.C. Tsai, *Modeling, simulation and kinetic parameter estimation in batch crystallization processes.* AIChE journal, 1994. **40**(4): p. 586-593.
3. Soare, A., et al., *Minimization of Attrition and Breakage in an Airlift Crystallizer.* Industrial & Engineering Chemistry Research, 2012. **51**(33): p. 10895-10909.
4. Lakerveld, R., J.J. Van Krochten, and H.J. Kramer, *An air-lift crystallizer can suppress secondary nucleation at a higher supersaturation compared to a stirred crystallizer.* Crystal growth & design, 2014. **14**(7): p. 3264-3275.
5. Joshi, J., et al., *Sparged loop reactors.* The Canadian Journal of Chemical Engineering, 1990. **68**(5): p. 705-741.
6. Merchuk, J.C., *Airlift Bioreactors: a Review of Recent Advances.* Canadian journal of chemical engineering, 2003. **81**(3/4): p. 324-337.
7. Lewis, A., et al., *Industrial Crystallization: Fundamentals and Applications*. 2015: Cambridge University Press.
8. Mullin, J.W., *Crystallization*. 2001: Butterworth-Heinemann.
9. Mersmann, A., *General prediction of statistically mean growth rates of a crystal collective.* Journal of crystal growth, 1995. **147**(1-2): p. 181-193.
10. Imran, A., et al. *Contribution of crystal-impeller and crystal-crystal collisions to secondary nucleation*. in *Proceedings of European Congress of Chemical Engineering*. 2007.
11. Ottens, E.P.K., *Nucleation in continuous agitated crystallizers*. 1973, TU Delft, Delft University of Technology.
12. Gahn, C. and A. Mersmann, *Brittle fracture in crystallization processes Part B. Growth of fragments and scale-up of suspension crystallizers.* Chemical Engineering Science, 1999. **54**(9): p. 1283-1292.
13. Gahn, C. and A. Mersmann, *Theoretical prediction and experimental determination of attrition rates.* Chemical Engineering Research and Design, 1997. **75**(2): p. 125-131.
14. Evans, T., G. Margolis, and A. Sarofim, *Mechanisms of secondary nucleation in agitated crystallizers.* AIChE Journal, 1974. **20**(5): p. 950-958.
15. Evans, T., A. Sarofim, and G. Margolis, *Models of secondary nucleation attributable to crystal-crystallizer and crystal-crystal collisions.* AIChE Journal, 1974. **20**(5): p. 959-966.
16. Neumann, A.M., et al., *The effect of the impeller speed on the product crystal size distribution (CSD) a 22 liter draft tube (DT) crystallizer.* Journal of crystal growth, 1999. **198**: p. 723-728.
17. Pérez-Calvo, J.F., S.S. Kadam, and H.J. Kramer, *Determination of kinetics in batch cooling crystallization processes—A sequential parameter estimation approach.* AIChE Journal, 2016.
18. Bermingham, S., P. Verheijen, and H. Kramer, *Optimal design of solution crystallization processes with rigorous models.* Chemical Engineering Research and Design, 2003. **81**(8): p. 893-903.
19. Westhoff, G.M., et al., *Modeling growth rate dispersion in industrial crystallizers.* Chemical engineering & technology, 2003. **26**(3): p. 286-291.
20. Gerhardt, G. and R.N. Adams, *Determination of diffusion coefficients by flow injection analysis.* Analytical chemistry, 1982. **54**(14): p. 2618-2620.
21. Winkelmann, J., *Diffusion coefficient of L-ascorbic acid in water*, in *Diffusion in Gases, Liquids and Electrolytes*. 2018, Springer. p. 860-861.
22. Denk, E.G. and G.D. Botsaris, *Fundamental studies in secondary nucleation from solution.* Journal of Crystal Growth, 1972. **13**: p. 493-499.

23. Daudey, P.J., *Crystallization of ammonium sulfate.* Secondary nucleation and growth kinetia in suspension, CHEM, 1987. **26**.
24. Neumann, A.M., *Characterizing industrial crystallizers of different scale and type*. 2001: TU Delft, Delft University of Technology.
25. Nowee, S.M., A. Abbas, and J.A. Romagnoli, *Optimization in seeded cooling crystallization: A parameter estimation and dynamic optimization study.* Chemical Engineering and Processing: Process Intensification, 2007. **46**(11): p. 1096-1106.
26. Nagy, Z.K., et al., *Determination of the kinetic parameters for the crystallization of paracetamol from water using metastable zone width experiments.* Industrial & Engineering Chemistry Research, 2008. **47**(4): p. 1245-1252.
27. Ploß, R. and A. Mersmann, *A new model of the effect of stirring intensity on the rate of secondary nucleation.* Chemical engineering & technology, 1989. **12**(1): p. 137-146.
28. Botsaris, G.D., *Secondary nucleation—a review*, in *Industrial crystallization*. 1976, Springer. p. 3-22.
29. Vetter, T., et al., *Modeling nucleation, growth, and Ostwald ripening in crystallization processes: a comparison between population balance and kinetic rate equation.* Crystal Growth & Design, 2013. **13**(11): p. 4890-4905.
30. Cao, Y., V. Kariwala, and Z.K. Nagy. *Parameter Estimation for Crystallization Processes using Taylor Method*. in *Advanced Control of Chemical Processes*. 2012.
31. Lieb, A. and M. Kind, *Determination of the attrition behaviour of ammonium sulphate and of pentaerythritol crystals using a Forced Circulation Crystalliser.* Powder technology, 2004. **143**: p. 273-279.
32. Kalbasenka, A., A. Huesman, and H. Kramer, *Modeling batch crystallization processes: Assumption verification and improvement of the parameter estimation quality through empirical experiment design.* Chemical engineering science, 2011. **66**(20): p. 4867-4877.
33. Gahn, C. and A. Mersmann, *Brittle fracture in crystallization processes Part A. Attrition and abrasion of brittle solids.* Chemical Engineering Science, 1999. **54**(9): p. 1273-1282.
34. Merchuk, J. and I. Berzin, *Distribution of energy dissipation in airlift reactors.* Chemical Engineering Science, 1995. **50**(14): p. 2225-2233.
35. Gherras, N. and G. Fevotte, *On the use of process analytical technologies and population balance equations for the estimation of crystallization kinetics. A case study.* Aiche Journal, 2012. **58**(9): p. 2650-2664.

This chapter is based on the published article:

Anisi F, Mathew Thomas K, Kramer H.J.M, Membrane-assisted Crystallization: Membrane Characterization, Modelling and Experiments, Chemical Engineering Science, 158 (2017) 277-286.

Chapter 3

Membrane-assisted Crystallization: Membrane Characterization, Modelling and Experiments

ABSTRACT

A hollow fiber membrane module was assessed for its potential in assisting crystallization processes. The membrane module was characterized in the sweeping gas membrane distillation configuration considering various solution and sweeping gas flow rates, temperatures and solution concentrations. A model, coupling mass and heat transfer, was developed to predict the membrane flux. The effect of the process conditions on the membrane flux was experimentally determined and the results were used to validate the model. Feed temperature and air flow rate were found to have a significant effect on the membrane flux. Having found the optimal process conditions for membrane distillation process, batch seeded crystallization experiment were performed to confirm the potential of membrane distillation in the generation of adequate rate and level of supersaturation. Since the desired supersaturation level could be maintained in the crystallizer while seeds were growing, it is confirmed that membrane distillation can be an efficient alternative to conventional supersaturation generation processes. Finally, comparing the modelling results with experiments confirms the acceptable accuracy and predictability capability of the developed model.

3.1 INTRODUCTION

Crystallization is one of the oldest and the most widely applied separation process in the chemical and pharmaceutical industries [1]. Supersaturation is the driving force for the crystallization. Generation of supersaturation can generally be achieved by either reducing the solubility of solution (e.g. cooling) or by removing the solvent from the solution by evaporation [2, 3]. However, evaporation in a crystallizer is limited by the area available for evaporation and the entrainment of liquid droplets in the condenser. Furthermore, it is challenging to produce thermally labile compounds by evaporative crystallization, because of the high investment cost involved in evaporating the solvent at lower temperatures [4].

A viable alternative to evaporation can be found in the desalination industry. Membranes are being widely used to substitute evaporation for obtaining the solvent (pure water) from the solution (saline water) [5-7]. Membranes can perform the similar task to concentrate a solution thereby generating supersaturation required for crystallization. Such an innovative combination of membranes and crystallization, Membrane-assisted Crystallization (MaC), has the potential to overcome the previously mentioned limitations of evaporative crystallization. MaC of several compounds has been investigated [4, 8, 9], and in a theoretical study it has been suggested that MaC can be applied to a large variety of systems [2].

Among the various membrane processes, Reverse Osmosis (RO), Osmotic Distillation (OD) and Membrane Distillation (MD) are the most commonly used processes in MaC. The high potential of MaC-RO and MaC-OD to control the generation of supersaturation and to concentrate a solution was found in the precipitation and crystallization processes [8, 10]. The potential of using MaC-RO process was investigated by optimization of final mean size with minimal energy conversion for adipic acid [4]. MaC-RO was successfully used for NH_4SO_4/water and adipic acid/water systems. It was observed that selectivity and membrane flux depend on the level of solubility and dependency of solubility on temperature [2]. In case of temperature sensitive compounds OD is most often used to remove water from liquid foods since the driving force for OD is the concentration difference and it can be operated in relatively low temperatures [11, 12].

MD is a promising alternative for compounds with high osmotic pressure. It is a thermally driven process in which the volatile components are transported across a porous hydrophobic membrane due to the difference in the vapor pressures across the membrane [7, 13]. MD gets its name from the similarity with conventional distillation process. Both processes are based on vapor-liquid equilibrium for separation and both processes require heat supplied to the feed for achieving the latent heat of vaporization [13]. It can be carried out in various configurations, out of which Direct Contact Membrane Distillation (DCMD) is the most studied and the commonly used in MaC. However, DCMD suffers from severe heat loss due to conduction across the membrane resulting in high temperature polarization.

The objective of this work is to use a relatively less studied configuration of MD, Sweeping Gas Membrane Distillation (SGMD), to generate the required supersaturation to carry out crystallization in an L-ascorbic acid (AA)/water solution system. In SGMD, an inert gas is used in the permeate side to sweep away the vapor transferred through the membrane. The use of the inert sweeping gas reduces the conductive heat loss and the mass transfer resistance [5]. SGMD remains the least studied MD configuration, as MD was primarily developed for the desalination industry, and hence would require an external condenser to condense the water vapor from the sweep gas, thus complicating the system [13]. However, this complication does not apply when the objective is to merely concentrate a solution, which means that SGMD is potentially favorable in MaC.

In order to successfully implement SGMD in MaC, a detailed study on the characterization of the membrane module has been performed considering the crucial concepts mentioned in literature [9, 14, 15]. The Liqui-Cel® Extra-Flow contactor used in this study is a transverse flow module. It has been reported that transverse flow has a larger shell side mass transfer coefficient and a more accurate performance prediction. The process fluid enters the module through a porous central tube and presence of a baffle in the middle of the fiber improves the mass transfer efficiency by providing a component of velocity normal to the membrane surfaces [16, 17].

The influence of various operating conditions (feed inlet temperature, feed flow rate and sweeping gas (air) flow rate) and the concentration of the feed on the membrane flux were investigated experimentally using this module with the novel focus for crystallization purposes. Based on the results, a feasible optimized operating conditions to carry out MaC was selected.

A model to describe the behavior of SGMD experiments is generated and validated based on experimental results. The model uses the coupling of mass and heat transfer, in combination with the free surface model for the specific geometry of the membrane module, and the resistance-in-series model in order to determine the membrane flux and to estimate temperature and concentration polarization. Such a model is an essential tool to design and optimize future application of the MaC systems.

3.2 MATERIALS AND METHOD

3.2.1 Materials

The membrane module used in this research was a Liqui-Cel® 2.5 x 8 Extra-Flow supplied by Membrana. The membrane in the module is a hydrophobic micro-porous hollow fiber membrane. Some of the membrane characteristics are shown in Table 3-1:

Table 3-1 *Membrane specifications*

Membrane Characteristics	
Material	PVDF
Module diameter, d_m, [cm]	4.5
Porous central tube diameter, d_t [cm]	0.6
Tube inside diameter, d_i [μm]	340
Tube outside diameter, d_o [μm]	420
Pore size, r, [μm]	0.04
Thickness, δ, [μm]	40
Porosity, ε	0.4
Inner fiber diameter, d_i [μm]	300
Area, A_m, [m^2]	1.4
Length, L, [m]	0.2564
Tortuosity, τ, [-]	2
Number of fibers, N	6400
Thermal conductivity, λ_{mm}, [$W/m.K^{-1}$]	0.18

According to the manufacturer recommendation temperature should not exceed 70 °C. The sweep gas was directed through the lumen side of the membrane module and the liquid feed was directed through the shell side, flowing counter current to the sweep gas (see Figure 3-1).

Distilled water solution as the feed and air as the sweeping gas were used. To investigate the effect of concentration on the membrane flux, AA/water solution was used which is the model compound also for the crystallization process.

3.2.2 Experimental Setup

The experimental setup for MaC primarily consists of a membrane unit, a buffer vessel and a crystallizer. A schematic illustration of the experimental setup is given in Figure 3-2. To prevent crystal formation and deposition on the surface of the membrane the stream fed to the membrane is heated in a separate

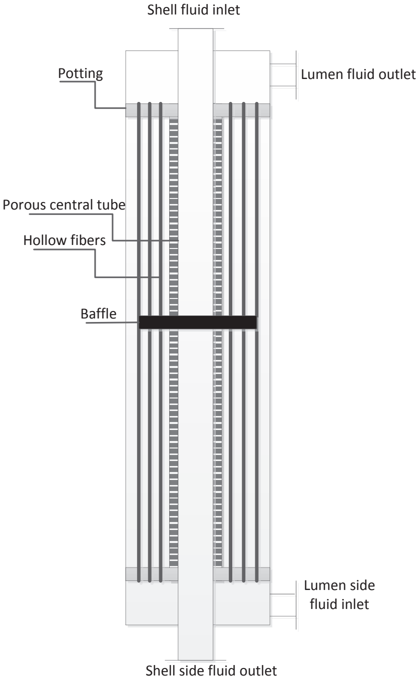

Figure 3-1 *Overview of Liqui-cel® Extra Flow module*

vessel, here referred to as the buffer vessel, until the solution is undersaturated. Since the solution oxidizes on exposure to the oxygen, nitrogen is used in blanketing to keep oxygen level low in an around the solution in the buffer vessel. In the crystallizer, which is operated at a lower temperature, supersaturation is generated by the recirculation of crystal free solution between the crystallizer and the buffer vessel in which the solution is at higher concentration due to the solvent removal by the membrane module.

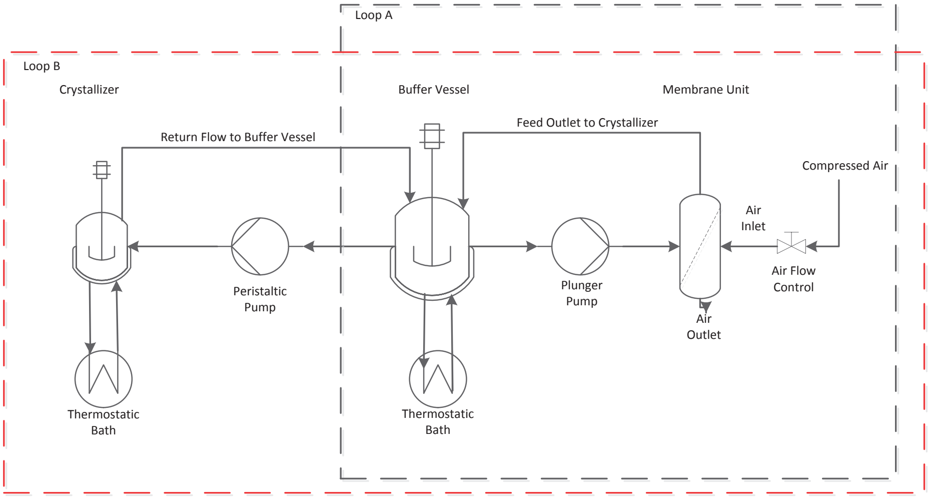
Loop A
Loop B
Crystallizer
Buffer Vessel
Membrane Unit
Return Flow to Buffer Vessel
Feed Outlet to Crystallizer
Compressed Air
Air Inlet
Air Flow Control
Peristaltic Pump
Plunger Pump
Air Outlet
Thermostatic Bath
Thermostatic Bath

Figure 3-2 *Schematic representation of MaC setup*

A stirred 1.5 L jacketed vessel was used as a crystallizer in which a funnel combined with an overflow was used to maintain a constant liquid level and a crystal free flow to the buffer vessel. The buffer vessel was a 30 L jacketed vessel in which mixing was carried out by a stirrer (Heidolph, RZR2051). The buffer vessel and tubes were jacketed and connected to a thermostatic bath (Lauda ECO RE 1050) which was connected to an external Pt-100 to control the temperature inside the vessel. The solution from the buffer vessel was pumped through the membrane module with a reciprocal pump with three plungers (Cat Pump, 5CP6221), which enabled both the pressure and the flow rates to be controlled. A peristaltic pump (Watson Marlow 323 U/D) was used between the buffer vessel and the crystallizer. A pulsation dampener (Cat Pump, 6028) was installed to minimize fluctuations in flow and pressure. A volume flow meter (KDG series, Kobold) was used to regulate and monitor the flow rate of air. A level sensor (Omega, LVCN414) was used in the buffer vessel to measure the level of the liquid in the buffer vessel which, in turn, is used to derive the MD flux. The concentration of the solution in the buffer vessel was measured online using Liquisonic concentration sensor. The velocity of sound in the solution and the temperature of the solution was obtained from the Liquisonic concentration sensor. A VBA based spreadsheet was used to obtain the concentration from the recorded data. The density of the solution was also obtained offline using a density meter (Anton Paar DMA 5000). Temperature sensors (Pt100) were used to measure the temperature of the feed inlet and outlet as well as the air inlet and outlet.

Figure 3-2 shows two loops (A and B) with individual flow rates and temperatures. Loop A connects the buffer vessel with the membrane module and in loop B exchange of crystal free liquid between the crystallizer and the buffer vessel is added.

Using this setup, firstly, characterization of membrane performance was conducted within loop A with pure water. Once the optimized process conditions attained, MaC-MD experiments considering loop B were carried out with AA/water solution to show the potential of MD to assist the crystallization processes in generation of the supersaturation.

3.3 PROCESS MODEL

MD is a membrane separation process requiring a driving force to establish the necessary transmembrane chemical potential or partial vapor pressure difference. Theoretical models have been developed for various membrane modules and configurations [8, 13, 18, 19]. The prevailing intention of all is to predict the values of the membrane flux and its dependence on membrane module design and configuration, membrane properties and process conditions.

SGMD involves evaporation of a volatile compound (water here) at the hot feed side, transport of the vapor through the pores of the hydrophobic membrane driven by the transmembrane vapor pressure difference, collection of the permeating vapor by an inert cold sweeping gas and finally condensation outside the membrane module [13]. Therefore, the flux through the membrane depends on the gradient in the partial vapor pressure of the water across the membrane. Noting the presence of a temperature gradient over the membrane and realizing that the flux is proportional to the partial pressure gradient across the pores, which is on its turn strongly temperature dependent, an appropriate model is required. The model needs to describe the coupled mass and heat transfer in the membrane module.

In this section the developed model for the SGMD process is described.

Initially, contribution of mass and heat transfer is described. Next, membrane flux is introduced coupling the mass and heat transfer models. Finally the approach to solve the equations is represented.

3.3.1 Heat Transfer

The heat transfer models are generally based on the correlations originally derived for heat transfer through non-porous/rigid surfaces (semi-empirical models) [20]. The heat fluxes in SGMD which are shown in Figure 3-3 consist of Q_f, Q_m, Q_v and Q_a corresponding to feed (heat transferred from the feed solution to the membrane surface across the thermally boundary layer at the feed side), membrane (heat transport by conduction across both the membrane matrix and the gas filled pores), MD flux (heat associated to the latent heat of vaporization and therefore to the mass transfer through the membrane pores) and air (heat transfer from the membrane surface to the permeate solution across the thermally boundary layer in the permeate side). Likewise, h_f, h_m, h_v and h_a are the heat transfer coefficients of feed, membrane, MD flux and sweeping gas side respectively [6, 8, 13, 19, 21, 22].

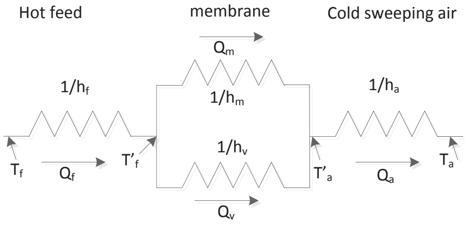

Figure 3-3 *Heat fluxes and heat transfer resistances in SGMD (redrawn from [6])*

The heat fluxes can be defined with the temperatures corresponding to them where T_f and T_a are bulk temperatures and T'_f and T'_a are the temperatures on the surface of membrane for feed and air side respectively. It is worth noting that, in steady state, the heat flux of the feed side is equal to that of the air side and they are both equal to sum of heat fluxes of membrane and MD flux.

h_f and h_a are estimated from the Nusselt numbers corresponding to feed and air side, which will be discussed later as they are dependent on the local flow and contacting conditions at the shell and lumen side. Heat transfer coefficient of membrane, h_m, can be calculated using the membrane porosity and the thermal conductivity of the membrane, the air entrapped in the pores and the membrane material [8, 13, 19, 23, 24]. And h_v which is the heat transfer coefficient corresponding to MD flux is calculated as:

$$h_v = \frac{J\Delta H_v}{T_a^{'} - T_f^{'}} \tag{3-1}$$

Where J ($kg/s.m^{-2}$) is the vapor flux through the membrane which will be defined later and ΔH_v (kJ/kg) is the heat of vaporization of water, which can be described as:

$$\Delta H_v = (1.7535 T_f + 2024.3) \tag{3-2}$$

Figure 3-3 shows the resistance-in-series model. With the help of this model the fluid and the total heat transfer coefficients, h_{fluid} and h_{tot}, are calculated [7, 19].

The temperatures at the feed-membrane and membrane-permeate interfaces can be determined as [13]:

$$T'_f = \frac{h_m\,[\,T_a + \frac{h_f}{h_a}\,T_f\,] + h_f\,T_f \text{ - } J.\Delta H_v}{h_m + h_f(1 + \frac{h_m}{h_f})}\;,\; T'_f = \frac{h_m\,[\,T_f + \frac{h_a}{h_f}\,T_a\,] + h_a\,T_a \text{ - } J.\Delta H_v}{h_m + h_a\,(1 + \frac{h_m}{h_a})} \tag{3-3}$$

3.3.2 Mass transfer

The mass transfer models are based on the dusty gas model [25, 26], in which the transmembrane flux can take place via both contribution of Knudsen flow (Equation 3-4) and molecular diffusion flow (Equation 3-5) in series [5-7, 22, 23, 27-39]. Knudsen and ordinary molecular diffusion, D_{kn} and D_{mol} (m^2/s), can be described as:

$$D_{kn} = \frac{2r}{3}\left(\frac{8RT}{\pi m_w}\right)^{1/2} \tag{3-4}$$

$$D_{mol} = \frac{0.926}{10^3 P}\left(\frac{T^{2.25}}{T + 245}\right) \tag{3-5}$$

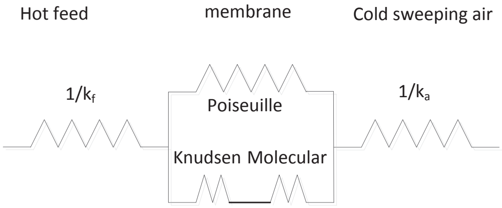

Figure 3-4 *Resistances to transmembrane mass transport of water vapor in SGMD. (based on drawing from [13])*

Where *R*, *P*, m_w and *T* are the gas constant (8.314 J/ K. mol^{-1}), the total local pressure (Pa), the molecular mass of water (18 kg/mol) and the temperature (K) respectively [35]. Since the membrane pore size is relatively small, molecule-pore collisions are dominant over molecule-molecule collisions and hence a Poiseuille type of flow can be neglected.

Combined Knudsen/ordinary molecular diffusion can be introduced as D_{mem} (m^2/s) with the help of resistance-in-series model [5-7, 22, 23, 27-39].

The resistance-in-series model can be applied to the mass transfer coefficients as well. (see Figure 3-4) The total mass transfer coefficient, k_{tot} (m^2/s), can be defined as [34, 36]:

$$k_{tot} = \left(\frac{1}{k_{mem}} + \frac{1}{k_a}\right)^{-1} \tag{3-6}$$

Where $1/k_{mem}$ and $1/k_a$ (m/s) are resistances of water vapor transport through the membrane (based on Knudsen and molecular diffusion) and in the air side boundary layer respectively. Since the solution is in direct contact with the membrane, the resistance in the boundary feed layer, k_f, is considered negligible.

3.3.3 Coupling of Mass and Heat Transfer

Nusselt number, Nu, for both the shell and the lumen side can be calculated using the Chilton-Colburn analogy to couple mass and heat transfer in gas liquid systems [40].

Heat transfer coefficients for feed and sweeping gas side can be calculated using Nu number and hydraulic diameter, d_h:

$$h=\frac{\lambda Nu}{d_h} \tag{3-7}$$

Where λ is the thermal conductivity. Based on indicated heat and mass transfer models and the coupling a flux equation can be developed, *J* (kg/s.m^{-2}) which depicts the mass transport of water vapor through the membrane:

$$J=\frac{m_w}{RT}k_{tot}(P'_{v,f}-P_{v,a}) \tag{3-8}$$

Where $P'_{v,f}$ is the vapor partial pressure in the pores on the surface of the membrane for the feed side. It is assumed that the vapor partial pressure changes on the surface and in the bulk for the permeate side is negligible. Therefore, $P_{v,a}$ (Pa) is the vapor partial pressure of the permeate side.

Assuming phase equilibrium at the vapor-liquid interface, the vapor pressure in the pores at the feed side of the membrane, $P'_{v,f}$, is directly determined by the temperature and composition of the liquid at the vapor-liquid interface.

The vapor partial pressure of pure water, $P^0_{v,f}$, on the feed side can be determined from the temperature of the feed on the membrane surface, T'_f (K), using Antoine equation [21]:

$$P^0_{v,f}=exp\left(A_{ant}-\frac{B_{ant}}{T'_f+C_{ant}}\right) \tag{3-9}$$

To calculate the partial pressure of water in a solution, $P'_{v,f}$ has to be corrected for the presence of the dissolved solute at the interface which will lower the activity. For many solutions of dissolved salts in water it has been shown that the activity can be represented by a polynomial expression in the non-volatile solute mole fraction on the membrane interphase, x'_s [27, 41]:

$$P'_{v,f}=P^0_{v,f}a_w \tag{3-10}$$

$$a_w=1-\sum C_i x'^{i}_s \tag{3-11}$$

Where a_w is the water activity coefficient and C_i are the polynomial coefficients given for the solute and x'_s is calculated as [13]:

$$\frac{x'_s}{x_s} = exp\,(\frac{J}{k_s \rho_f}) \qquad (3\text{-}12)$$

Where x_s is the solute mole fraction in the bulk and k_s is the solute mass transfer coefficient for the diffusive mass transfer through the boundary layer which can be calculated from the Sherwood number in the feed side.

The partial pressure of water vapor on the lumen side, $P_{v,a}$, can be written as a function of the total pressure on the lumen side, P (Pa), and the humidity ratio, ω [5]:

$$P_{v,a} = \frac{\omega P}{\omega + 0.622} \qquad (3\text{-}13)$$

3.3.4 Calculation Algorithm: Segmentation

Up to now the membrane module was taken into account as a single section considering a mean temperature and pressure. However, temperature and pressure variations along the module length must be taken into account for a better understanding of membrane flux behavior [23, 33, 42]. Correspondingly, a step-wise mass and heat transfer calculations was used in this study. The module length, L, was divided into a finite number of elements. Each of these segments were assumed to have uniform properties. A number of grid points, i, was used for discretization of the module length.

The membrane flux, J, accordingly, was calculated in each grid point based on feed and sweeping gas flowrates, ϕ, humidity, ω, density, ρ, heat and mass transfer coefficients in each segment for both sides of the membrane. Since feed and air are flowing counter current to each other, the single segment mass and energy balances are driven by its previous segment.

In order to calculate the flow rates and temperatures the geometry of the membrane should be defined properly. Depending on the fluids flow directions co-, counter-, and cross-flow configurations different flow vectors are considered. In plate and frame membranes different adaptation of heat and mass transfer models are considered compared to hollow fiber membranes [7, 23, 30, 31].

Liqui-cel® Extra flow membrane module is a transverse flow module. One fluid go through the fibers which are bundled in a regular arrangement. The other fluid enters the porous central tube and is distributed radially and axially along the shell side of the module. In the following shell and lumen side are specified:

3.3.4.1 Lumen Side

For the lumen side the hydraulic diameter is the inner tube diameter, d_i, and the Sherwood number for the lumen side, Sh_a, in a hollow fiber membrane module can be defined as [31, 43, 44]:

$$Sh_a = 1.62\ (\frac{d_i^2 u_a}{LD_{mol}})^{\frac{1}{3}} \qquad (3\text{-}14)$$

Where u is the linear velocity inside the fiber which is calculated as a function of sweeping gas volumetric flowrate respectively.

Using equation 3-14 the contribution of water transport resistances in the air side, k_a, in Equation 3-15 can be calculated as:

$$k_a = \frac{Sh_a D_{mol}}{d_i} \qquad (3\text{-}15)$$

Accordingly, the membrane mass transfer coefficient, k_{mem}, can be defined according to the geometry of the membrane which is a hollow fiber one as:

$$k_{mem} = \frac{2\tau D_{mem}}{\varepsilon d_i ln(\frac{d_o}{d_i})} \qquad (3\text{-}16)$$

3.3.4.2 Shell Side

Since the flow in the shell side is distributed radially through porous central tube, the geometry of the shell side is defined through adaptation of free surface model [14]. (see Figure 3-5)

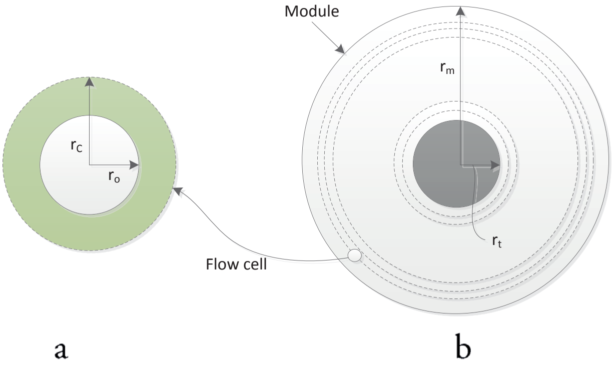

Figure 3-5 *Schematic representation of applying free surface model, a) for a fiber, and b) for a module with free surface (redrawn from [30])*

In this model fibers are regularly arranged in layers between the central tube and the wall of the module. Hence the packing fraction, ϵ_p, is defined as [14, 30, 45-47]:

$$\epsilon_p = \frac{Nd_o^2}{d_m^2 - d_t^2} \qquad (3\text{-}17)$$

Where d_o, d_m, d_t and N are fiber outer diameter, module diameter, central tube diameter and number of the fibers in the module respectively. The cell diameter, d_c, assuming that the cell and the module have the same packing fraction is defined as:

$$d_c = \frac{d_o}{\sqrt{\epsilon_p}} \tag{3-18}$$

Since the feed (liquid) flows through the central tube and is distributed into the shell, the velocity has an extra component normal to the flow direction. In order to calculate the effective shell side velocity, u_e, firstly, the average cell free surface velocity is calculated as a function of shell side volumetric flow rate, ϕ_f (m^3/s). The method proposed by Zeng et al was applied to obtain the expression for average effective velocity [30]:

$$u_e = \frac{Ln\epsilon_p}{4\,(\sqrt{\epsilon_p}-1)} \; \frac{ln\dfrac{2d_m-d_c}{2d_t+d_c}}{(d_m-d_t-d_c)} \; \frac{\varphi_f}{\pi\,(L/2)} \tag{3-19}$$

In Equation 3-19 it is assumed that the feed flow rate ϕ_f is constant through the module and u_e is the average velocity of the feed considering the radial distribution.

For mass and heat transfer calculations the hydraulic diameter for the shell side can be defined as [30]:

$$d_{h,f} = \frac{d_c^2 - d_o^2}{d_o} = \frac{1-\epsilon_p}{\epsilon_p}\, d_o \tag{3-20}$$

According to the investigation and comparison of different relationships for Sherwood number, Sh_f, when liquid flows in the shell side the following relationship was used [30]:

$$Sh_f = 2.15 Re_f^{0.42} Sc_f^{0.33} \tag{3-21}$$

Where Re_f and Sc_f are Reynolds and Schmidt numbers respectively. Re_f and Sc_f can be calculated applying the average effective velocity in equation 3-19 and the properties of the liquid.

3.3.4.3 Temperature Changes

Since temperature changes on the feed side is not large, a linear profile for feed temperature was considered. Air pressure changes inside the module was also considered as linear. But for the air temperature a relationship based on heat of vaporization of water, $\Delta H_{v,}$ driven from energy balance equation in a hot water chamber was applied which was solved analytically [6, 20]:

$$T_a = T_f - ((T_{f,out} - T_{a,in} - \frac{T_{f,out} - T_{f,in}}{L\alpha}) \times exp\left[\alpha(1-x)\right] - \frac{T_{f,out} - T_{f,in}}{L\alpha} \tag{3-22}$$

$$\alpha = \left\{\left[h_{tot} - \frac{k_m}{\delta}\left(1 - \frac{h_{tot}}{h_{fluids}}\right)\right]\frac{\Delta H_v^0}{\Delta H_v} - h_{tot}\right\}\frac{d_i}{\varphi_a \rho_a C_{ha}} \tag{3-23}$$

Where C_{ha} is the specific heat of humid air, ϕ_a is the air flow rate and $\Delta H_v{}^0$ is the heat of vaporization of water at temperature 0 °C. T_a and T_f are the air and feed bulk temperatures in location x which is defined for number of grids, i, as:

$$x(i) = (i-1)\,\frac{L}{number\ of\ grids} \tag{3-24}$$

$T_{a,in}$, $T_{f,in}$, $T_{a,out}$ and $T_{f,out}$ are air and feed inlet and outlet temperatures respectively. Inlet and outlet pressures were assigned and a linear profile for pressure changes was considered. Initial feed concentration was also assigned.

3.4 EXPERIMENTAL PROCEDURE

3.4.1 Characterization of the Membrane Performance

Initially, experiments were carried out to evaluate the dependence of MD flux on the various operating conditions. The operating conditions that were varied during the experiments include the feed temperature, flow rate and concentration and sweeping gas (air) flow rate. The feed inlet temperature was varied between 30 °C and 60 °C to study the influence on the MD flux. Similarly, feed and air flow rate were varied between 276 L/hr to 552 L/hr and 1900 L/hr to 5700 L/hr respectively. The influence of the feed concentration on the MD flux was also studied for a feed concentration in the range of between 0 kg solute/kg solvent to 0.5 kg solute/kg solvent.

The experimental process conditions are given in Table 1S in the supplementary materials. These 40 experiments were accomplished with distilled water.

The experimental process conditions for 13 experiments using concentrated solution starting with different concentrations are given in Table 2S in supplementary materials. The feed temperature and flowrate are 50 °C and 552 L/hr for all the experiments and the saturation concentration in 50 °C is 0.74 kg solute/kg solvent.

3.4.2 Membrane-assisted Crystallization

MaC experiments were performed in two steps: first, supersaturation was generated from an unsaturated solution in the crystallizer by solvent removal via the membrane. After achieving a certain level of supersaturation seeds were added which marked the start of crystallization process while the membrane unit generated the supersaturation needed for the crystallization process. Starting from an unsaturated solution (S_1), the solution was continuously circulated between the buffer vessel and the crystallizer. When the desired level of supersaturation (S_2) was reached, the crystallization was initiated by adding seed crystals. The crystallizer was maintained at 30 °C and the buffer vessel at 50 °C to ensure that the solution in the membrane module remains undersaturated throughout the experiment.

The added seed crystals were obtained by sieving AA using a 200 µm sieve (Retch AS300). The addition of seeds to the supersaturated solution would mark the beginning of the crystallization process (growth of seeds). The flow rate from the buffer vessel to the crystallizer (ϕ_{bf}) was set at 6 L/hr. A perforate funnel was fixed on top of the crystallizer to avoid overflow of the crystals from the crystallizer to the buffer vessel. An overflow is present above the funnel through which the crystal-free solution flows into the buffer vessel through a tube. The experimental process conditions are summarized in Table 3S in supplementary materials.

3.5 RESULTS AND DISCUSSION

3.5.1 Sweeping Gas Membrane Distillation

First, experimental results for characterization of the membrane unit with pure water are discussed and compared with literature results. Next, experimental results with a solution of AA under optimized process conditions for solvent removal by the membrane module are presented. In all cases the results from the model using the same process conditions are compared with the experimental results. In the figures, the symbols represent the experimental results while the lines are modelling results for the same experiment. Finally the accuracy of the model regarding membrane flux calculation is discussed.

3.5.1.1 Membrane Characterization (Effect of Process Conditions on Membrane Flux)

3.5.1.1.1 Effect of Feed Temperature

The feed temperature has been varied from 30 °C to 60 °C. Figure 3-6 shows that the MD flux has an exponential dependence on the feed inlet temperature which is due to the exponential increase of vapor pressure of the feed solution with temperature which increases the transmembrane vapor pressure difference and consequently the flux. A similar dependence of MD flux on feed inlet temperature can be found in literature [5, 7, 23, 31, 34, 36, 48, 49]. At high feed temperature evaporation is inevitable and additionally, a pressure drop was reported for tangential flow membrane when increasing feed temperature [33]. These effects were reported for temperatures higher than 50 °C.

It can be observed from Figure 3-6 that the effect of the feed temperature is stronger in case of higher air flow rates. A possible reason is that the higher air flow rates prevent higher vapor pressures at the permeate side of the membrane.

From Figure 3-6 it can be observed that results from the model are in good agreement with the experimental results which means the model is capable to describe the influence of feed temperature for different feed and air flow rates on the membrane flux.

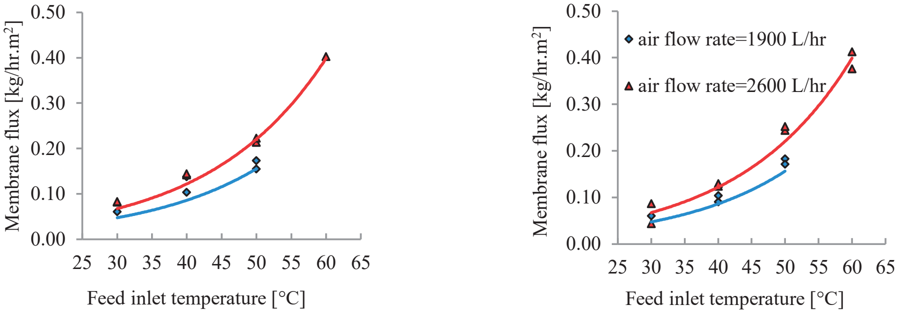

a b

Figure 3-6 *Effect of feed temperature on membrane flux for two different air flow rates. The feed flow rate was a) 276 L/hr and b) 552 L/hr (markers represent the experimental value and lines are the modelling results)*

3.5.1.1.2 Effect of Feed Flow Rate

The influence of the feed flow rate on the MD flux was studied over a wide range of feed temperatures and air flow rates. The results from the experiments showed that feed flow rate had negligible effect on the MD flux. Similar trends were reported in the literature [5, 7, 23, 34, 36, 48].

The feed flow rate is known to have a direct effect on the temperature polarization. The increase in the feed flow rate leads to a reduction of the boundary layer thickness along the membrane and thereby reducing the difference between the feed and air temperatures at the membrane surface and the bulk (Temperature Polarization). However, the temperature polarization on the feed side of the membrane is already close to unity, hence, the increase in feed flow rate will have a very low (almost negligible) influence on the MD flux. The slight or negligible increase of the MD flux due to change of feed flow rate has also been reported in the literature [5-7, 50].

3.5.1.1.3 Effect of Air Flow Rate

It can be observed from Figure 3-7 that the sweep gas (air) volume flow rate has strong linear influence on the MD flux. The positive influence of the air flow rate on the MD flux is also seen in the literature for SGMD [5-7, 23, 36, 48]. The increase in the air flow rate has two effects. The first effect is the increase in the water vapor capacity of air. With an increase in the flow rate of air it can carry along a larger amount of water vapor. The second effect is the decrease in the thickness of the boundary layer adjoining the membrane on the sweep gas side which decreases the resistance for both heat and mass transfer. As the heat transfer coefficient in the permeate side increases, the temperature at the membrane surface approaches the temperature in the bulk and consequently the driving force as well as the permeate flux increases slightly [33].

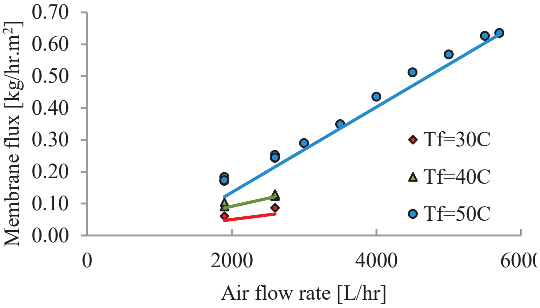

Figure 3-7 *Effect of air flow rate on membrane flux in different feed temperatures and feed flow rate of 552 L/hr (markers represent the experimental value and lines are the modelling results)*

3.5.1.1.4 Effect of Feed Concentration

It can be observed from Figure 3-8 that the MD flux decreases only slightly with the increase in the concentration of AA in the solution. The decrease in flux is approximately linear with the solute concentration and similar trends can be seen in literature [5].

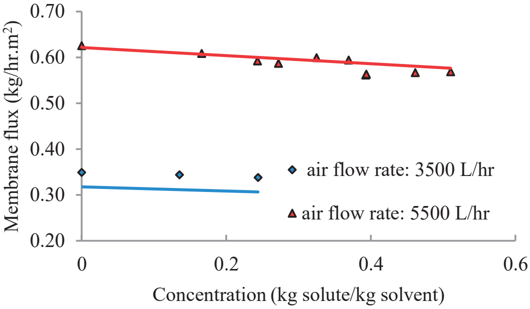

Figure 3-8 *Effect of concentration on membrane flux in different air flow rates (markers represent the experimental value and lines are the modelling results)*

The increase in the concentration of non-volatile solute in the solution, in this case AA in water, has effect on reduction of water vapor partial pressure on the feed side of the membrane due to the presence of AA molecules in the feed solution. This in turn leads to a reduced driving force [13, 27].

It must be noted that the decrease in MD flux depends on the mole fraction of AA in the solution. In Figure 3-8, concentration has been reported as the mass of solute per unit mass of solvent. The molar mass of AA is high (176.12 g/mol), hence the solution is very dilute in terms of mole fraction of AA (a concentration of 0.5 kg solute/kg solvent is equivalent to 0.0486 moles of solute per mole of solution). This is the reason for having only a small reduction in the MD flux.

Furthermore the SGMD flux is in agreement with the reported fluxes in literature for the similar process conditions [18, 30, 31, 51]. However, since the most frequent application of membrane distillation is in desalination and waste water treatment processes, process conditions and membrane module requirements are mainly different from the intended application in this study. Therefore, higher membrane fluxes are generally reported using membranes with pore diameter of approximately 10 times larger and double porosity than Liqui-Cel® Extra flow [7, 13, 52, 53].

It is worth mentioning that although no specific study has been done about the long term performance of this module, it has been used for MD and MaC purposes for over two years with more than 300 hours of operation within the process conditions recommended by the supplier and no fouling/wetting have been detected.

3.5.1.2 Crystallization

The results of the membrane characterization revealed that only the feed temperature and air flow rate have strong influence on the MD flux. The higher the feed temperature the higher the membrane flux. Some studies reported an increased effect of temperature polarization and a drop in selectivity operating in high feed temperatures [27, 29, 54]. However, based on manufacturer recommendation for the Liqui-cel® Extra flow membrane module the temperature should not exceed 70 °C and besides that, AA is a heat sensitive compound. It was observed that oxidation rate increases in temperatures higher than 50 °C despite de-aerating the vessel with a nitrogen stream. Therefore, feed temperature of 50 °C was chosen as the optimized feed temperature. To control the rate and level of supersaturation generation air flow rate can be altered which immediately affect the membrane flux. Therefore, crystallization experiments have been designed to integrate the crystallization with membrane unit. In all the experiments the solution is undersaturated at the beginning and once the sufficient level of supersaturation (as was aimed in Table 3S) is achieved in the crystallizer (the end point of first part of the discontinuous lines in Figure 3-9) seeds are applied which marks the start of crystallization in the crystallizer. In Figure 3-9 the concentration trend in the buffer vessel can be seen. The less steeper slope in the second part shows the consumption of supersaturation by the crystals in the crystallizer. Figure 3-9 shows the concentration change in two phases of the experiments (generating the supersaturation followed by crystallization process). The lines which belong to the modelling results predict the concentration change in the first part relatively perfect but it lacks the perfect prediction when crystallization process starts (second part). The reason is probably the unknown rate of supersaturation consumption by the seed crystals. Nevertheless, the level of supersaturation provided by membrane unit in all experiments remains in the supersaturated region which confirms the potential of membrane distillation technology to operate as an assistant for crystallization processes in providing supersaturation.

Since the production rate is not measured, only the overall yield (percent), being the ratio between the actual yield to that of the theoretical yield, for crystallization experiment 1 was found out to be 27 %. The low yield in this study is the result of using a buffer vessel considerably larger than the crystallizer. This resulted in a large volume of unavailable concentrated solutions being stored in the buffer vessel resulting in a low yield for the MaC process. However, for industrial applications, the buffer vessel can be considerably smaller (or even avoided), resulting in a much higher yield.

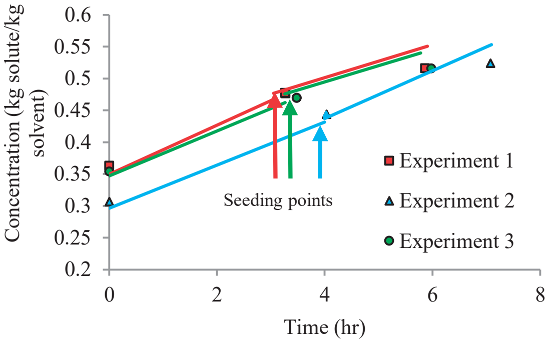

Figure 3-9 *Generation of supersaturation in a crystallization process (markers represent the experimental value and lines are the modelling results)*

3.5.2 Model Accuracy

In order to check the accuracy of the model compared to experimental results, membrane fluxes resulted from experiments and model considering all the experimental conditions listed in Table 1S and S2 are plotted. The results can be seen in Figure 3-10. The result implies that the predicted values are in reasonable agreement with the experimental data and consequently confirms the acceptable predication capability of the developed model.

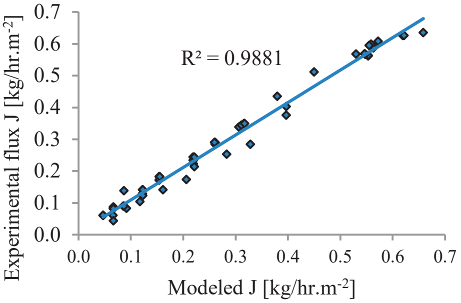

Figure 3-10 *Comparison of predicted and experimental membrane fluxes (markers represent the experimental value and line are the modelling results)*

3.6 CONCLUSIONS

In this study the feasibility of membrane-assisted crystallization using membrane distillation was investigated. The results show that sweeping gas membrane distillation (SGMD) can successfully be applied for compounds with high osmotic pressures and allows for crystallization at low temperatures and forms an attractive alternative for evaporative crystallization. The application of MaC-SGMD enhances the application field for membrane assisted crystallization considerably [2].

A Liqui-Cel® Extra flow membrane module was used in this study to concentrate a solution of AA in water with the aim of supersaturation generation for crystallization processes. Characterization of this membrane module was done altering the process conditions, feed flow rate, temperature, concentration and air flow rate. A model coupling mass and heat transfer was developed to predict the membrane flux and to investigate the temperature and concentration polarization. To define the shell flow behavior a free surface model [30] was adapted to resemble the transverse flow properly. To consider temperature and pressure changes along the length of membrane module, a step-wise mass and heat transfer model was developed. The results show that the model is capable of predicting the flux to an acceptable extent. Having the membrane module characterized and optimized crystallization processes were operated in order to confirm the potential of membrane unit to provide sufficient rate and amount of supersaturation. According to the characterization experiments it has been found that it is straightforward to manipulate the rate of solvent removal by means of changing process conditions. Feed temperature and air flow rate have been found as controlling parameters. Air flow rate has been found as the best parameter for this manipulation since it influences the flux promptly.

The accuracy of the model was tested considering the experiments with distilled water and the experiments with AA/water solution. Since the predicted membrane flux is in accordance with the results from the experiments, the model can be used for further MaC investigations.

Questions that are necessary to be answered are related to the scale up of the process. The characterization of the membrane module presented in this study can be used to design further experiments with larger crystallizers. Moreover, if the rate and level of supersaturation generation can be controlled in MaC-MD, it could enhance the crystal quality.

3.7 REFERENCES

1. Drioli, E., G. Di Profio, and E. Curcio, *Progress in membrane crystallization.* Current opinion in chemical engineering, 2012. **1**(2): p. 178-182.
2. Lakerveld, R., et al., *Membrane assisted crystallization using reverse osmosis: Influence of solubility characteristics on experimental application and energy saving potential.* Chemical engineering science, 2010. **65**(9): p. 2689-2699.
3. Curcio, E., A. Criscuoli, and E. Drioli, *Membrane crystallizers.* Industrial & engineering chemistry research, 2001. **40**(12): p. 2679-2684.
4. Kuhn, J., et al., *Characterization and dynamic optimization of membrane-assisted crystallization of adipic acid.* Industrial & engineering chemistry research, 2009. **48**(11): p. 5360-5369.
5. Khayet, M., M. Godino, and J. Mengual, *Theoretical and experimental studies on desalination using the sweeping gas membrane distillation method.* Desalination, 2003. **157**(1): p. 297-305.
6. Khayet, M., P. Godino, and J.I. Mengual, *Theory and experiments on sweeping gas membrane distillation.* Journal of membrane Science, 2000. **165**(2): p. 261-272.
7. Khayet, M., P. Godino, and J.I. Mengual, *Nature of flow on sweeping gas membrane distillation.* Journal of membrane science, 2000. **170**(2): p. 243-255.
8. Curcio, E. and E. Drioli, *Membrane distillation and related operations—a review.* Separation and Purification Reviews, 2005. **34**(1): p. 35-86.
9. Gryta, M., *Concentration of NaCl solution by membrane distillation integrated with crystallization.* Separation science and technology, 2002. **37**(15): p. 3535-3558.
10. Azoury, R., J. Garside, and W. Robertson, *Habit modifiers of calcium oxalate crystals precipitated in a reverse osmosis system.* Journal of crystal growth, 1986. **76**(2): p. 259-262.
11. Gryta, M., *Osmotic MD and other membrane distillation variants.* Journal of membrane science, 2005. **246**(2): p. 145-156.
12. Warczok, J., et al., *Application of osmotic membrane distillation for reconcentration of sugar solutions from osmotic dehydration.* Separation and Purification Technology, 2007. **57**(3): p. 425-429.
13. Souhaimi, M.K. and T. Matsuura, *Membrane distillation: principles and applications*. 2011: Elsevier.
14. Sengupta, A., et al., *Large-scale application of membrane contactors for gas transfer from or to ultrapure water.* Separation and purification technology, 1998. **14**(1): p. 189-200.
15. Wickramasinghe, S., M.J. Semmens, and E. Cussler, *Mass transfer in various hollow fiber geometries.* Journal of Membrane Science, 1992. **69**(3): p. 235-250.
16. Al Obaidani, S., et al., *The role of membrane distillation/crystallization technologies in the integrated membrane system for seawater desalination.* Desalination and Water Treatment, 2009. **10**(1-3): p. 210-219.
17. Ji, X., et al., *Membrane distillation-crystallization of seawater reverse osmosis brines.* Separation and Purification Technology, 2010. **71**(1): p. 76-82.
18. Khayet, M., *Membranes and theoretical modeling of membrane distillation: A review.* Advances in colloid and interface science, 2011. **164**(1): p. 56-88.
19. Alkhudhiri, A., N. Darwish, and N. Hilal, *Membrane distillation: A comprehensive review.* Desalination, 2012. **287**: p. 2-18.
20. Incropera, F. and D. DeWitt, *Introduction to heat transfer.* 1985.
21. Gryta, M. and M. Tomaszewska, *Heat transport in the membrane distillation process.* Journal of membrane science, 1998. **144**(1): p. 211-222.

22. Schofield, R., A. Fane, and C. Fell, *Heat and mass transfer in membrane distillation.* Journal of membrane Science, 1987. **33**(3): p. 299-313.
23. Khayet, M., M. Godino, and J. Mengual, *Thermal boundary layers in sweeping gas membrane distillation processes.* American Institute of Chemical Engineers. AIChE Journal, 2002. **48**(7): p. 1488.
24. Onsekizoglu, P., *Membrane Distillation: Principle, Advances, Limitations and Future Prospects in Food Industry*. 2012: INTECH Open Access Publisher.
25. Webb, S.W., *Gas-phase diffusion in porous media: Evaluation of an advective-dispersive formulation and the dusty-gas model including comparison to data for binary mixtures*. 1996: Sandia National Laboratories.
26. Ho, C.K. and S.W. Webb, *Gas transport in porous media*. Vol. 20. 2006: Springer.
27. Lawson, K.W. and D.R. Lloyd, *Membrane distillation.* Journal of membrane Science, 1997. **124**(1): p. 1-25.
28. Phattaranawik, J., R. Jiraratananon, and A. Fane, *Heat transport and membrane distillation coefficients in direct contact membrane distillation.* Journal of Membrane Science, 2003. **212**(1): p. 177-193.
29. Rivier, C., et al., *Separation of binary mixtures by thermostatic sweeping gas membrane distillation: I. Theory and simulations.* Journal of membrane science, 2002. **201**(1): p. 1-16.
30. Zheng, J.-M., et al., *Shell side mass transfer in a transverse flow hollow fiber membrane contactor.* Journal of membrane science, 2005. **261**(1): p. 114-120.
31. Karanikola, V., et al., *Sweeping gas membrane distillation: numerical simulation of mass and heat transfer in a hollow fiber membrane module.* Journal of Membrane Science, 2015. **483**: p. 15-24.
32. Martínez-Díez, L. and M.I. Vazquez-Gonzalez, *Temperature and concentration polarization in membrane distillation of aqueous salt solutions.* Journal of membrane science, 1999. **156**(2): p. 265-273.
33. El-Bourawi, M., et al., *A framework for better understanding membrane distillation separation process.* Journal of membrane science, 2006. **285**(1): p. 4-29.
34. Basini, L., et al., *A desalination process through sweeping gas membrane distillation.* Desalination, 1987. **64**: p. 245-257.
35. Mahmud, H., et al., *A study of mass transfer in the membrane air-stripping process using microporous polyproplylene hollow fibers.* Journal of Membrane Science, 2000. **179**(1): p. 29-41.
36. Boi, C., S. Bandini, and G.C. Sarti, *Pollutants removal from wastewaters through membrane distillation.* Desalination, 2005. **183**(1): p. 383-394.
37. Sherwood, T.K. and R.L. Pigford, *Absorption and extraction*. Vol. 66. 1952: McGraw-Hill New York.
38. El Diasty, R., P. Fazio, and I. Budaiwi, *The dynamic modelling of air humidity behaviour in a multi-zone space.* Building and Environment, 1993. **28**(1): p. 33-51.
39. Zhang, L.-Z. and S.-M. Huang, *Coupled heat and mass transfer in a counter flow hollow fiber membrane module for air humidification.* International Journal of Heat and Mass Transfer, 2011. **54**(5): p. 1055-1063.
40. Zhang, L.-Z., *An analytical solution to heat and mass transfer in hollow fiber membrane contactors for liquid desiccant air dehumidification.* Journal of Heat Transfer, 2011. **133**(9): p. 092001.
41. Tang, I. and H. Munkelwitz, *Water activities, densities, and refractive indices of aqueous sulfates and sodium nitrate droplets of atmospheric importance.* Journal of Geophysical Research, 1994. **99**(D9): p. 18801-18808.

42. Cath, T.Y., V.D. Adams, and A.E. Childress, *Experimental study of desalination using direct contact membrane distillation: a new approach to flux enhancement.* Journal of Membrane Science, 2004. **228**(1): p. 5-16.
43. Gabelman, A. and S.-T. Hwang, *Hollow fiber membrane contactors.* Journal of Membrane Science, 1999. **159**(1): p. 61-106.
44. Shen, S., S.E. Kentish, and G.W. Stevens, *Shell-side mass-transfer performance in hollow-fiber membrane contactors.* Solvent Extraction and Ion Exchange, 2010. **28**(6): p. 817-844.
45. Schöner, P., et al., *Mass transfer in the shell side of cross flow hollow fiber modules.* Chemical Engineering Science, 1998. **53**(13): p. 2319-2326.
46. Yang, M.C. and E. Cussler, *Designing hollow-fiber contactors.* AIChE Journal, 1986. **32**(11): p. 1910-1916.
47. Lipnizki, F. and R.W. Field, *Mass transfer performance for hollow fibre modules with shell-side axial feed flow: using an engineering approach to develop a framework.* Journal of Membrane Science, 2001. **193**(2): p. 195-208.
48. Charfi, K., M. Khayet, and M. Safi, *Numerical simulation and experimental studies on heat and mass transfer using sweeping gas membrane distillation.* Desalination, 2010. **259**(1): p. 84-96.
49. Qi, B., B. Li, and S. Wang, *Investigation of shell side heat transfer in cross-flow designed vacuum membrane distillation module.* Industrial & Engineering Chemistry Research, 2012. **51**(35): p. 11463-11472.
50. Khayet, M., C. Cojocaru, and A. Baroudi, *Modeling and optimization of sweeping gas membrane distillation.* Desalination, 2012. **287**: p. 159-166.
51. Creusen, R., et al., *Integrated membrane distillation–crystallization: process design and cost estimations for seawater treatment and fluxes of single salt solutions.* Desalination, 2013. **323**: p. 8-16.
52. Tun, C.M., et al., *Membrane distillation crystallization of concentrated salts—flux and crystal formation.* Journal of Membrane Science, 2005. **257**(1): p. 144-155.
53. García-Fernández, L. and M. Khayet, *Membranes used in Membrane Distillation: Preparation and Characterization.* 2015.
54. Banat, F.A. and J. Simandl, *Membrane distillation for dilute ethanol: separation from aqueous streams.* Journal of membrane science, 1999. **163**(2): p. 333-348.

Table S1 *Overview of membrane characterization experiments (process conditions and experimental results)*

Exp **#**	**Feed inlet T** (°C)	**Feed outlet T** (°C)	**Air inlet T** (°C)	**Air outlet T** (°C)	**Feed flow rate** (L/hr)	**Air flow rate** (L/hr)	**Duration** (hr)
1	40	39.5	20	38	276	1900	2.40
2	40	39.5	21	37	276	2600	2.90
3	30	29.5	20	28	276	1900	4.38
4	30	29.5	20.5	28.8	276	2600	3.74
5	30	29.5	19.5	27	552	1900	3.90
6	30	29.5	20	28.2	552	2600	3.68
7	40	39.5	20	36.3	552	1900	4.09
8	40	39.5	21	37	552	2600	3.87
9	50	49.5	19	45	552	1900	4.26
10	50	49.5	19.7	45	552	2600	3.97
11	50	49.3	22	47	276	1900	3.75
12	40	39.5	23	37	552	1900	6.81
13	40	39.5	23	37	276	1900	7.09
14	30	29.5	23	29	552	2600	6.58
15	40	39.5	25	38	552	2600	2.20
16	40	39.5	23	37	276	2600	7.91
17	50	49	21	47	276	2600	7.24
18	30	29.5	21	28	276	2600	3.67
19	40	39.5	20.5	37	552	2600	7.62
20	50	49.5	23	38	276	1900	7.34
21	50	49.5	24	48.5	276	2600	8.52
22	50	49.5	24	49	552	1900	7.50
23	50	49.5	23	48.5	552	2600	8.42
24	60	59.5	23	56.5	552	2600	4.53
25	50	49.5	28	47	552	2600	7.90
26	50	49.5	28	47	552	1900	6.97
27	50	49.5	27	47	276	1900	7.77
28	50	49.5	25	47	276	2600	7.65
29	50	49.5	24	47	552	3000	7.04
30	50	49.5	25	47	276	3000	7.54
31	50	49.5	25	47	414	2600	6.73
32	50	49.5	25	46.5	414	1900	7.31
33	50	49.5	25	47	552	3500	7.63
34	50	49	24	47	552	5700	4.78
35	50	49.5	24	47	552	5500	4.13
36	50	49.5	24	47	552	4500	3.07
37	50	49.5	24	47	552	5000	2.65
38	50	49.5	20	47	552	4000	4.54
39	60	58	23	56	276	2600	2.88
40	60	59	24	57	552	2600	3.31

Table S2 *Overview of membrane characterization experiments with solution of AA/water (process conditions and experimental results)*

Exp	**Concentration range**	**Feed inlet T**	**Feed outlet T**	**Air inlet T**	**Air outlet T**	**ϕ_f**	**ϕ_a**
#	Kg solute/kg solvent	(°C)	(°C)	(°C)	(°C)	L/hr	L/hr
1	0.0	50	49.5	24	47	552	3500
2	0.0	50	49.5	23	47	552	5500
3	0.135	50	49.5	25	48	552	3500
4	0.244	50	49.5	21	48	552	3500
5	0.166	50	49.5	23	47	552	5500
6	0.243	50	49.5	24	47	552	5500
7	0.272	50	49.5	20	47	552	5500
8	0.325	50	49.5	25	48	552	5500
9	0.369	50	49.5	27	48	552	5500
10	0.393	50	49.5	25	48	552	5500
11	0.394	50	49.5	30	49	552	5500
12	0.461	50	49.5	27	48	552	5500
13	0.510	50	49.5	24	48	552	5500

Table 3S *Overview of membrane-assisted crystallization experiments (process conditions and experimental results)*

S_1	**S_2**	**Feed inlet T**	**Feed outlet T**	**Air inlet T**	**Air outlet T**	**ϕ_f**	**ϕ_{bf}**	**ϕ_a for part 1**	**ϕ_f for part 2**	**Buffer vessel T**	**Crystallizer T**	**duration part 2**
[-]	[-]	(°C)	(°C)	(°C)	(°C)	[L/hr]	[L/hr]	[L/hr]	[L/hr]	[°C]	[°C]	[hr]
0.83	1.098	50	49.5	22	47	552	6	5500	3000	50	30	2.6
0.72	1.035	50	49.5	21	46	552	6	5500	3000	50	30	3.05
0.84	1.112	50	49.5	24	47	552	6	5500	3000	50	30	2.90

Chapter 4

Continuous Crystallization of L-ascorbic acid Using Airlift Crystallizer and Membrane Distillation

ABSTRACT

Research on continuous crystallization is increasingly growing due to the chemical and pharmaceutical industries turning into fully operated in continuous mode plant. This work demonstrates how an airlift crystallizer performs in a continuous cooling process and whether the kinetics estimated for batch processes in such a crystallizer are still valid for continuous processes. Next, the airlift crystallizer is integrated with a membrane distillation unit and the feasibility of using membrane distillation technology to assist crystallization process is analyzed.

The kinetic model developed for batch crystallization in the airlift crystallizer demonstrated acceptable results for the continuous process. Simulation results showed that level of supersaturation generation and seeding strategy in the crystallizer need to be optimized in order to achieve a stable process. Membrane-assisted crystallization experiments have shown the feasibility of such experiments and the good fit with the model suggests that model-based process optimization can lead to pretty in advance determined product specifications.

4.1 INTRODUCTION

Batch-wise operation of chemical processes, though still relevant to specific applications, is often replaced with continuous operation over the years. Nowadays, most chemicals are produced continuously with the exception of pharmaceutical and fine chemicals, which are still mainly manufactured batch-wise. Crystallization forms an important unit operation step in the manufacturing of pharmaceutical and chemical compounds either as an intermediate purification step or a final solid production step [1-3].

Although both batch and continuous crystallization processes can be designed to share similar process conditions and to produce same products, the process itself occurs differently and the product demonstrates different properties. Every aspect of the batch process is transient, while the content of the vessel is transformed from the initial to the end state during which the process conditions undergo certain trajectories. Difficulties to control the gradients in the trajectory of process conditions often lead to variations in the product quality between different batches [4, 5]. As the conditions inside the crystallizer are continually changing, process analysis (monitoring and control) is known as a complex issue for a batch operated processes. On the other side, a continuous crystallization process is, in general, operated in a steady state meaning that the conditions inside the crystallizer are those of the end points and are thus easier to control [6]. Although a continuous process is inflexible and cannot be easily adapted to fit different products, more consistent product quality and rate of production, lower footprint and more stable product are possible when optimized for a single product [1, 4, 7-15]. However, continuous operation suffers from the problem that it delivers a broad size distribution which is mostly not desirable. Moreover the current conventional crystallizers have problems to manipulate this size distribution. Therefore, research is increasingly directed towards design of systems where better control of the supersaturation (such as membrane-assisted systems), residence time (such as (plug) flow crystallizers) and crystallization kinetics (such as airlift crystallizer (ALC) and US induced seed generation techniques) is possible.

In this chapter membrane distillation technology and ALC are investigated in further details.

Membrane technology has attracted a lot of attention; in this regard, generating supersaturation via solvent removal by membrane and feeding the supersaturated solution to the crystallizer. Reverse osmosis (RO), osmotic distillation (OD) or membrane distillation (MD) are various types of applying membrane technology in assisting crystallization processes. In addition to assisting the crystallization process in generation of supersaturation, membranes have the potential to replace conventional energy intensive techniques such as evaporative crystallization. They can be coupled with low-grade waste and/or alternative energy sources with consequent reduction of energy costs. In several studies integration of the membrane directly with the crystallizer, however, promotes heterogeneous nucleation on the membrane surface [16-22]. On the other hand, in hybrid systems a circulating flow is generated between the crystallizer and a buffer vessel to ensure a clear undersaturated solution from the crystallizer at a higher temperature to avoid nucleation and growth on the membrane surface [21, 23-25]. Selecting proper operating conditions (temperature and flowrates) and membrane process (RO, OD or MD) are crucial to prevent undesired crystallization [16, 17, 21, 24, 26-32].

Membranes work independent from the type of the crystallizer but influence the performance of the crystallizer by minimizing the encrustation due to absence of cooling surface and they are not limited by evaporation process conditions. Moreover, they can use waste energy and therefore it makes them a more sustainable technology compared to other techniques [23, 33].

As have already mentioned, problems such as broad residence time distribution which gives rise to a broad CSD result in new types of crystallizers such as continuous tubular crystallizers in the form of plug flow crystallizers (PFCs), segment flow ones and oscillatory baffled crystallizers (OBC) [9, 13, 34, 35] or other types of crystallization processes such as membrane-assisted ones [25]. Tubular flow crystallizers are able to produce crystals of small sizes and a narrow size distribution. In such a crystallizer a long tube is required in order to achieve the desired residence time. An oscillatory baffled crystallizer (COBC) showed improved mass transfer and mixing profile [7, 9, 35-37]. However, careful characterization of the dispersed phase and influence of operating variables are required to be considered in order to effectively operate such a crystallizer.

ALCs combine the flexibility and simplicity of a stirred vessel in the absence of moving internal parts, an impeller or a slurry circulating pump, known as the main source of the secondary nucleation. The extensive knowledge and experience obtained from application of ALC in biotechnology involving reactions and salting-out of minerals [38-40] helped to perform batch seeded cooling crystallization of slow growing L-ascorbic acid (AA) in an 18 L ALC [41]. Theoretical and experimental studies have shown that secondary nucleation in an ALC can be suppressed at levels of supersaturation where in a stirred crystallizer a clear contribution of secondary nucleation is inevitable [41, 42]. This means that the design space for continuous experiments in an ALC is broader and therefore, a higher gain can be expected.

Due to the strong suppression of nucleation in the ALC seeding might be required using this type of crystallizer both for batch as well as for continuous operation. Primary nucleation at the start-up of the batch process, which requires high supersaturation levels, are not advisable in such a crystallizer. In continuous operation continuous seeding might be needed in the ALC.

As properly stated by Price, 2017, the underlying message in a continuous crystallization process is that the product size is determined by “nucleation” and “growth” linked to supersaturation level and residence time which may be manipulated by seeding strategy, classification and recycling [43]. However, design of a new crystallizer and crystallization processes requires a lot of optimization. Model development is, therefore, important to facilitate the development of these innovations. Many crystallization models have been developed for batch processes but due to complicated differences in kinetics of batch processes with continuous ones, it is not always possible to apply the same kinetic models developed for batch in a continuous process. For instance, secondary nucleation becomes essential in the last steps of a batch process whereas in a continuous process it can be effective at any moment. Suppression of secondary nucleation in the ALCprovides the advantage where one single kinetic model might be capable of describing crystallization kinetics in the ALC in the course of a batch process as well as the continuous one.

4.1.1 Chapter outline

Continuous experiments have been designed in the 18 L ALC integrated with membrane unit in order to see how the ALC performs under the continuous operation and to answer the following questions:

Normally the kinetics of batch crystallization processes differ from the ones for continuous processes since in a batch processes secondary nucleation occurs late in the process but in a continuous one it competes with the growth at any time under certain process conditions.

- Can the crystallization kinetics derived and validated in batch operated processes [42] be applied to describe the continuous process?
- Is continuous seeding required? And how should it be optimized?
- Can we perform continuous crystallization in the ALC using continuous seeding?
- Can we perform continuous membrane-assisted crystallization in an ALC?

Therefore, firstly, continuous cooling crystallization experiments are performed in the ALC. The results are compared with the simulation results from the developed kinetic model [42] to answer the first research question of this chapter.

Secondly, continuous periodically seeded crystallization of AA in an 18 L ALC assisted with the membrane module has been performed using the same membrane module as used in [25] with two possible configurations, with and without fine removal. Samples for he supersaturation level and the crystal size distribution (CSD) are collected and analysed. It should be emphasized that the continuous experiments have been performed in the same 18 L ALC and membrane unit as used in [25, 41, 42] which enables us to assume same working volume, hydrodynamics and modelling assumptions.

It is worth to mention that the experiments had limitations regarding the duration because no night shift was possible. Therefore they were only continued to maximum of 3 residence times. The objective of these experiments was, then, to give us a proof for the feasibility of the continuous experiments in the ALC integrated with membrane distillation technology.

4.2 MATERIALS AND METHODS

4.2.1 Model development

Continuous crystallization in an ALC is modelled with(out) membrane distillation to generate the supersaturation for cooling and membrane-assisted crystallization process.

A population balance equation (PBE) coupled with the kinetic expressions validated for AA in our previous study [42] is considered here. The PBE can be formulated as:

$$\frac{\partial n(L,t)V(t)}{\partial t} = - V(t)\,\frac{\partial (n(L,t).G(L,\sigma))}{\partial L} + V(t).B(L) + V(t).D(L) + \sum_j^{Ni} \varphi_{in} n_{in,j} - \sum_j^{Ni} \varphi_{out} n_{out,j} \tag{4-1}$$

Where n is the number density of the crystals, V is the volume of the crystallizer and L is the size of crystals. The left term in equation 4-1 is number rate of accumulation, the first term in the right represents the rate of number gain by crystal growth (G) and the two following terms represent production and consumption rate due to birth (B) and death (D) of crystals. The last two terms takes the crystallizer inlet and outlet flow considering the flow to membrane unit and the evaporation rate if any into account. The assumptions for this equation are as follows:

- The process is operated steady state which means no accumulation of mass occurs in the control volume.
- Vapour contains only solvent (water) and the feed stream is crystal free.
- No agglomeration and breakage
- Well-mixed volume meaning no spatial variations in temperature, concentration and the CSD
- Single-solute single-solvent system and the solid phase only contains a single pure component.
- The compartment is an open system, capable of exchanging mass and energy with its environment by means of fluxes through one or more of its surfaces.

Growth and nucleation are the two interconnected crystallization kinetic phenomena which have been extensively studied for ALC in our previous study [42]. Based on this study the Mersmann model for a combined diffusion integration mechanism, the so called two-step model, is the finally validated model for growth:

$$\frac{G(L)}{2k_d(L)} = \frac{\Delta C}{C_s} + \frac{k_d(L)}{2k_r C_s}\left(\frac{C_{sat}}{C_s}\right)^2 - \sqrt{\left(\frac{k_d(L)}{2k_r}\right)^2 \left(\frac{C_{sat}}{C_s}\right)^4 + \frac{k_d(L)}{k_r}\left(\frac{C_{sat}}{C_s}\right)^2 \frac{\Delta C}{C_s}} \tag{4-2}$$

Where C_s is molar density in solid phase and C_{sat} is molar saturation concentration. k_r is the coefficient for surface integration and k_d is mass transfer coefficient.

The secondary nucleation in the ALC was best described by a supersaturation dependent surface nucleation model which activates only when high levels of supersaturation is reached:

$$N_{SN}= K_{SN1} m_2 \frac{D_{AB}}{d_m^4} e^{(-\pi \frac{K_{SN2}}{lnS})} \tag{4-3}$$

Where S is the relative supersaturation, m_2 is the second moment equation:

$$m_2 \left[\frac{m^2}{m^3}\right] = \int_{L0}^{\infty} n(L,t) L^2 dL \tag{4-4}$$

K_{SN1} and K_{SN2} in equation 4-3 and k_r and k_d are the parameters which are estimated and calculated in our kinetic study (Table 2-5 in chapter 2) based on which other forms of secondary nucleation are negligible in an ALC.

4.2.2 Seeding

All of the experiments are seeded and the size of the final product is dictated by the initial size distribution. A mathematical expression for the initial distribution is obtained by fitting two additive log normal distributions to the volume density distribution. The five parameters, $L_{g,1}$, $L_{g,2}$, σ_1, σ_2 and F_1, in equation 4-5 are used as fitting parameters. $L_{g,iI}$ is the geometric mean (location parameter), σ_i the geometric standard deviation (spread parameter) and F_1 gives the relative weighting of the two log-normal distributions.

$$\tilde{v}_0(L) = \frac{F_1}{L} \frac{1}{ln\sigma_1\sqrt{2\pi}} exp(- \frac{ln^2\left(\frac{L}{L_{g,1}}\right)}{2ln^2\sigma_1}) + \frac{1-F_1}{L} \frac{1}{ln\sigma_2\sqrt{2\pi}} exp(- \frac{ln^2\left(\frac{L}{L_{g,2}}\right)}{2ln^2\sigma_2}) \tag{4-5}$$

And it is transformed to an initial number density with:

$$n_{seeds}\left[\frac{\#}{m^3 m}\right] = \frac{\tilde{v}_0(L)}{k_V L^3} \frac{\rho_{seeds}}{\rho_c} \tag{4-6}$$

In where ρ_{seeds} denotes the initial concentration of seeds.

Additional seeding is simulated as a function of time with the same distribution as equation 4-5.

4.2.3 CSD representation

The quantile, symbolically denoted as L_q, is defined as the crystal size for which q% of the observed volume density distribution has a size smaller than or equal to this value:

$$\frac{q}{100} = \bar{V}(L_q) \tag{4-7}$$

Where

$$\bar{V}(L) = \frac{\int_{Lmin}^{L} n(L) k_v L^3 dL}{\int_{Lmin}^{Lmax} n(L) k_v L^3 dL} \tag{4-8}$$

The CSD width is expressed as L_{90}/L_{10} and the median size is L_{50}.

To follow the previous studies, two main ideas must be taken into account: (1) multiple (in both terms of measured parameters and measurement frequency) experimental data and (2) quantification of CSD or quantiles are essential to properly study the continuous process [44] and decide if batch kinetics are still valid for the continuous process.

4.2.4 Seeding procedure

Commercial AA crystals (DSM, Universal grade) were put through sieves in a shaker machine (Retch, AS200 Basic). Depending on the experiments the desired sieve tray of 125 and 212 µm size fraction were collected with median size of 173 and 245 µm. The seeds were prepared by introducing them into a flask of 100 ml saturated solution of AA in water with the aim of removing crystalline dust. The seed slurry is then introduced to the experiment.

During all continuous experiments seed preparation was done similarly to prevent additional seeding procedure influences on the results.

4.2.5 Experimental setup

An 18 L ALC equipped with a gas disengagement zone, an image probe and temperature and pressure monitoring and control is used in this study for which the detailed design is presented in [45]. 100% nitrogen was introduced into the riser at the flowrate of 400 L/h similar to our previous batch experiments [41]. The general procedure of a continuous experiment in the ALC includes feed flowrate from the bottom of the riser, product removal from the bottom of the downcomer, an overflow from the ALC and a returning flow from the membrane to the ALC.

Monitoring and control of the crystallization processes is necessary though challenging. Therefore, during the experiments, product samples were taken at different times, quickly weighed and filtered using a vacuum filter to reduce the time for possible alteration of the sample characteristics.

After two and three residence times are passed samples are taken from top and bottom of the crystallizer, filtered, carefully washed with water, dried and prepared for CSD measurements. Characterization of CSD was performed using a laser diffraction instrument (Microtrac s3500), offline microscope images (Eclipse Ti-S Inverted Research Microscope) and the in-situ particle video microscope (PVM). Following is the description of the experimental process for continuous cooling and membrane-assisted crystallization with ALC:

4.2.6 Continuous cooling crystallization (CCC) of L-ascorbic acid

Based on the results from the batch experiments in our previous study [41] preliminary continuous cooling experiments have been designed and conducted in the ALC with the aim of finding the optimized process conditions such as seed size and load and the strategy to introduce seeds into the continuous process, the temperature and the level of supersaturation in the crystallizer. An average saturated concentration of 0.566 g/g at 40 ºC with a standard deviation of 0.00920 g/g (1.6%) and the metastable zone width of 9 degrees in the ALC were used as was measured and reported in the previous study [41]. Accordingly, the experiments have been designed in such a way to stay within the metastable zone where spontaneous, uncontrolled primary nucleation is kinetically inhibited. Figure 4-1 shows a schematic view of the continuous cooling crystallization process:

Experiments listed in Table 4-1 are performed with periodic seeding. For a residence time of 2 hours 30 minute intervals have been chosen to seed the crystallizer. T_s and T_{cr} are the saturation (feed) and crystallizer temperature. The process conditions used for these experiments are given in Table 4-1. The solubility curve made in [41] is used through these experiments.

Table 4-1 *Process conditions for continuous cooling experiments. Residence time for all experiments is 2 hours and seeds are added every 30 minutes.*

Exp #	Total duration [hr]	Feed concentration	Seed size [µm]	Seed amount per 30 min [gr]	T_s [ºC]	T_{cr} [ºC]
1C	3	0.5026	245	-	40	34
2C	2	0.4659	245	-	37	33
3C	3	0.4977	245	8	40	36
4C	6	0.5080	245	4	40	36
5C	6	0.4977	173	8	40	36
6C	6	0.5026	173	16	40	36
7C	6	0.4362	173	33	40	36

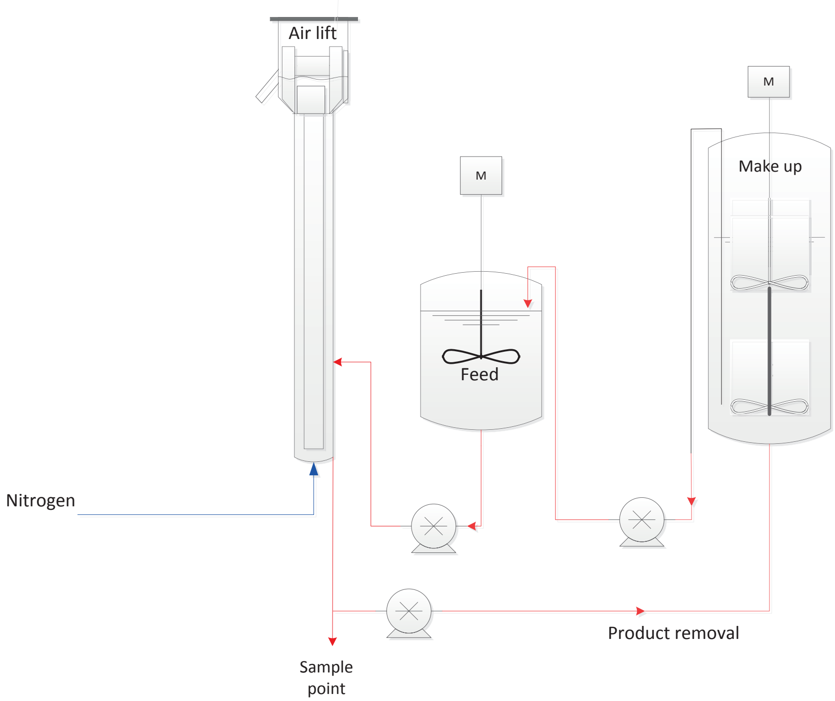

Figure 4-1 *Schematic view of the continuous cooling crystallization process*

4.2.7 Continuous membrane-assisted crystallization (CMaC) experiments with L-ascorbic acid

In a CMaC process a membrane setup is connected to the ALC. The crystallizer and the buffer system are filled with a solution saturated at 40 ºC and also the feed stream is saturated and kept at 40 ºC. The temperature of the crystallizer is chosen 2 degrees lower than saturation point. The supersaturation is generated by the membrane system. To make sure no crystallization occurs on the surface of the membrane the solution is firstly heated in the buffer vessel to become undersaturated before entering the membrane module. Two configurations have been studied to integrate the membrane system to the ALC. In configuration 1 (Figure 4-2a) feed and the product flow rates are considered the same. The residence time is kept as 2 hours. A liquid overflow is designed for the ALC feeding buffer vessel and a stream of a similar flow rate is pumped to the ALC. A baffle is installed before the overflow to prevent the large crystals leaving the crystallizer.

In configuration 2 (Figure 4-2b), the feed stream flows directly to the buffer vessel avoiding the solid liquid separation in the crystallizer and therefore the feed stream for the crystallizer is the one flowing from the buffer vessel to ALC. The feed and product flow are accordingly adjusted to maintain the 2 hours residence time. Higher initial concentration is used in the buffer vessel in order to minimize the time to reach the desired supersaturation.

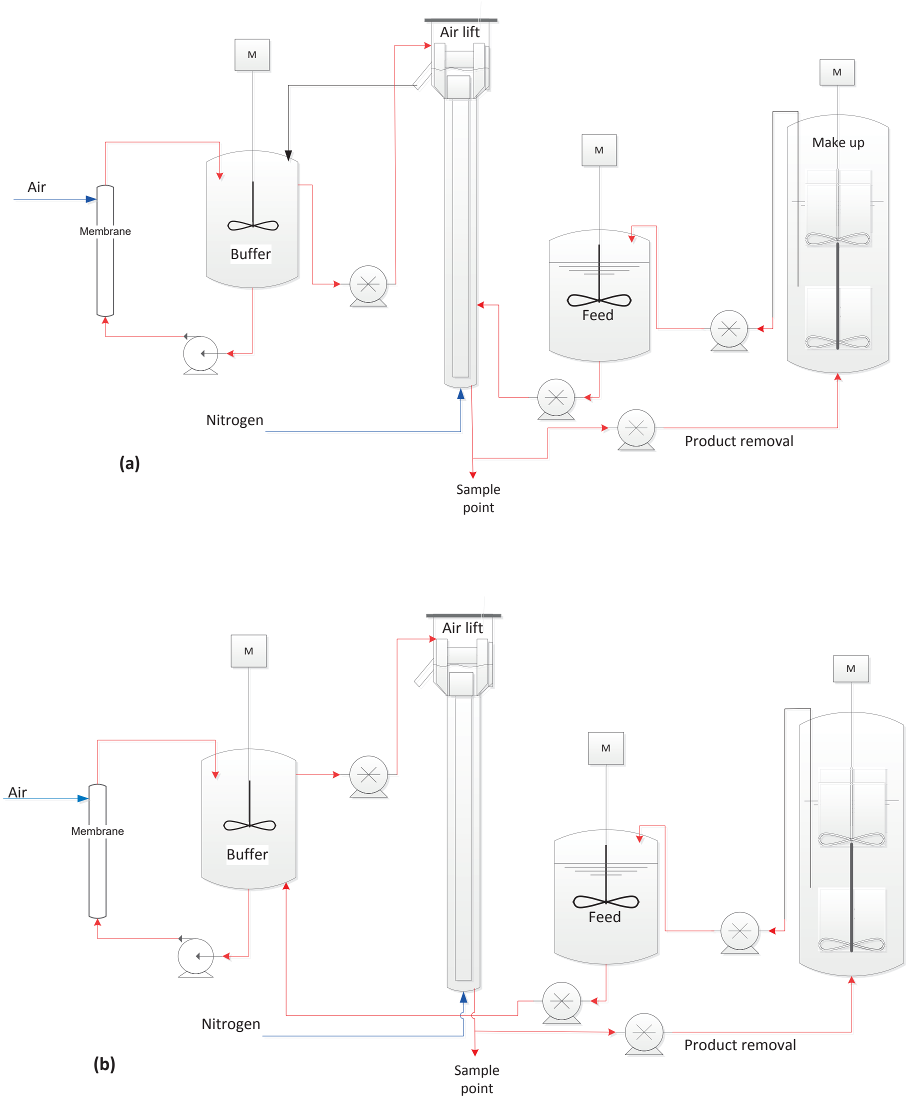
Air lift
M
M
M
Make up
Air
Membrane
Buffer
Feed
Nitrogen
Product removal
(a)
Sample point
Air lift
M
M
M
Air
Membrane
Buffer
Feed
Nitrogen
Product removal
(b)
Sample point

Figure 4-2 *Schematic view of the continuous membrane-assisted crystallization process a) configuration 1, b) configuration 2*

Based on our previous study [25] a membrane flux of 0.3 kg.m^{-2}.hr^{-1}, for which air flow rate of 3000 l/hr and buffer vessel temperature of 50 ºC is used, for the generation of the supersaturation during these processes. The products from these two configurations are analyzed and compared. Each set of experiments are performed twice to check their reproducibility. Table 4-2 shows the process conditions for these experiments.

Table 4-2 *Process conditions for CMaC experiments. Residence time for all experiments is 2 hours and 33 gr seeds of 173 µm is added every 30 minutes.*

Exp #	Conf	Duration [hr]	φ_{feed} [ml/min]	$\varphi_{product}$ [ml/min]	$\varphi_{buffer\_airlift}$ [ml/min]
1&2	1	4.5	137	137	170
3 &4	2	6	137	137	137
5 to 7	2	4.5	137	137	137

4.3 RESULTS AND DISCUSSIONS

4.3.1 Seeding

Figure 4-3 illustrates the volume density of the seed crystals and the fit to the model equation 4-5. Parameters used to fit the model are given in Table 4-3. A good fit for seed crystals size distribution is necessary in order to have similar initial conditions in the model to the ones in the experiments.

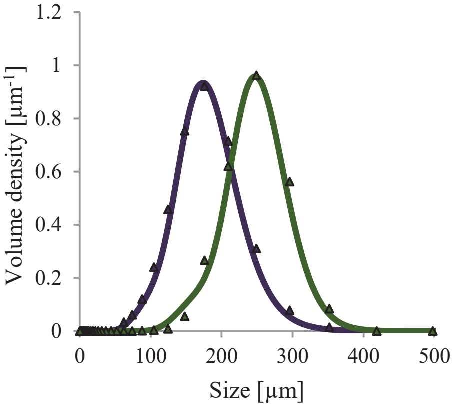

Figure 4-3 *Seeds size distribution; Markers displaying the experimental results and lines displaying the model fit, purple and green presenting seeds of 173 and 245 µm.*

Parameter	Fitted amount for 245 µm	Fitted amount for 173 µm
$L_{g,1}$	255×10^{-6}	185×10^{-6}
$L_{g,2}$	190×10^{-6}	140×10^{-6}
σ_1	1.16	1.25
σ_2	1.25	1.40
F_1	0.85	0.81

Table 4-3 *Fitted parameters for equation 4-5 for two seed sizes used in the experiments*

4.3.2 Continuous cooling crystallization

A number of continuous cooling experiments (exp 1–7) have been performed primarily to investigate the influence of the continuous operation on the product quality in the ALC and to study the influence of the process conditions especially with respect to the seeding policy and the residence time on the product quality. The second objective of these experiments was to check the ability of the previously developed kinetic model to describe continuous experiments in the ALC. The crystallization model has been previously derived on the basis of a number of batch experiments in the ALC [41, 42].

Experiments #1C and #2C are performed with different initial supersaturations and duration in which seeding only occurred at the start of the experiment. Figure 4-4 shows the relative supersaturation profile for these two experiments.

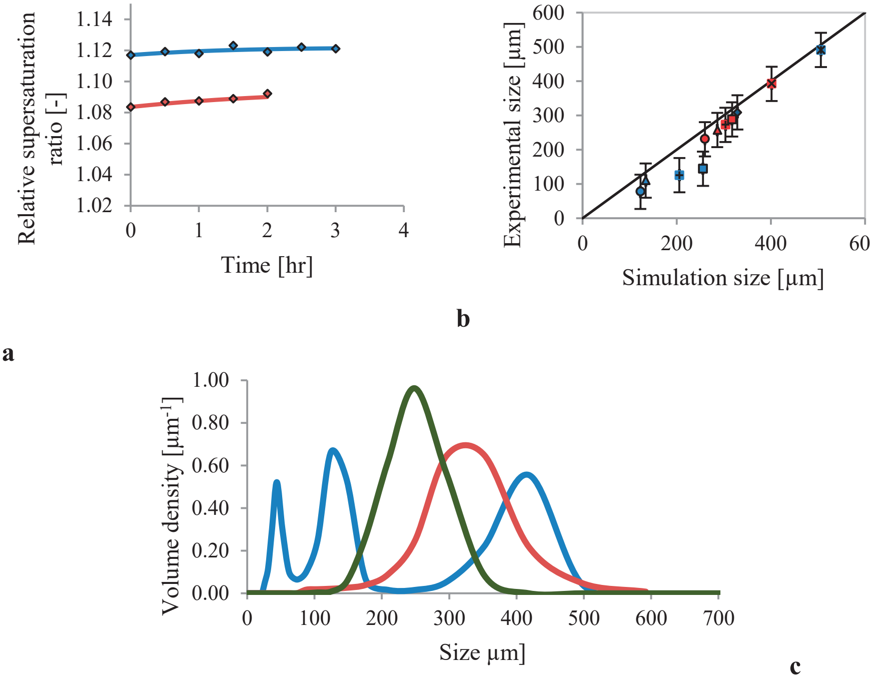

Figure 4-4 *Simulation (lines) and experimental (markers) results for (a) Relative supersaturation, (b) quantiles (L_{10}(○), L_{20}(Δ), L_{30}(+), L_{40}(□), L_{50}(◊), L_{90}(χ)) at the end of experiments and (c) CSD of initial seeds (green) and the products of experiments #1C (blue) and #2C (red)*

In Figure 4-4, it can be seen that the supersaturation level increases a bit in the beginning and remains almost constant afterwards. This supersaturation level is influenced by the generation of supersaturation by the hotter and more concentrated feed stream (Table 4-1) and the (mass) growth rate of the seed crystals, which is proportional to the growth rate and the available surface area of the crystals. This surface area of the crystals increases by the growth induced increase of the crystal diameter, but decreases at the same time by washing out of the crystals via the product removal.

Depending on these factors the trend of supersaturation profile can vary from increasing to constant and even to a decreasing profile. Within current process conditions the supersaturation difference between these two experiments (#1C and #2C) remains also more or less constant.

Due to the short duration of the experiments no stationary value is obtained from the CSDs, which was also not the aim of these experiments. Comparing the CSDs after 1 residence time for experiment #1C and 1.5 residence time for experiment #2C shows that in experiment #2C larger crystals were produced, due to the higher supersaturation during the experiment and the longer duration of the experiment. However, also a considerable amount of smaller crystals were present in the product of this experiment possibly due to an inevitable secondary nucleation or disturbance during the operation. Operating the crystallizer close to the nucleation threshold, such as in experiment #2C, could result in secondary nucleation which could actually be used to avoid the continuous seeding. This will however require a precise control system regulating the amount of secondary nuclei by the manipulation of the supersaturation in the crystallizer. This was beyond the scope of this study and therefore it is tried to avoid conditions where secondary nucleation can be stimulated. Thus, a lower level of supersaturation (the one for experiment #1C or lower) is used for the next experiments.

Comparing the simulation results with the ones from the experiments indicates that the simulated supersaturation profile overlaps nicely with the measured supersaturation supporting the explanation given above. The simulated quantiles L_{10}, L_{20} L_{30} and L_{40} are lower than the ones of the experiments; while L_{50} and L_{90} are predicted very well by the model in these experiments. The reason is that in the model the supersaturation remains always below the limit value for surface nucleation, whereas in the experiment some surface nucleation can occur in zones where the supersaturation is slightly higher such as close to the cooling walls. For experiment #2C all quantiles are predicted precisely by the model.

The results of experiments #1 and #2 raise the need for more seeding. In Experiments #3C and #4C periodically seeding is used in intervals of 30 minutes. The initial supersaturation, seeds size and crystallizer residence time are kept the same in these two experiments. Only different amount of seeds crystals were used (8 and 4 grams/30'' for experiments #3c and #4c respectively) while also the initial supersaturation is slightly different. Figure 4-5 shows results for these two experiments. The solution concentration reaches a steady state value after about two residence times. The increase in the supersaturation level before it reaches the steady state value in experiment #4C is due to the balance of the supersaturation generation, partly by the feed stream and partly by the unavoidable evaporation and the supersaturation depletion by the growth of the crystals. However, the experiment needs to be continued for a longer period (longer than 3 residence time) in order to enable us to explain the profile.

The steeper slope of supersaturation profile in the first 3 hours for experiment #4C compared to that of experiment #3C can be also explained by the lower amount of seeds introduced in experiment #4C and therefore lower depletion rate is expected. The quantiles related to large crystals for both experiments are almost similar both in the simulation and the experiments.

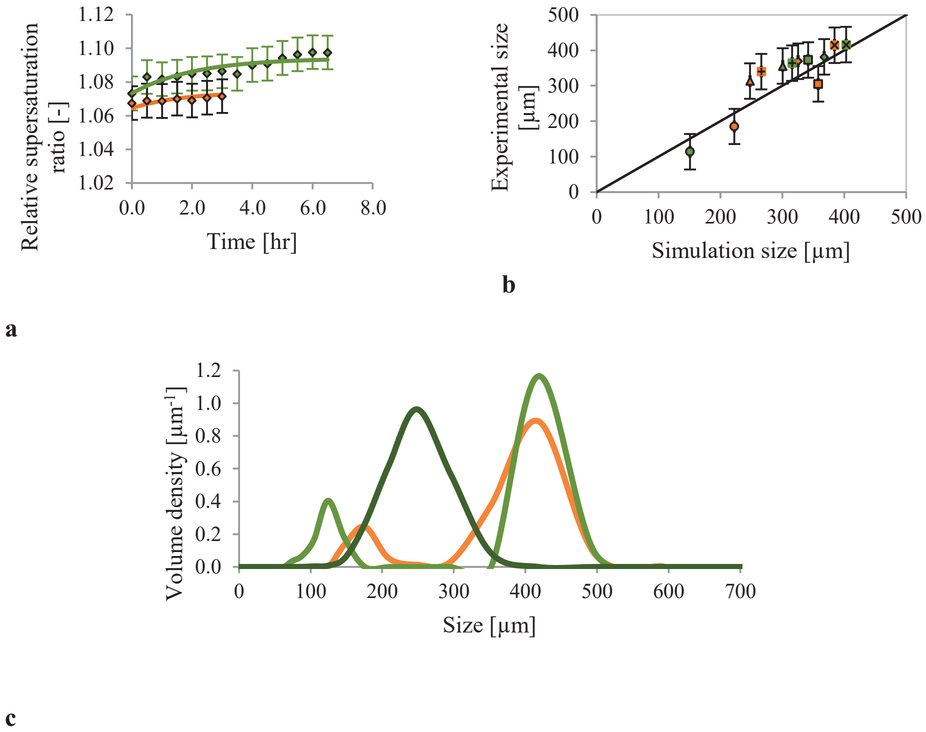

Figure 4-5 *Simulation (lines) and experimental (markers) results for effect of amounts of seeds on (a) Relative supersaturation during the whole experiments (b) quantiles from the product (L_{10}(○), L_{20}(Δ), L_{30}(+), L_{40}(□), L_{50}(◊), L_{90}(χ)) and (c) experimental CSD of the seeds (dark green) and product in the last hour for experiments #3C (orange) and #4C (light green)*

Experiments #5C to #7C are performed using different amount of seeds per interval and using seed crystal of a smaller size. Figure 4-6a shows the relative supersaturation for these three experiments. Although the increasing trend can be still seen in the first residence time of all three experiments, the higher the amount of seeds used the faster it tends to level off. Figure 4-6b and c show the quantiles and the CSD for these experiments. Smaller product crystals compared to the ones from experiments #1C to #4C was expected due to the smaller size (and thus a higher number) of the seed crystals and the lower initial supersaturation level. It is also expected that the more seeds used, the smaller the size of the product crystals. Experiment #5C shows the largest mean size accordingly. The presence of the peaks below 100 µm must be attributed to some secondary nucleation, while the peaks present between 100 and 150 µm can be attributed to the seed crystals added during the experiment.

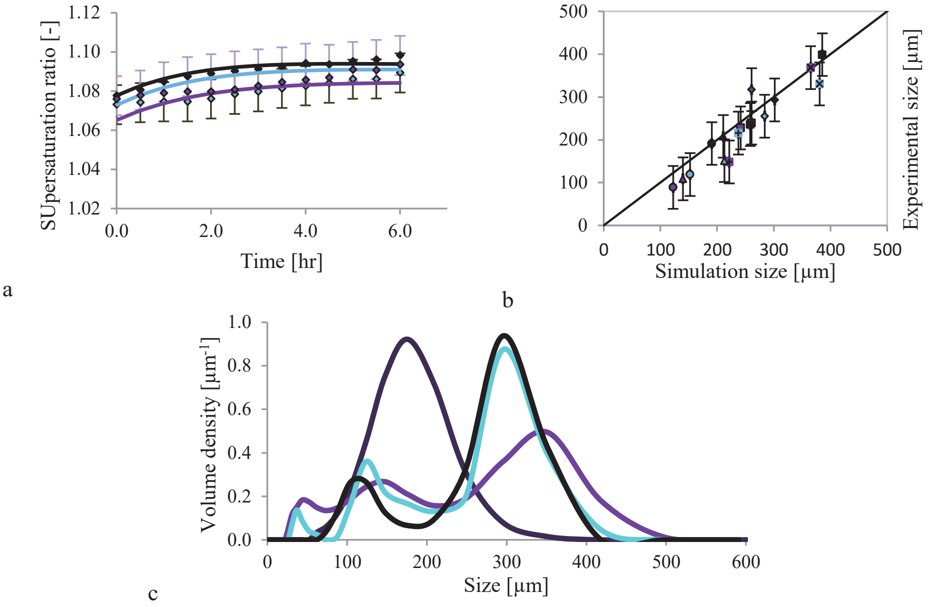

a

b

c

Figure 4-6 *Simulation (lines) and experimental (markers) results for (a) Relative supersaturation, (b) comparison of simulation and experimental quantiles (L_{10}(○), L_{20}(Δ), L_{30}(+), L_{40}(□), L_{50}(◊), L_{90}(χ)) at the end of experiments and (c) CSD of initial seeds (dark purple) and the products of experiments #5C (light purple), #6C (light blue) and #7C (black)*

To summarize the validated model for batch cooling experiments in ALC has been used in a sensitivity study for continuous cooling experiments in the same crystallizer and the results show that the model is capable of producing reasonable results for the continuous experiments using same kinetics.

The availability of such a model is necessary in order to enable us to design further experiments in this crystallizer or, if needed, to design another crystallizer based on desired requirements. The process conditions used in experiment #7 is further used for the continuous membrane-assisted crystallization experiments.

4.3.3 Continuous membrane-assisted Crystallization (CMaC) of L-ascorbic acid

The continuous MaC experiments have been performed with and without overflow according to the setups shown in Figure 4-2. Experiments #1 and #2 are performed with configuration (a) and experiments #3 to #7 with configuration (b). The only difference is that experiments #6 and #7 are performed with a higher concentration in the buffer vessel than the one for the other experiments.

The results show lower crystal fractions for experiments #1 and 2 where the overflow is being used. The objective of using an overflow is to allow for flexibility in choosing the flow to the membrane. Although a baffle has been used in order to avoid the crystals to be removed via this overflow to the buffer vessel, crystal fraction and median size for samples from the overflow are also measured. The crystal fraction is determined as mass of dried crystals per mass of suspension. Results indicate that the solution removed by the overflow has a crystal fraction of 0.2% with the median size of 230 µm. This amount of crystal loss can be also seen in the increase in the concentration in the buffer vessel shown in Figure 4-7 compared to the one for experiments #3 to #5 where the overflow is not used. In both cases (set a: experiments #1 and #2 and set b: experiments #3 to #5) the concentration in the buffer vessel is increasing which is partly contribution of membrane action and partly the addition of fines from the overflow.

Table 4-4 *Crystal fraction for CMaC experiments*

Exp #	1	2	3		4		5	6	7
Crystal fraction [%]	4 hrs	4 hrs	4 hrs	6 hrs	4 hrs	6 hrs	4 hrs	4 hrs	4 hrs
	0.45	0.45	1.20	1.35	0.65	1.0	0.75	0.75	0.75

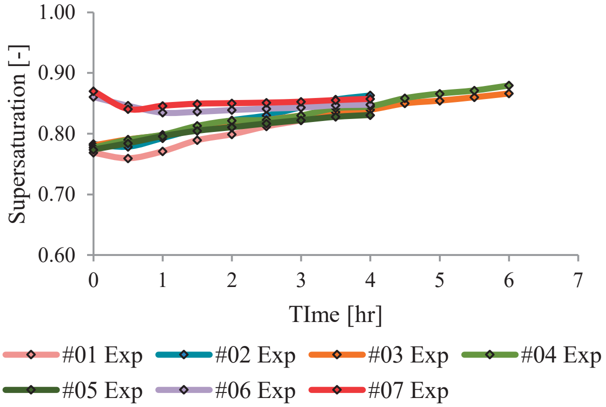

Figure 4-7 *Level of relative supersaturation of L-ascorbic acid in the buffer vessel for experiments #1 to #7.*

The markers in Figure 4-8 show the supersaturation level in the ALC and the quantiles measured and calculated from the product flow after 4 hours of experiment. The lines indicate the same values predicted with the model.

Supersaturation level for both experiments is increasing in the first two residence times but the increase is slowly levelling off in the second residence time as was also expected based on the results from CCC experiments. The increase in the beginning similar to CCC experiments can be again attributed to the small surface area unable to consume the provided supersaturation. Modelling results indicate that the steady state is almost reached after 2 residence time is passed. The duration of the experiments was limited to 2 residence times and it can be only seen that the increase in the supersaturation is levelling off in the second residence time. The quantiles are predicted perfectly with the model as can be seen in Figure 4-8b. The CSD of experiments (shown in Figure 4-8c) clearly contains a peak for grown crystals being removed via the product flow which has a median size of ~300 µm.

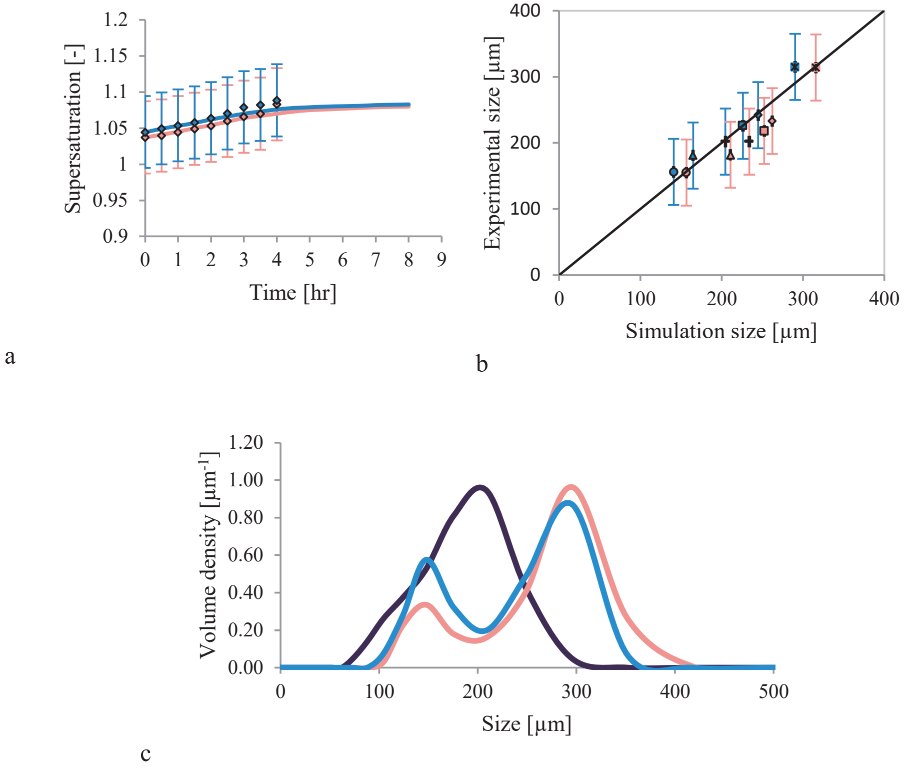

Figure 4-8 *Simulation (lines) and experimental (markers) results for (a) Supersaturation level, (b) quantiles (L_{10}(○), L_{20}(Δ), L_{30}(+), L_{40}(□), L_{50}(◊), L_{90}(χ)) and (c) CSD of seeds (dark purple) and product after 4 hours for experiments #1 (pink) and #2 (blue)*

The results from experiments #3 to #7 are shown in Figure 4-9. The initial concentration of buffer vessel for experiments #3 to #5 is almost the same and it increases in the course of the experiment. Therefore, a larger initial concentration in the buffer vessel for experiments #6 and #7 is considered to minimize the time for concentration stabilization in the buffer vessel. It can be seen in Figure 4-7 that the concentration of buffer vessel stabilizes after the first hour of these two experiments.

The supersaturation increases in the first two residence times for all experiments and it slows down and stabilizes afterwards. Median size of ~350 µm for these experiments is measured and the reproducibility of the results is confirmed by comparing the CSD for these experiments.

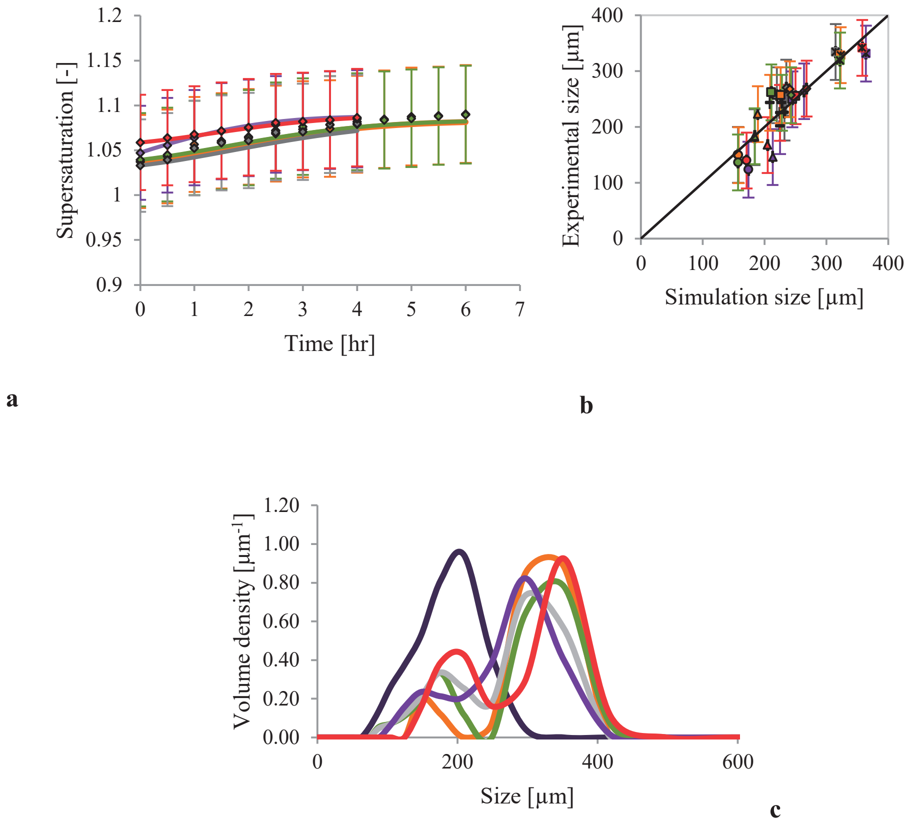

Figure 4-9 *Simulation (Lines) and experimental (markers) results for (a) Relative supersaturation, (b) quantiles (right) comparison of simulation and experimental quantiles (L_{10}(○), L_{20}(Δ), L_{30}(+), L_{40}(□), L_{50}(◊), L_{90}(χ)) at the end of experiments #3 (orange), #4 (green), #5 (grey), #6 (light purple) and #7 (red) and (c) the CSD of seeds (dark purple) and experiments as indicated*

These experiments show the ability of membrane distillation unit to assist the ALC in a continuous crystallization process. They have also confirmed the feasibility of continuous crystallization in the ALC. The results of feasibility study are encouraging. Unfortunately it was not possible to perform long experiments in practice. However, the very good predictive capability of the model enables us to optimize the process further.

One of the important questions to be answered via the model is: 'Can the period of start-up be shorter or even discarded with better flow adjustment between the membrane unit and the crystallizer?' This has been evaluated by changing the membrane flow rate and the crystallizer residence time and analysing their influence on supersaturation profile in the crystallizer and the product median size. In Figure 4-10 four different membrane flow rates are considered while the crystallizer residence time is constant 2 hours. The higher the membrane flow rate the more supersaturation available to be consumed by the seed crystals and the larger the median. In Figure 4-11 three different crystallizer residence time are considered while the membrane flow rate is constant 0.3 kg/hr. Though the relation between the residence time and the median size is not linear, the higher the residence time the larger the median size. The influence of crystallizer residence time on supersaturation profile is very low and can be neglected. Based on the result shown in Figure 4-12 if larger median size would be the objective, residence time of 2 hours and membrane flow rate of 0.45 kg/hr are the optimized values to be implemented as used in experiments CMaC #1 to #7.

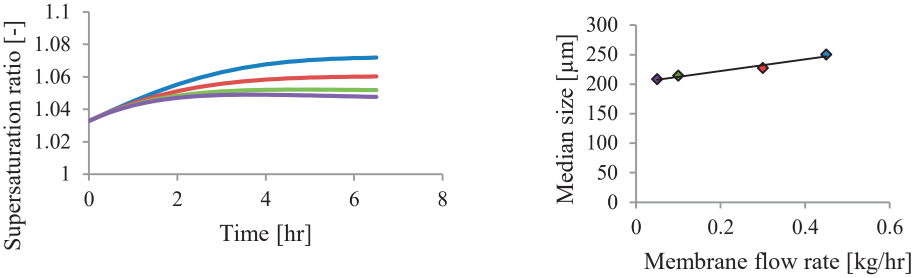

Figure 4-10 *Effect of membrane flow on supersaturation profile and median size (M=0.05 (purple), M=0.1 (green), M=0.3 (red), M=0.45 (blue))*

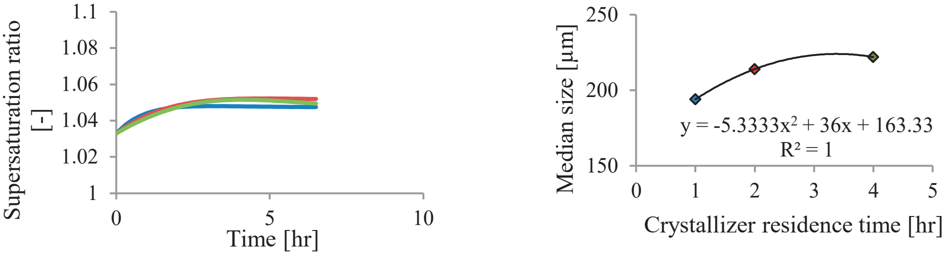

Figure 4-11 *Influence of crystallizer residence time on supersaturation profile and product median size (RT=1 (blue), RT=2 (red), RT=3 (green))*

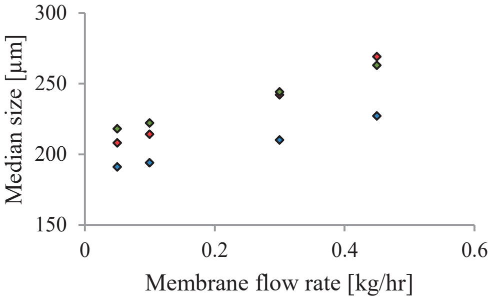

Figure 4-12 *Influence of membrane flow rate and crystallizer residence time on product median size (RT=1 (blue), RT=2 (red), RT=3 (green))*

Besides the size and size distribution, the facet of the crystals are also important which can be only traced by inline imaging or offline microscopic image of the product.

Figure 4-13 shows the inline and offline images of the crystals in the crystallizer for one of CMaC experiments without the overflow and with the feed to buffer flow.

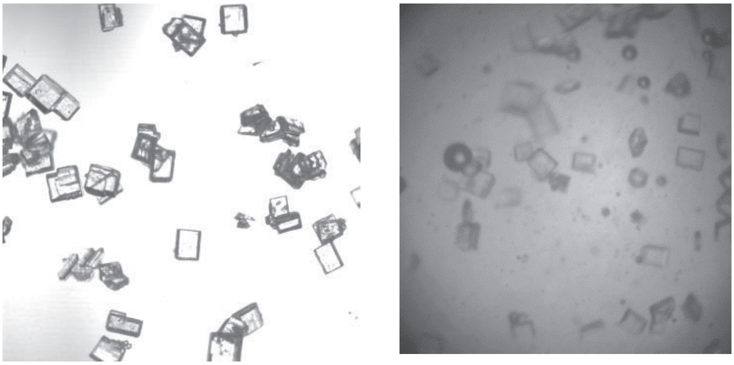

Offline microscopic image

Inline image from the camera

Figure 4-13 *Offline and inline image of the product crystals from one of the CMaC experiments*

4.4 CONCLUSIONS AND FURTHER RECOMMENDATIONS

In this study the continuous cooling and membrane-assisted crystallization experiments are performed based on which following conclusions are driven:

- Batch cooling crystallization experiments have been performed in the ALC applying different process conditions. Supersaturation was selected low enough to ensure no secondary nucleation occurs. In the model growth was only active and secondary nucleation was completely suppressed.
- The kinetic model developed and validated for batch cooling crystallization experiments has been tested for continuous cooling crystallization and resulted in acceptable outcome for different process condition.
- Continuous membrane-assisted crystallization experiments in an ALC have been performed for the first time and the results confirm the possibility and present the flexibility of designing such experiments.
- The developed model can be used to design new processes and equipment. It can be also used to design experiments based on optimized process conditions for different objectives such as large median size or high yield.
- It is recommended to perform the experiments for a long period (more than 4 residence times) in order to ensure the process stability.
- It is recommended to use other model compounds to ensure the capacity of CMaC to be applied to different systems.

4.5 REFERENCES

1. Quon, J.L., et al., *Continuous crystallization of aliskiren hemifumarate.* Crystal Growth & Design, 2012. **12**(6): p. 3036-3044.
2. Randolph, A. and M. Larson, *Theory of Particulate Processes, Acad.* Press, New York, 1988.
3. Gao, Z., et al., *Recent Developments in the Crystallization Process: Toward the Pharmaceutical Industry.* Engineering, 2017. **3**(3): p. 343-353.
4. Gros, H., T. Kilpiö, and J. Nurmi, *Continuous cooling crystallization from solution.* Powder technology, 2001. **121**(1): p. 106-115.
5. Mollan Jr, M.J. and M. Lodaya, *Continuous processing in pharmaceutical manufacturing.* American Pharmaceutical Review, 2004.
6. Roberts, K.J., R. Docherty, and R. Tamura, *Engineering Crystallography: From Molecule to Crystal to Functional Form*. 2017: Springer.
7. Morris, G., et al., *Estimation of Nucleation and Growth Kinetics of Benzoic Acid by Population Balance Modeling of a Continuous Cooling Mixed Suspension, Mixed Product Removal Crystallizer.* Organic Process Research & Development, 2015. **19**(12): p. 1891-1902.
8. Mascia, S., et al., *End-to-end continuous manufacturing of pharmaceuticals: Integrated synthesis, purification, and final dosage formation.* Angewandte Chemie International Edition, 2013. **52**(47): p. 12359-12363.
9. Wong, S.Y., et al., *Development of continuous crystallization processes using a single-stage mixed-suspension, mixed-product removal crystallizer with recycle.* Crystal Growth & Design, 2012. **12**(11): p. 5701-5707.
10. Quintana-Hernández, P.A., et al., *Nonlinear MIMO control of a continuous cooling crystallizer.* Modelling and Simulation in Engineering, 2012. **2012**: p. 36.
11. Lakatos, B., *Stability and dynamics of continuous crystallizers.* Computers & chemical engineering, 1994. **18**: p. S427-S431.
12. Lakatos, B.G., T.J. Sapundzhiev, and J. Garside, *Stability and dynamics of isothermal CMSMPR crystallizers.* Chemical engineering science, 2007. **62**(16): p. 4348-4364.
13. Alvarez, A.J. and A.S. Myerson, *Continuous plug flow crystallization of pharmaceutical compounds.* Crystal Growth & Design, 2010. **10**(5): p. 2219-2228.
14. Zhang, H., et al., *Application of continuous crystallization in an integrated continuous pharmaceutical pilot plant.* Crystal growth & design, 2014. **14**(5): p. 2148-2157.
15. Johnson, M.D., et al., *Development and scale-up of a continuous, high-pressure, asymmetric hydrogenation reaction, workup, and isolation.* Organic Process Research & Development, 2012. **16**(5): p. 1017-1038.
16. Azoury, R., J. Garside, and W. Robertson, *Crystallization processes using reverse osmosis.* Journal of Crystal Growth, 1986. **79**(1): p. 654-657.
17. Curcio, E., A. Criscuoli, and E. Drioli, *Membrane crystallizers.* Industrial & engineering chemistry research, 2001. **40**(12): p. 2679-2684.
18. Curcio, E., G. Di Profio, and E. Drioli, *Membrane crystallization of macromolecular solutions.* Desalination, 2002. **145**(1): p. 173-177.
19. Curcio, E., G. Di Profio, and E. Drioli, *A new membrane-based crystallization technique: tests on lysozyme.* Journal of Crystal Growth, 2003. **247**(1): p. 166-176.
20. Gryta, M., *Direct contact membrane distillation with crystallization applied to NaCl solutions.* CHEMICAL PAPERS-SLOVAK ACADEMY OF SCIENCES, 2002. **56**(1): p. 14-19.

21. Tun, C.M., et al., *Membrane distillation crystallization of concentrated salts—flux and crystal formation.* Journal of Membrane Science, 2005. **257**(1): p. 144-155.
22. Kim, J., et al., *Membrane distillation (MD) integrated with crystallization (MDC) for shale gas produced water (SGPW) treatment.* Desalination, 2016.
23. Kuhn, J., et al., *Characterization and dynamic optimization of membrane-assisted crystallization of adipic acid.* Industrial & engineering chemistry research, 2009. **48**(11): p. 5360-5369.
24. Edwie, F. and T.-S. Chung, *Development of simultaneous membrane distillation–crystallization (SMDC) technology for treatment of saturated brine.* Chemical Engineering Science, 2013. **98**: p. 160-172.
25. Anisi, F., K.M. Thomas, and H.J. Kramer, *Membrane-assisted crystallization: Membrane characterization, modelling and experiments.* Chemical Engineering Science, 2017. **158**: p. 277-286.
26. Gryta, M., *Concentration of NaCl solution by membrane distillation integrated with crystallization.* Separation science and technology, 2002. **37**(15): p. 3535-3558.
27. Guan, G., et al., *Analysis of membrane distillation crystallization system for high salinity brine treatment with zero discharge using Aspen flowsheet simulation.* Industrial & engineering chemistry research, 2012. **51**(41): p. 13405-13413.
28. Chen, G., et al., *Performance enhancement and scaling control with gas bubbling in direct contact membrane distillation.* Desalination, 2013. **308**: p. 47-55.
29. Mariah, L., et al. *Membrane distillation for the recovery of crystalline products from concentrated brines*. in *WISA Biennial Conference, Durban, South Africa*. 2006. Citeseer.
30. Charcosset, C., et al., *Coupling between membrane processes and crystallization operations.* Industrial & engineering chemistry research, 2010. **49**(12): p. 5489-5495.
31. Pramanik, B.K., et al., *A critical review of membrane crystallization for the purification of water and recovery of minerals.* Reviews in Environmental Science and Bio/Technology, 2016. **15**(3): p. 411-439.
32. Martínez, M.B., et al., *Membrane crystallization for the recovery of a pharmaceutical compound from waste streams.* Chemical Engineering Research and Design, 2014. **92**(2): p. 264-272.
33. Kramer, H.J., et al., *4.1 Membrane Crystallization Technology and Process Intensification.* 2017.
34. Lawton, S., et al., *Continuous crystallization of pharmaceuticals using a continuous oscillatory baffled crystallizer.* Organic Process Research & Development, 2009. **13**(6): p. 1357-1363.
35. Kacker, R., S.I. Regensburg, and H.J. Kramer, *Residence time distribution of dispersed liquid and solid phase in a continuous oscillatory flow baffled crystallizer.* Chemical Engineering Journal, 2017. **317**: p. 413-423.
36. Kwon, J.S.-I., et al., *Modeling and control of crystal shape in continuous protein crystallization.* Chemical Engineering Science, 2014. **107**: p. 47-57.
37. Alvarez, A.J., A. Singh, and A.S. Myerson, *Crystallization of cyclosporine in a multistage continuous MSMPR crystallizer.* Crystal Growth & Design, 2011. **11**(10): p. 4392-4400.
38. Arimatsu, Y., et al., *Continuous production of calcium gluconate crystals in an integrated bioreaction–crystallization process using external loop airlift bubble columns with immobilized glucose oxidase gel beads.* Journal of chemical engineering of Japan, 2004. **37**(8): p. 1035-1040.
39. Gonzalez-Contreras, P., J. Weijma, and C. Buisman, *Bioscorodite crystallization in an airlift reactor for arsenic removal.* Crystal Growth & Design, 2012. **12**(5): p. 2699-2706.
40. Jenkins, D., *Salting-out crystallisation using NH3 in a laboratory-scale gas lift reactor.* The Canadian Journal of Chemical Engineering, 2009. **87**(6): p. 869-878.

41. Lakerveld, R., J.J. Van Krochten, and H.J. Kramer, *An air-lift crystallizer can suppress secondary nucleation at a higher supersaturation compared to a stirred crystallizer.* Crystal growth & design, 2014. **14**(7): p. 3264-3275.
42. Anisi, F. and H.J.M. Kramer, *Crystallization kinetics in an airlift and a stirred draft tube crystallizer; Secondary nucleation models revisited.* Chemical Engineering Research and Design, 2018.
43. Price, C.J., *Continuous Pharmaceutical Crystallization from Solution*, in *Engineering Crystallography: From Molecule to Crystal to Functional Form*. 2017, Springer. p. 315-329.
44. Gherras, N. and G. Fevotte, *On the use of process analytical technologies and population balance equations for the estimation of crystallization kinetics. A case study.* Aiche Journal, 2012. **58**(9): p. 2650-2664.
45. Soare, A., et al., *Minimization of Attrition and Breakage in an Airlift Crystallizer.* Industrial & Engineering Chemistry Research, 2012. **51**(33): p. 10895-10909.

Chapter 5

Ultrasound-Assisted Seed Generation for Continuous Crystallization Processes

ABSTRACT

Gaining control over crystallization phenomenon, primary nucleation, has always been and still is a challenge in crystallization science. However, new technologies such as ultrasound not only can facilitate the control over primary nucleation but also enhance the rate by several factors. The effect of ultrasound on primary nucleation on three different model compounds with different solubilities has been investigated in this study. A few preliminary experiments have been performed in which the generated ultrasound seeds have been introduced to an airlift crystallizer in order to grow the seed crystals to a desired larger size within a batch cooling process. A narrow crystal size distribution has been achieved for the cooling batch experiments in the airlift crystallizer with larger number of counts of seed crystals, and the previously developed model for airlift crystallizer showed a good agreement in results. The model can be used to design new experiments in order to optimize process conditions such as size and amount of seeds, initial supersaturation level and temperature profile.

5.1 INTRODUCTION

Continuous operation in general is attracting interest due to the potential benefits such as low operation cost, reduction in operating volume and improved safety and controllability. Design based on continuously operated stirred crystallizers or use of tubular flow systems with plug flow-like mixing regime are being developed for continuous crystallization processes. With respect to the crystallization process, the plug flow systems offer enhanced process control opportunity such as homogeneous temperature and supersaturation distribution, narrow residence time distribution and flexibility to ‘scale out’ the operation instead of scale up. Tubular crystallizer employing interaction of the oscillating fluid flow with the baffles in the tubes to achieve plug flow-like mixing conditions is a promising design in this regard. Since the mixing conditions mostly depend on the generation of the vortices from the interaction of the oscillating flow with the baffles, a flowrate independent control over mixing is achieved. Thus, the oscillatory flow baffled crystallizer allows for large residence times to be realized in relative short tube lengths.

On the other hand the reliability and the operation know-how of the stirred tank systems have favored the implementation of such systems for continuous operation at industrial scale [1]. A number of challenges are associated with the stirred tank systems which include among others, poor control over mixing, low heat transfer rates and varying shear rates which results in non-uniform conditions in the crystallizer and hence in poor control over the quality of the crystals. New generation of crystallizers provide opportunities to improve the crystallization process control. The airlift crystallizer (ALC) is an example of a new design in which the crystallization kinetics are controlled by suppression of secondary nucleation known as the main cause of crystal attrition followed by a wide crystal size distribution (CSD). An airlift system consists of a riser and a downcomer, which are in open connection. A density difference between the content of the riser and the downcomer is created by gas injection in the riser resulting in a higher gas hold-up. This density difference is the driving force for a circulation flow around the draft tube which separates the riser and the downcomer. Therefore, suppression of secondary nucleation is achieved by eliminating the moving objects (impellers) avoiding the high local shear and the particle-impeller collisions.

Control of nucleation is important, irrespective of the type of the crystallizer, as the onset of the crystallization process is critical for controlling the end product quality. However, due to the stochastic nature of the nucleation process and its strong nonlinear dependence on the supersaturation making it sensitive to small spatial inhomogeneity in the supersaturation, gaining precise control over primary nucleation is a challenge. Nucleation outbursts cause issues such as broad multi-modal size distribution and changes in crystal structure which need to be avoided.

Several strategies have been proposed and implemented to control the nucleation. Seeding the batch or continuous operation is a popular choice as it eliminates the need for nucleation to generate the required number of crystals in the process. Avoiding the primary nucleation through seeding, allows the process to be operated at low supersaturations where growth is dominant. Seeding is often applied even in continuous mixed-suspension mixed-product removal (MSMPR) crystallization to ensure quick and reliable start-up. However, due to the dominance of secondary nucleation in continuously operated stirred tank crystallizers no additional seeding is needed. On the other hand, in the case of ALC for example, where secondary nucleation is strongly suppressed, seeding might be required to ensure that no primary nucleation outbursts occur [2]. In case of continuous plug flow tubular crystallizers, seeding is continuously required as there is no back mixing of nuclei formed by attrition. In tubular crystallizers, the larger surface area can cause heterogeneous nucleation and presents a risk of fouling of the walls (encrustation). Thus seeding might be advisable to ensure sufficient crystal surface area in the first part of the crystallizer to keep the supersaturation low enough to avoid the unwanted nucleation. Hence, various studies have focused on optimizing the seeding strategy by studying the influence of parameters such as the seed mass, the seed size distribution or the ratio of the crystallized mass to the seeded mass on the crystallization process [3-6].

However, ensuring an optimal number of seeds narrowly distributed around a specific mean size, is challenging. Agglomeration of the seed crystals is a problem which is often encountered and the seed crystal characteristics change due to aging during hold up. As a result of agglomeration and growth of the seed crystals by aging, the available surface area for rapid consumption of the supersaturation is reduced, leading to poor process control. Transferring of the seeds from the hold-up vessel to the crystallizer is also critical, as correct supersaturation needs to be ensured; otherwise secondary nucleation occurs, which causes excessive fines production. Recycling the product as seed crystal is the most common solution, but it is costly as additional processing steps and control is required to ensure the optimum amount and quality of the seeds. Thus, an efficient process which ensures continuous supply of the optimum seed crystals is demanding.

The complexities and the challenges involved with the seeding process and with the recirculation of the product crystals as seeds can be avoided by having a dedicated system where seeds can be generated through controlled nucleation. One of the potential nucleation control approaches is the use of external energy fields to control the nucleation rates. Application of external energy fields such as ultrasound (US) and laser pulses have been shown to be promising tools for gaining control over the nucleation rate for manipulating the number of crystals to obtain the desired size distribution and the crystal structure. Especially, US as a potential tool for generation of seed has been studied and demonstrated to produce crystals with narrow size distribution [7-9]. This approach needs to be further developed by identifying the optimum process conditions such as supersaturation, mixing and the energy of external fields required to gain the desired manipulability of the nucleation rates. Both process design and equipment configurations for controlled application of external energy fields require development to ensure application of the technology to industrial processes. Ideally a multistage process is envisaged, where the use of external fields allows optimum seeding through direct generation of the seeds in the process, which can then be grown to the desired characteristics under controlled growth conditions.

5.2 OVERVIEW OF APPLICATION OF ULTRASOUND IN THE CRYSTALLIZATION PROCESSES

Use of US in crystallization (sono-crystallization) has continued to be an area of active research. Application of US has been targeted to achieve a reduction in MSZW, increased productivity due to the increased nucleation rates, control over purity and polymorph of the crystals, inhibition of agglomeration, improved micro-mixing to enhance diffusion limited mass transport and most commonly for manipulating the particle size distribution. US has been used as a nucleation process actuator and explored for crystallization process control due to the enhanced nucleation rate reported upon its application [10]. It has been shown that the application of US promotes nucleation at relative low supersaturations levels, as was determined by a reduction of the induction time, meaning that the required number of nuclei in a batch process can be generated at much lower supersaturation levels [9, 11-17]. Qiu et al. have reported a reduction in induction time from 340 s to 48 s for magnesium ammonium phosphate, with the application of US in the range of 350 W [18]. Application of US during crystallization was found to overcome problems with agglomeration [8]. Studies in the field of particle size reduction have used US to enhance the attrition and therefore induce a faster deracemization [19], improved solubility and faster dissolution kinetics of the APIs by increasing the specific surface area [15, 20-22]. Good control over particle size distribution has been reported by inducing nucleation at low supersaturations, which helped in avoiding an uncontrolled outburst of nuclei leading to fines generation [14, 15, 23]. Enhanced US induced nucleation rates have been utilized to promote nucleation in systems which are notoriously difficult to nucleate. Through use of US, the nucleation rate improvements have been reported for aminoacids [24], adipic acid [7, 25], roxithromycin [14], ice [26], $CaSO_4$ [27], dodecandioic acid in different solvents [28], L-Aspargine monohydrate [29], paracetamol [9], Dextrose Monohydrate [30] and K_2SO_4 [31]. However, there are studies which also report that the effect of US on nucleation is not strong; for example the use of US to study nucleation of calcium carbonate crystals [32] or with ammonium sulphate system [33].

The inability to detect nucleation before the nuclei grow to the minimum detectable size of the commonly used PAT tools, such as FBRM or imaging probes, makes the identification of the optimum conditions for application of US difficult. The inability to precisely characterize nucleation also leads to poor understanding of the US-assisted nucleation mechanism, which makes it difficult to predict the nucleation rates. Often the effect of US on the crystallization process is evaluated based on the end product quality which can be misleading as the shape, size or the number of crystals change due to the growth, secondary nucleation or agglomeration. Furthermore, poor understanding of US-assisted nucleation has also led to limited designs of US equipment and as a result mostly ultrasonic cleaning bath, US horns immersed directly into a batch crystallizer or transducer attached to the wall of batch crystallizers are utilized to study US-assisted nucleation [34]. Often, these configurations are suboptimal as the spatial distribution of the US field or the power introduced into the system is poorly controlled, leading to poor results. Overall, limited development of US-assisted crystallizers, where spatial and temporal control of the cavitation events can be achieved, has hindered the realization of US as an industrial tool to control the crystallization process.

Cavitation has been the predominant phenomenon believed to lend a sufficient explanation to the US-induced nucleation [11, 35]. On applying the US, cavitation bubbles are created which induce very high local temperatures and pressures upon collapse [11, 31, 36, 37]. However, high temperature reduces the supersaturation and high pressures mostly increase the work for nucleation making the exact mechanism unclear. Therefore, other mechanisms have been proposed. A rapid increase in supersaturation during bubble expansion or after collapse of the cavitation bubbles has been proposed to be responsible for the enhanced nucleation rates due to creation of thermal gradients with rates approximated to be in the range of 10^7 to 10^{10} K/s [38]. A distinction can be made between transient and stable cavitation bubbles. Transient bubbles are short-lived and create the extreme local conditions upon collapse, whereas the stable cavitation stay for longer acoustic cycles and implode less violently when compared to transient bubbles [19, 20]. Stable cavitation has been attributed to act as nucleation site and promote nucleation through heterogeneous nucleation mechanism [39]. Another explanation of the enhanced nucleation rates during sono-crystallization is the segregation of the solute species in the vicinity of the bubbles due to large pressure gradients, especially the bubble oscillations before collapsing promotes creation of high density regions favouring nucleation [40]. The enhanced mass transfer resulting from the improved micromixing upon application of the US has also been attributed to the nucleation rate enhancement and the resulting crystal shape and surface properties [37, 41, 42]. Devarakonda et al. reported a US-assisted crystallization process where an increase in growth rate was observed owing to breakage of crystals which resulted in increased surface area, whereas Nalajala et al. described higher nucleation rate but lowered growth rate due to the increased turbulence and breakage of crystals when sonication was applied [35]. The major contribution to the crystal breakage is reported to be particle-shock wave interaction while minor contributions are from interparticle collisions, particle-horn collisions and particle-wall collisions. Most importantly a consistent agreement has been observed with respect to production of smaller particles on application of US [16, 21]. In order to facilitate the design of US application various studies are now focused on, for example, evaluating the effect of US frequency (30-1140 kHz) and US power (4-200 W) on crystal nucleation and breakage, effect of batch or continuous configurations and process conditions on cavitation [33, 43], milli-flow devices to gain spatial control over cavitation [44, 45] and energy efficient application of US [9, 17, 46, 47].

Overall, a vast variety in investigations have demonstrated, on one hand, the potential of US to manipulate the nucleation rate in crystallization processes which can be further developed into a process control tool. On the other hand, the strong system dependent effects of US highlight the requirement to identify first the dominant phenomenon at which US induces the formation of the nuclei, either by primary or secondary nucleation processes according to different available models, Single Nucleus Mechanism (SNM) or Classical Nucleation Theory (CNT) [48, 49]. Also, as nucleation rate has a strong non-linear dependence on process conditions, controlled nucleation through use of US can only be ensured at conditions where spontaneous nucleation can be prevented from forming excessive nuclei which leads to poor crystal specifications. The metastable zone is the region between the saturation temperature of a solution and the temperature at which the crystals are first detected. The width of this zone is commonly used to determine the crystallization operating window for the process in which uncontrolled nucleation can be prevented. However, Metastable Zone Width (MSZW) not only depends on the system (solute and solvent) but also on process conditions such as temperature, volume, degree of turbulence, cooling rate etc [10].

In this chapter, firstly, the effect of US on nucleation for a number of different solutes with large variety in solubilities and MSZW is studied. Secondly, US setup is used as an alternative to overcome the drawbacks of external seed sources and solution preparation. There are several literature studies on Paracetamol as model compound used in US-assisted experiments as a relatively low-soluble compound but there exist no study (to the knowledge of the author) on L-ascorbic acid (AA) and Melamine which have higher and much lower water solubilities than Paracetamol respectively. Therefore it is interesting to study the effect of US on these three compounds in order to investigate if the effect of US is dependent on the compounds' solubility and MSZW.

For these model compounds we first identify a reasonable supersaturation regime at which primary nucleation can be induced by application of US. This reasonable supersaturation is chosen low enough, well within the MSZW, to avoid excessive nucleation which leads to fines formation and hence poor size distribution. Secondly, the two commonly used designs of US application system have been tested in their capability for *in-situ* seed generation, i.e. to provide supply of seeds with optimal quality.

Two different US configurations tested were; one for batch application in which the US horn was inserted directly in a batch crystallizer, and one for continuous seed generation in which the US was applied in a flow-through-cell.

A measure is required in order to characterize the nucleation kinetics. Since nucleation seldom occurs instantaneously after generation of supersaturation (depending on the nucleation rate), the time required to observe nucleation in a supersaturated solution, defined as induction time is, often used as a tool to compare the nucleation rates.

Finally, the US generated seeds have been applied to an ALC which provides controlled growth conditions. FBRM has been used where possible to characterize the crystallization phase in the process.

5.3 MATERIALS AND METHODS

5.3.1 Metastable zone width (MSZW) determination without US

Use of US in producing seeds is interesting because the nuclei can be generated at lower supersaturation (within MSZ). This initial supersaturation ratio at which the US initiates the generation of nuclei is the most important parameter to be optimized [39]. In order to determine this supersaturation the MSZW is measured and identified. According to the literature the working volume has a large influence on the MSZW. The stochastic nature of nucleation is shown to be very evident at small batch volumes [10]. For Paracetamol-water system variation up to 20 °C have been found in the MSZW between independent measurements at 1 ml scale, whereas, with experiments at a volume of 500 ml or 1000 ml the variation is only around 2 °C. The more deterministic MSZW in large volumes was attributed to the higher probability of a single nucleus to form, which is followed by secondary nucleation leading to what can be observed as nucleation according to Single Nucleus Mechanism (SNM) [10, 50, 51]. Thus, the supersaturation required to induce nucleation at small volumes can show a high variability and be much higher than the measurements for larger volumes. Moreover, use of US introduces new mechanism which may influence nucleation, such as cavitation events and may result in higher nucleation probability at a constant supersaturation reducing the variability in nucleation, especially at low working volumes, but we have not studied in depth the effect of US on the MSZW as function of volume. Therefore the volumes of 500 ml and 1000 ml are chosen in this study to avoid large dependency of MSZW on volume in low volumes.

Three systems have been studied, namely, aqueous solution of AA, paracetamol and melamine. The clear saturated solution is made by keeping the solution at 5 °C above the saturation temperature to ensure complete dissolution of the solids. A linear cooling profile (-0.1 °C/min) is applied to the solution and the nucleation observed visually. Volumes of 1000 ml for Paracetamol and AA and 500 ml for Melamine have been considered. A lower volume for Melamine is due to its very low solubility compared to the other two compounds. The batch setup used to characterize the MSZW is shown as configuration ‘a’ detailed in the next section and in Figure 5-1.

5.3.2 US device and setup

A 20 kHz US horn with a diameter of 34 mm and output power rated to be 500 W (model UIP 500HD, Heilscher) has been used throughout this work to apply US. Two equipment configurations have been used in the study 1) Direct contact of the US probe with supersaturated solution in a 1 L jacketed glass crystallizer, and 2) The US probe coupled to a flow-through-cell in which the supersaturated solution is pumped for continuous or batch operation with recirculation. The two configurations are schematically shown in Figure 5-1 as b and c respectively.

It should be noted here that the working volumes of the configurations are different. Configuration ‘b’ allows 1000 ml batch of supersaturated solution to be sonicated, whereas configurations ‘c’ has a hold up volume of 150 ml which is exposed to US (the volume of the US cell) and the volume of the feed vessel is 3 L. Moreover, configuration ‘b’ operates in batch mode only whereas the other one allows both batch and continuous operation.

In our setup, the input energy to the US horn could be regulated from the signal generator (attached to the US horn) by selecting the mode of operation to be between 50 to 100% (in steps of 10%). In our study the input power selection was fixed at 50% which implied that only half of the maximum rated power (500 W @100%) was supplied to the US horn. We also had a reducer attached to the horn which resulted in the output energy from the horn to be reduced by 50%. The direct characterization of the US energy transferred into the medium is not straightforward. A commonly used measure is the calorimetric energy input due to the heating of the medium by the US energy [52]. The rise in temperature of the medium upon application of the US is measured and the total heat energy is quantified. The calorimetric powers used in our study were in the range of 20-50 W.

In our study, the effect of US on nucleation has been quantified in the batch system (configuration ‘b’). Configuration ‘c’ has been used as an alternative to configuration b for AA to generate seeds of AA to be later applied to ALC where growth dominated operation was targeted. An FBRM has been used to detect nucleation when possible; otherwise nucleation has been detected visually. In all the experiments, clear supersaturated solution is present before the application of US. Final CSD is measured offline with laser diffraction device.

Configuration ‘c’ can be used in several ways; batch, recirculation in which the flow is recycled to the feed vessel, and in continuous mode in which the liquid passes only once the US cell.

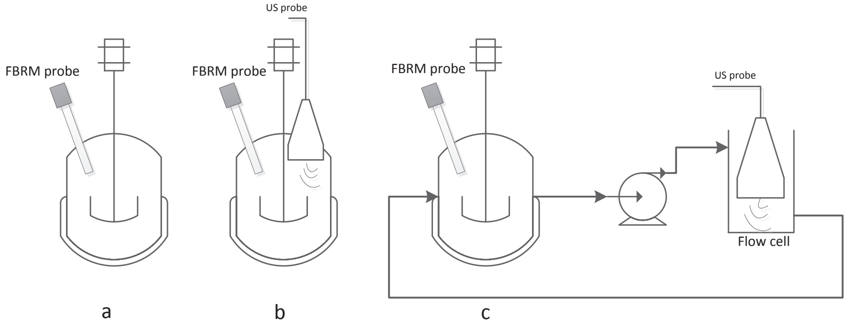

Figure 5-1 *Configurations of the setups used: a) without US for determination of MSZW, b) with direct application of US into the solution c) with US horn attached to and immersed in the flow through cell connected to a feed vessel either for recirculation or continuous flow*

5.4 RESULTS AND DISCUSSION

5.4.1 Determination of the process conditions for US application

As mentioned in section 5.3.1 before we can apply US the process conditions, which include among others the MSZW, are determined for the studied systems, AA, Paracetamol and Melamine. The results are summarized in Table 5-1. The measurement volumes and temperatures of the measurements are also given in Table 5-1.

As seen from Table 5-1, the MSZW for AA and for paracetamol is relatively large compared to Melamine. Due to the narrow MSZW with melamine-water system, the application window for US is only small and spontaneous nucleation is difficult to avoid.

Table 5-1 *Overview of the studied compounds with their corresponding process conditions. The nucleation has been detected visually. MSZW is derived as the difference between saturation and nucleation temperature at the given conditions.*

Compound	Concentration (g/L solvent)	Working Volume (mL)	Saturation Temp. (ºC)	Avg. Nucleation Temp (ºC)	MSZW
L-ascorbic acid (AA)	500	1000	40	24	16
Paracetamol	21	1000	38	25	13
Melamine	10.7	500	50	43	7

5.4.2 Effect of US on nucleation in batch operation

Nucleation under the influence of US was characterized in a batch process. The experiment has been performed in a 10 and a 3 L vessel using configuration b for AA in which US probe is directly in contact with the whole solution for a continuous period of time. The time within which nucleation is initially observed was not repeatable. It may be explainable with the proposed mechanism for US in literature that only a small number of primary nuclei are generated or exist in the system and undergo secondary nucleation by the violent interaction between the collapsing cavities and the crystals. Therefore configuration c is designed in order to expose a much lower volume of the solution to the US which may improve the control over nucleation. This is discussed in next section 5.4.3.

However, the Paracetamol-water system studied in configuration ‘b’ has led to outstanding results. Performing an induction time measurement, a clear saturated solution was cooled down to 35 °C to generate a desired supersaturation level (S=1.22) while remaining within the MSZW (according to Table 5-1). Experiments with and without the application of US were carried out. The nucleation was observed visually.

A significant reduction in induction time was observed when applying US. Under silent conditions (blank experiment with no US), no nucleation is observed for at least 5 hours. Upon use of US as soon as the supersaturation is generated, a short exposure of 5 minutes is enough to induce nucleation. The repeatability of the results has been confirmed through several trials. The solution is visually observed to become turbid indicating that a large number of nuclei have been produced. On the contrary, spontaneous nucleation under silent conditions proceeds considerably slower and hence no nuclei are observed within the limited observation time.

The effect of US on the nucleation in a melamine-water solution has been similarly studied under batch condition using configuration ‘b’. Figure 5-2 shows the reduction in induction time as a function of relative supersaturation. This is in accordance with literature for the many other compounds studied. The use of US shifted the induction time for all different supersaturation levels to a lower value for all supersaturation levels. However, the striking effect of US in reduction of induction time (reduction of MSZW) can be seen in specifically lower supersaturations compared to the ones for blank experiments [28, 53].

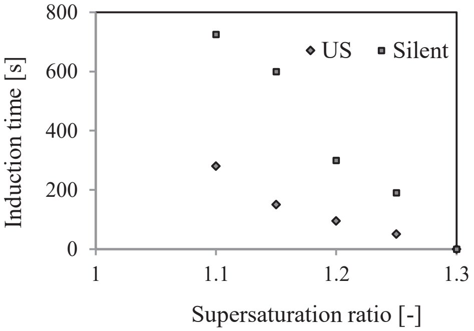

Figure 5-2 *Reduction in induction time observed upon application of US at various fixed intial supersaturation under batch operation (500 ml) using configuration ‘b’ for Melamine in various supersaturations, well within the MSZ*

5.4.3 Applicability of flow cell for seed generation

The effectiveness of the flow cell for seed generation was characterized based on configuration c for AA. In those experiments a stream of solution exits the feed vessel, passes the flow cell in which it undergoes the US and flows back from the bottom of the flow cell to the feed vessel. The results showed that one pass through the flow cell does not provide enough residence time to induce primary nucleation. Therefore, a recirculation loop has been considered in which the solution circulates continuously around the flow cell and the feed vessel. To facilitate the monitoring of nucleation an FBRM probe was placed in the 1000 ml feed vessel in which the saturated solution was prepared initially. The start-up process lasted for 20 minutes after preparation of the saturated solution as the solution was pumped (100 ml/min) through the flow cell and allowed to drain away for twice the residence time (90 s) before closing the loop for recirculation of the solution. The draining procedure allowed removal of any left-over contaminants from being recirculated. Once the loop was closed, the process was started cooling down the solution to a temperature within the MSZW. The US was turned on once the desired temperature was reached. The temperature is controlled in the whole system. The US probe was immersed in the solution inside the US cell. The FBRM was placed inside the feed vessel. The rise in the number of particles in the vessel was continuously recorded to monitor the occurrence of nucleation.

The initial supersaturation of 1.33 has been used both in the experiments with and without US (silent conditions). Figure 5-3 shows the rise in particle counts as recorded by the FBRM during these experiments. In the absence of US around 120 minutes are required before nucleation is observed whereas when applying US, the nucleation is observed within 30 minutes. It should be noted that the increased surface area the additional tubing from the feed vessel to the flow cell, the presence of the the circulation pump and the flow cell all contribute in promoting nucleation and are responsible for the rate of change of particle counts under silent conditions.

To estimate the induction time the rate of change of particle counts can be extrapolated back to the background level. Figure 5-3 shows how the induction time is determined. The narrow peaks appearing in the FBRM signal of the blank experiment after almost 30 minutes (Figure 5-3a) is not considered as the onset of nucleation. After 120 minutes when the nucleation is clearly initiated, the counts rose approximately with the rate of 3-4 counts/min. In case of the US experiment the first outburst of nuclei is followed by a sharp increase in the counts, approximately 50 counts/min.

Figure 5-4 shows the experiment at a lower level of initial supersaturation (S=1.18). Only the experiments applying US is shown in Figure 5-4, since the blank experiment showed a much longer induction time. From the counts recorded by FBRM for these experiments the induction time is estimated to be longer than 20 minutes less than the blank experiment with supersaturation level of 1.33. This confirms the power of US to induce nucleation in much lower levels of supersaturation [33].

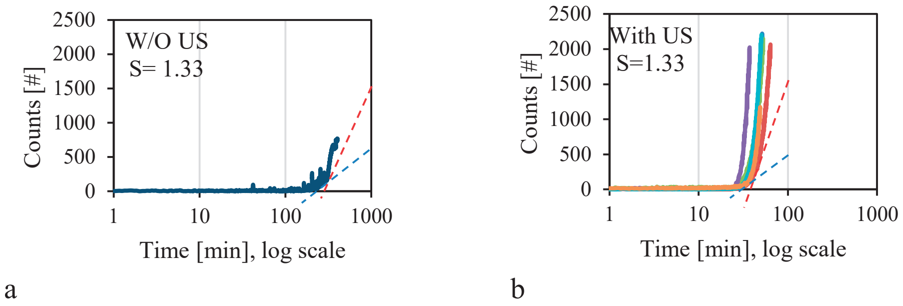

Figure 5-3 *Effect of US on nucleation kinetics of AA in batch operation a) blank experiment with initial supersaturation of 1.33, b) experiment with US at initial supersaturation of 1.33. The blue dashed lines indicating the slope of increase of counts before the outburst starts and red dashed lines show the outburst of crystals when the number of counts starts rising very sharply.*

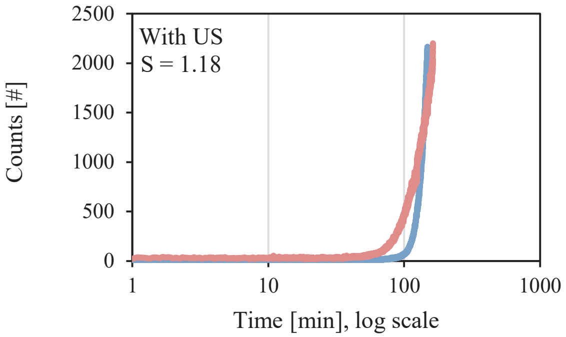

Figure 5-4 *US experiments with lower initial supersaturation of 1.18*

Figure 5-5 shows the laser diffraction based CSD of the samples collected at the exit of the flow cell. Samples of the suspension were taken at the time point when the FBRM indicated a value of 2000 counts, which was around 120 minutes for the blank experiment and 60 minutes when US was used. In the US experiment, almost a unimodal distribution with a peak at 40 µm is observed, while the experiment without US showed several peaks. It should be noticed that in the blank experiment the residence time is double due to the much lower count rate.

The peaks in the CSD of the blank experiment can be explained by multiple nucleation bursts at different timepoints during the experiment, which could result in peaks at 20 and 65 and 175 micron. The peaks in the FBRM total count trend between 30 and 120 minutes are caused by multiple nucleation bursts during the experiment. These multiple nucleation timepoints would lead to variations in the growth time in the experiment and thus to variation in crystals sizes resulting in a multimodal CSD. The occurrence of multiple nucleation events can be caused by the slower nucleation kinetics in the blank process resulting in a longer period of high, unconsumed supersaturation giving rise to additional nucleation events.

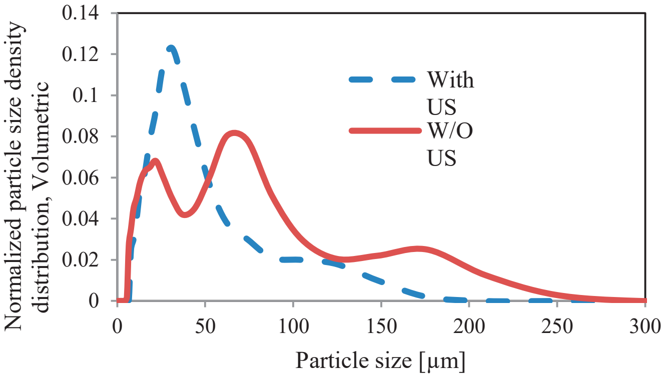

Figure 5-5 *Normalized particle size density distribution (volume based) of sample taken from US-assisted and blank process (S=1.33) at batch times of 60 min and 120 min corressponding to FBRM counts of 2000. (measured offline with laser diffraction device)*

Concluding the results show a clear effect of US influencing the induction time, the nucleation rate and the CSD. The mechanism with which US enables the nucleation in even low supersaturations is not fully known but several possibilities have been mentioned in the literature among which are primary nucleation via a reduction in the nucleation energy barrier, the high local supersaturation created by cavitation events [33, 43], or attrition of primary nuclei (probably generated earlier than can be visually observed). The latter can be either based on the spontaneous or US induced formation in the clear supersaturated solution of a single nucleus as described in the SNM or a low number of nuclei according to the CNT, which after growing to a certain size undergo secondary nucleation. As an alternative the primary nuclei could be formed by heterogeneous nucleation at the liquid air interface or at the wall and later undergo attrition [50]. Though it is essential to understand what mechanism is responsible when US-assisted experiments performs orders of magnitudes better in terms of nucleation rate and process yield, a repeatable procedure of seed generation is enough to proceed with the objective of this study, introduction of US generated seeds to the ALC and growing them to a desired size while having a narrow CSD due to suppression of secondary nucleation in the ALC.

In order to optimize the amount of seeds needed previously developed model validated for the kinetics of AA has been used [54]. A mathematical expression for the initial distribution is obtained by fitting two additive log normal distributions to the volume density distribution. The five parameters, $L_{g,1}$, $L_{g,2}$, σ_1, σ_2 and F_1, in equation 5-1 are used as fitting parameters. $L_{g,iI}$ is the geometric mean (location parameter), σ_i the geometric standard deviation (spread parameter), and F_1 gives the relative weighting of the two log-normal distributions.

$$\tilde{v}_0(L) = \frac{F_1}{L}\;\frac{1}{ln\sigma_1\sqrt{2\pi}}\;exp\left(-\;\frac{ln^2\left(\frac{L}{L_{g,1}}\right)}{2ln^2\sigma_1}\right) + \frac{1-F_1}{L}\;\frac{1}{ln\sigma_2\sqrt{2\pi}}\;exp\left(-\;\frac{ln^2\left(\frac{L}{L_{g,2}}\right)}{2ln^2\sigma_2}\right) \qquad (5\text{-}1)$$

The FBRM probe determines the chord length distribution (CLD) of the suspension and the number of crystals present in the solution. Very roughly we can assume that the square weighted chord length distribution recorded by the FBRM represents volume density distribution of the suspension [55] and the following fit was achieved for the seeds generated by US and ready to be introduced to ALC (Figure 5-6) and the counts corresponding to these distributions are 1000 and 2000. The fitting parameters are listed in Table 5-2. Since the number of seed crystals in experiment #2 was half of that of experiment #1, the residence time of the produced seeds in the seeding vessel was lower for experiment #2. Therefore the average size of these seeds was also smaller than the ones from experiment #1.

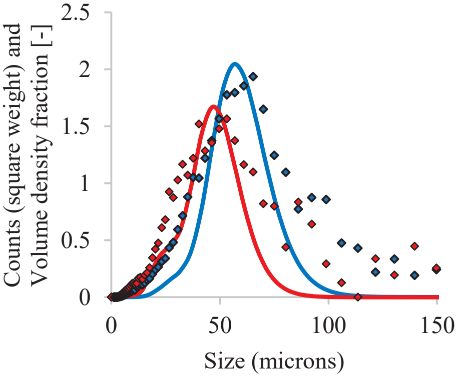

Figure 5-6 *FBRM chord length distribution of seeds generated with US (presented by markers) fitted with a volume density distribution equation in the model (presented by lines). Blue and red indicate the experiments with 2000 and 1000 counts of seeds respectively.*

Parameter	Fitted amount for 2000 counts	Fitted amount for 1000 counts
$L_{g,1}$	70×10^{-6}	50×10^{-6}
$L_{g,2}$	50×10^{-6}	30×10^{-6}
σ_1	1.23	1.23
σ_2	1.4	1.4
F_1	0.90	0.80

Table 5-2 *Fitting parameters of seeding population*

The initial distribution is fitted with the model estimating the crystal density to fit the supersaturation and the final quantiles. The following supersaturation profiles are expected as shown in Figure 5-7. Secondary nucleation in the ALC is formulated with surface nucleation in the developed model and the threshold is estimated as S=1.13 [54]. In these experiments the same threshold is used and is active through both experiments since both experiments are conducted with an intial supersaturation higher than 1.13.

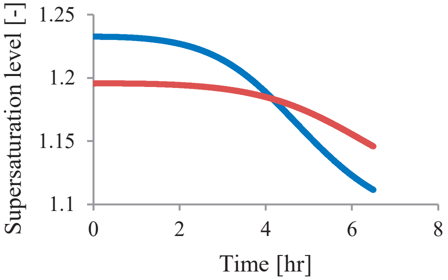

Figure 5-7 *Expected supersaturation level for seeds with counts of 2000 (experiment #1, blue) and 1000 (experiment #2, red)*

Having these preliminary results from the simulations shows that initial lower number of seeds leads to a slower reduction in supersatiuration level due to less available surface area. Therefore it takes much longer for experiment #2 than for experiment #1 to deplete the supersaturation. Achieving such an insight from the model experiments have been designed in which the seeds generated by US have been introduced to the ALC to grow larger in a cooling batch experiment.

5.5 US-ASSISTED SEED GENERATION FOR AN AIRLIFT CRYSTALLIZER

A fixed volume of the seeds (3 L) when reached the desired 2000 and 1000 counts based on FBRM results (experiments #1 and 2) were fed to the ALC, previously filled with a solution saturated at 40 °C and a batch cooling experiment was started applying a 3rd order cooling profile as follows (equation 5-2):

$$T(t) = T_s - (T_s - T_f)\left(\frac{t}{t_f}\right)^3 \qquad (5\text{-}2)$$

Where T_f is the temperature at the end of the batch time (t_f) and T_s is the seeding temperature. Figure 5-8 shows the ALC setup schematically.

The saturation temperature (T_{sat}), seeding temperature (T_s) and the final temperatures (T_f) for both experiments were 40 °C, 34.5 °C and 32.5 °C respectively. These selected temperatures are within the metastable zone at which no primary nucleation is expected to occur. This temperature range is selected in accordance with cooling batch experiments performed in ALC [2].

The evolution of the number of crystals inside the crystallizer was monitored and recorded using FBRM. Samples were collected from the ALC every 15 minutes in order to measure the density of the solution. At the end of the batch time samples are taken both from the top and bottom of the crystallizer to determine the final particle size distribution with the laser diffraction instrument.

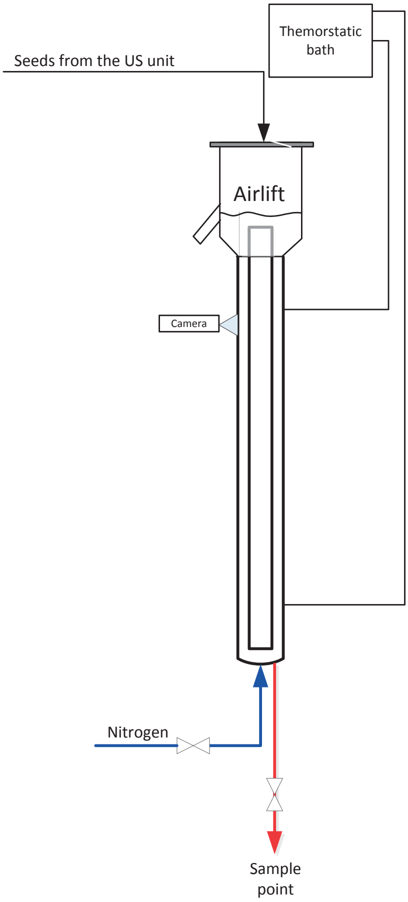

Figure 5-8 *Process flow diagram of the ALC setup for the cooling batch experiments*

Figure 5-9 shows the supersaturation profiles and final CSD of the products from these two experiments.

The supersaturation profile for both experiments shows three phases in the crystallization process in accordance with the simulation results; a drop of supersaturation in the first hour, a slight increase or stabilization of the supersaturation in the second hour and the drop of supersaturation for experiment #1 during last 4 hours and an almost constant supersaturation for experiment #2 in the same period.

Since in the third order cooling profile almost no supersaturation is generated in the first hour, the first drop can be explained by the consumption of supersaturation by the added seed crystals leading to their growth. Since the number of seeds in experiment #1 is double the one in experiment #2 this drop is sharper for experiment #1.

In the second hour the supersaturation is slightly rising or stabilizes which means that the generation of supersaturation via cooling is slightly higher or at least equal to the decrease caused by the growth of the crystals. This increase is stronger for experiment #2 since number and size of the added seeds is lower resulting in a lower surface area to consume the generated supersaturation.

In the third phase of these two experiments the consumption of supersaturation resulting in growth of seed crystals and secondary nuclei can be explained through the CSD (Figure 5-9b). The decreasing trend of supersaturation profile in the last 4 hours in experiment #1 has resulted in larger product size; however the bimodality of this CSD indicates that part of the drop in supersaturation profile is attributed to an ongoing event of secondary nucleation.

The constant supersaturation profile for experiment #2 indicates that the rates of generation and consumption of supersaturation were almost the same . The added seeds crystals of experiment #2 were smaller in size than the ones in experiment #1 due to shorter period of seed generation. The product crystals of this experiment were also smaller than the one from experiment #1. Apparently the lower number of seed crystals did not lead to a higher growth rate. The broader CSD of experiment #2 suggests a stronger secondary nucleation (surface nucleation) compared to experiment #1. Since the initial supersaturation for experiment #2 is lower, secondary nucleation (surface nucleation) might have started only in the third phase when the supersaturation has increased leading to a broader final CSD.

Comparing Figure 5-7 with Figure 5-9 suggests that the predicted trend in the supersaturation are in accordance with the results from the experiments, although the initial drop in the supersaturation is not well captured by the model. However the expected median size for experiment #2 is lower than the one predicted in the simulations which can be related to the different level of surface nucleation and the threshold used for the supersaturation in such experiments. It is recommended to optimize this threshold in the simulations based on these results in order to validate the model for such experiments.

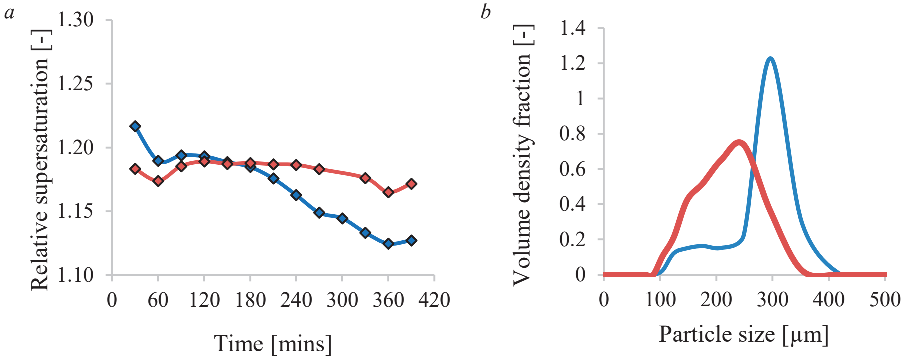

Figure 5-9 *Relative supersaturation profile and final CSD for experiments #1 and #2 in the ALC. Blue and red colors indicate the results for experiments #1 and #2 respectively.*

Figure 5-10 shows the relative supersaturation profile and final CSD for one of the conventional seeded batch experiments from [2] with similar initial supersaturation as used in experiments #1 and #2. T_{sat}, T_s and T_f for this experiment is 40 °C and 31.8 °C and 31 °C which are slightly different from the ones used in experiment #1 and 2. The desupersaturation in this experiment was stronger and therefore crystals grew to larger sizes.

Figure 5-11 shows a comparison between seeds prepared conventionally (size of 125 µm) [2] and the seeds of US after filtering and drying (size of 20-70 µm). Offline microscopic images are taken with Eclipse Ti-S Inverted Research Microscope. In-line images are taken with in-situ particle video microscope (PVM) which is placed beneath the gas disengagement zone in order to obtain live images of the crystals (Figure 5-8). What can be clearly seen when comparing offline microscopic images of seeds and products of [2] with the ones produced with US and later grown in ALC is the agglomeration/aggregation or maybe loose attachment of the latter. However, in the in-line images of the former agglomerated

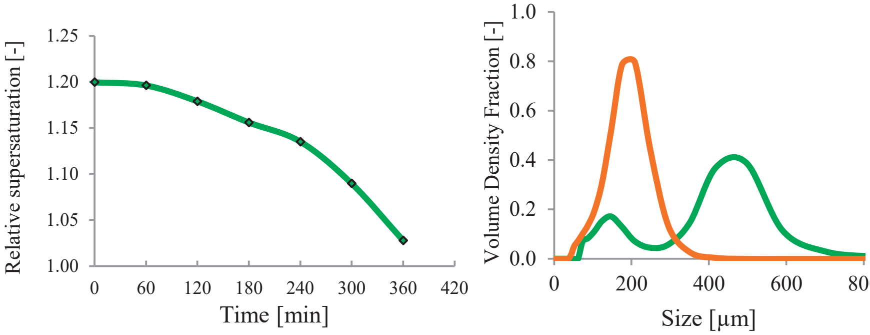

Figure 5-10 *Relative supersaturation profile and final CSD for experiment #9 from [2]. Orange and green indicate the results for seeds and experiment #9.*

crystals are also present (probably the fines) but the large product crystals (size of larger than 400 µm) are sharply faceted and not attached to each other. It is also stated in the literature that AA nuclei with size smaller than 50 µm tend to agglomerate due to its strong cohesive properties [56]. Therefore, it might be the reason why the in-line images of US seeds growing in ALC do not display clear single crystals. Nevertheless, a larger batch time might be the solution to let them grow larger and disaggregate later in the process.

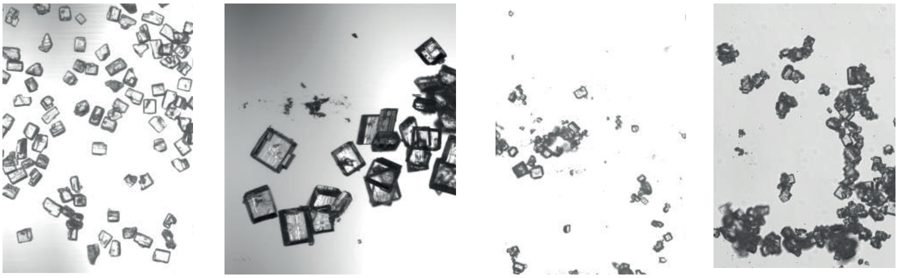

Seeds 125 µm from conventional method (Retch, AS200 Basic) with sieves, t=0

Product of ALC batch crystallization experiments with seeds 125 µm, t=6 hours

Seeds 20-70 µm from US, t=0

Product of ALC batch crystallization experiments with seeds 20-50 µm, t=6 hours

Microscopic images of the seeds and products

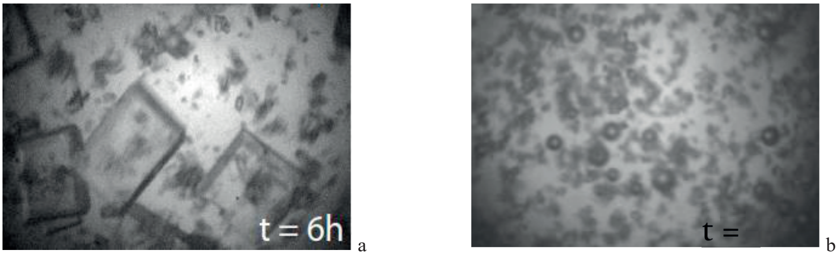

In-line photo taken at the end of the 6 hours batch experiment in ALC with seeds from a) Conventional seed preparation system and b) US

Figure 5-11 *Comparison of microscopic and in-line images of conventional and US generated seeds and product of ALC using these seeds*

All in all US as an alternative to conventional seed preparation methods has been tried out to generate seeds mainly to avoid the need for manual seed preparation and introduction to the system. Preliminary experiments using US generated seed crystals were successfully applied resulting in crystal product with a narrow CSD. The experiments showed, however, a high sensivity for the number of the seed crystals added to the crystallizer and the initial supersaturation of the solution at the seeding point. These process variables need further optimization, preferably making use of process model.

Also the reproducibility of the US seed generation needs further attentions. In our experience rather large variations in the rate of nuclei formation were found under similar conditions. On the other hand, the results using US generated seeds already gave comparable results to those of the conventional seeding optimised results [2].

In addition to the optimization of the seeding parameters, also the third order temperature profile, which causes the generation of the supersaturation to be slow in the first part and high in the last part of the batch was optimized for the experiments performed with seeds of 125 to 212 µm [2]. However, it may need to be once again exercised and optimized given the chance to apply various temperature profiles and initial supersaturation level for growth of US generated relatively small seeds.

From the current experiments we know that the US increases the nucleation rate and the size and volume density is somehow controllable but there is room to improve the seeds quality and to manipulate the US seed generation process to achieve the desired characteristics as well. Therefore, the question of “Is US seeding an alternative for conventional seeding?” can be preliminarily answered by “yes” but a more detailed study is needed considering all the aforementioned aspects before designing and optimizing continuous or semi-continuous US-seeded crystallization experiments in an ALC.

5.6 CONCLUSIONS AND RECOMMENDATIONS:

- Under batch configurations a clear effect of US on enhancing nucleation rates has been observed for three model compounds.
- Low supersaturation is critical to the success of nucleation control through the application of US, as at high supersaturation the risk of primary nucleation is high.
- Working with a model system which is difficult to nucleate (i.e. has a large MSZW) would be better suited to exploit US for nucleation control.
- Research is still needed to design US setups in which the residence time distribution is minimal and good spatial control of the power of the US is achieved.

- A narrow CSD has been achieved for the cooling batch experiments in ALC with larger number of counts of seed crystals. However, the probable contribution of secondary nucleation (surface nucleation) made the CSD bimodal. The lower number of counts meaning also smaller seed crystals resulted in broader CSD which suggest that the secondary nucleation has started later in the process.
- In some of the experiments settling of particles was visually observed. Our observations with the flow cell showed that the mixing in flow cell should be improved.
- The developed model validated for kinetics of AA was able to produce similar supersaturation profile as seen in the experiments. However, secondary nucleation (surface nucleation) should be optimized in order to achieve better agreement in CSD representation.
- Ideally, the idea is to directly attach the US seed generator to the ALC in order to design a continuous crystallization process from nucleation to growth to the desired product size and CSD. However, the design of the setup and the process conditions need to be initially optimized. Recommendation is to firstly extend the existing model based on the results presented here. Secondly, new experiments can be designed based on the optimization of simulation results.

5.7 REFERENCES

1. Su, Q., Z.K. Nagy, and C.D. Rielly, *Pharmaceutical crystallisation processes from batch to continuous operation using MSMPR stages: Modelling, design, and control.* Chemical Engineering and Processing: Process Intensification, 2015. **89**: p. 41-53.
2. Lakerveld, R., J.J. Van Krochten, and H.J. Kramer, *An air-lift crystallizer can suppress secondary nucleation at a higher supersaturation compared to a stirred crystallizer.* Crystal growth & design, 2014. **14**(7): p. 3264-3275.
3. Chung, S.H., D.L. Ma, and R.D. Braatz, *Optimal seeding in batch crystallization.* The Canadian Journal of Chemical Engineering, 1999. **77**(3): p. 590-596.
4. Ward, J.D., D.A. Mellichamp, and M.F. Doherty, *Choosing an operating policy for seeded batch crystallization.* AIChE Journal, 2006. **52**(6): p. 2046-2054.
5. Kalbasenka, A.N., et al., *Application of Seeding as a Process Actuator in a Model Predictive Control Framework for Fed-Batch Crystallization of Ammonium Sulphate.* Particle & Particle Systems Characterization, 2007. **24**(1): p. 40-48.
6. Eder, R.J.P., et al., *Seed loading effects on the mean crystal size of acetylsalicylic acid in a continuous-flow crystallization device.* Crystal Research and Technology, 2011. **46**(3): p. 227-237.
7. Narducci, O., A. Jones, and E. Kougoulos, *Continuous crystallization of adipic acid with ultrasound.* Chemical engineering science, 2011. **66**(6): p. 1069-1076.
8. Louhi-Kultanen, M., et al., *Crystallization of glycine with ultrasound.* International journal of pharmaceutics, 2006. **320**(1): p. 23-29.
9. Kaur Bhangu, S., M. Ashokkumar, and J. Lee, *Ultrasound Assisted Crystallization of Paracetamol: Crystal Size Distribution and Polymorph Control.* Crystal Growth & Design, 2016. **16**(4): p. 1934-1941.
10. Kadam, S.S., et al., *A new view on the metastable zone width during cooling crystallization.* Chemical engineering science, 2012. **72**: p. 10-19.
11. Hem, S.L., *The effect of ultrasonic vibrations on crystallization processes.* Ultrasonics, 1967. **5**(4): p. 202-207.
12. Amara, N., et al., *Crystallization of potash alum: effect of power ultrasound.* Ultrasonics sonochemistry, 2001. **8**(3): p. 265-270.
13. Li, H., et al., *Rapid sonocrystallization in the salting-out process.* Journal of Crystal Growth, 2003. **247**(1): p. 192-198.
14. Guo, Z., et al., *Effect of ultrasound on anti-solvent crystallization process.* Journal of Crystal Growth, 2005. **273**(3): p. 555-563.
15. De Castro, M.L. and F. Priego-Capote, *Ultrasound-assisted crystallization (sonocrystallization).* Ultrasonics sonochemistry, 2007. **14**(6): p. 717-724.
16. Mullin, J.W., *Crystallization*. 2001: Butterworth-Heinemann.
17. Castillo-Peinado, L.d.l.S., L. de Castro, and M. Dolores, *The role of ultrasound in pharmaceutical production: sonocrystallization.* Journal of Pharmacy and Pharmacology, 2016. **68**(10): p. 1249-1267.
18. Qiu, L., et al., *Effect of power ultrasound on crystallization characteristics of magnesium ammonium phosphate.* Ultrasonics Sonochemistry, 2017. **36**: p. 123-128.
19. Xiouras, C., et al., *Attrition-enhanced deracemization of NaClO3: Comparison between ultrasonic and abrasive grinding.* Crystal Growth & Design, 2015. **15**(11): p. 5476-5484.
20. Sander, J.R., B.W. Zeiger, and K.S. Suslick, *Sonocrystallization and sonofragmentation.* Ultrasonics sonochemistry, 2014. **21**(6): p. 1908-1915.

21. Wohlgemuth, K., F. Ruether, and G. Schembecker, *Sonocrystallization and crystallization with gassing of adipic acid.* Chemical Engineering Science, 2010. **65**(2): p. 1016-1027.
22. Jordens, J., et al., *Sonofragmentation: Effect of Ultrasound Frequency and Power on Particle Breakage.* Crystal Growth & Design, 2016.
23. Ruecroft, G., et al., *Sonocrystallization: the use of ultrasound for improved industrial crystallization.* Organic Process Research & Development, 2005. **9**(6): p. 923-932.
24. McCausland, L.J., P.W. Cains, and P.D. Martin, *Use the power of sonocrystallization for improved properties.* Chemical engineering progress, 2001. **97**(7): p. 56-61.
25. Anderson, H.W., et al., *Crystallization of adipic acid*. 1995, Google Patents.
26. Chow, R., et al., *A study on the primary and secondary nucleation of ice by power ultrasound.* Ultrasonics, 2005. **43**(4): p. 227-230.
27. Yaminsky, V., et al., *Nucleation and coagulation effects of ultrasound during precipitation in solution.* Kolloidnyi Zhurnal, 1991. **53**(1): p. 100-104.
28. Kordylla, A., et al., *Towards an optimized crystallization with ultrasound: effect of solvent properties and ultrasonic process parameters.* Journal of Crystal Growth, 2008. **310**(18): p. 4177-4184.
29. Bhoi, S. and D. Sarkar, *Modelling and experimental validation of ultrasound assisted unseeded batch cooling crystallization of l-asparagine monohydrate.* CrystEngComm, 2016.
30. Devarakonda, S., J.M. Evans, and A.S. Myerson, *Impact of ultrasonic energy on the crystallization of dextrose monohydrate.* Crystal growth & design, 2003. **3**(5): p. 741-746.
31. Lyczko, N., et al., *Effect of ultrasound on the induction time and the metastable zone widths of potassium sulphate.* Chemical Engineering Journal, 2002. **86**(3): p. 233-241.
32. Nishida, I., *Precipitation of calcium carbonate by ultrasonic irradiation.* Ultrasonics Sonochemistry, 2004. **11**(6): p. 423-428.
33. Virone, C., et al., *Primary nucleation induced by ultrasonic cavitation.* Journal of crystal Growth, 2006. **294**(1): p. 9-15.
34. Devarakonda, S., J.M. Evans, and A.S. Myerson, *Impact of ultrasonic energy on the flow crystallization of dextrose monohydrate.* Crystal growth & design, 2004. **4**(4): p. 687-690.
35. Nalajala, V.S. and V.S. Moholkar, *Investigations in the physical mechanism of sonocrystallization.* Ultrasonics sonochemistry, 2011. **18**(1): p. 345-355.
36. Cains, P.W., P.D. Martin, and C.J. Price, *The use of ultrasound in industrial chemical synthesis and crystallization. 1. Applications to synthetic chemistry.* Organic process research & development, 1998. **2**(1): p. 34-48.
37. Guo, Z., A. Jones, and N. Li, *The effect of ultrasound on the homogeneous nucleation of BaSO4 during reactive crystallization.* Chemical engineering science, 2006. **61**(5): p. 1617-1626.
38. Skorb, E.V., H. Möhwald, and D.V. Andreeva, *Effect of Cavitation Bubble Collapse on the Modification of Solids: Crystallization Aspects.* Langmuir, 2016. **32**(43): p. 11072-11085.
39. Kordylla, A., et al., *Modeling ultrasound-induced nucleation during cooling crystallization.* Chemical Engineering Science, 2009. **64**(8): p. 1635-1642.
40. Grossier, R., O. Louisnard, and Y. Vargas, *Mixture segregation by an inertial cavitation bubble.* Ultrasonics Sonochemistry, 2007. **14**(4): p. 431-437.
41. Li, H., et al., *The application of power ultrasound to reaction crystallization.* Ultrasonics sonochemistry, 2006. **13**(4): p. 359-363.
42. Jordens, J., et al., *The effects of ultrasound on micromixing.* Ultrasonics sonochemistry, 2016. **32**: p. 68-78.

43. Gielen, B., et al., *Characterization of stable and transient cavitation bubbles in a milliflow reactor using a multibubble sonoluminescence quenching technique.* Ultrasonics Sonochemistry, 2015. **25**: p. 31-39.
44. Jiang, M., et al., *Indirect ultrasonication in continuous slug-flow crystallization.* Crystal Growth & Design, 2015. **15**(5): p. 2486-2492.
45. Jamshidi, R., et al., *Investigation of the Effect of Ultrasound Parameters on Continuous Sonocrystallization in a Millifluidic Device.* Crystal Growth & Design, 2016. **16**(8): p. 4607-4619.
46. Gielen, B., et al., *Energy efficient crystallization of paracetamol using pulsed ultrasound.* Chemical Engineering and Processing: Process Intensification, 2017. **114**: p. 55-66.
47. Gielen, B., et al., *Ultrasonic precipitation of manganese carbonate: Reactor design and scale-up.* Chemical Engineering Research and Design, 2016. **115**: p. 131-144.
48. Myerson, A., *Handbook of industrial crystallization*. 2002: Butterworth-Heinemann.
49. Kashchiev, D., *Nucleation*. 2000: Elsevier.
50. Kadam, S.S., H.J. Kramer, and J.H. ter Horst, *Combination of a single primary nucleation event and secondary nucleation in crystallization processes.* Crystal Growth & Design, 2011. **11**(4): p. 1271-1277.
51. Gahn, C. and A. Mersmann, *Brittle fracture in crystallization processes Part A. Attrition and abrasion of brittle solids.* Chemical Engineering Science, 1999. **54**(9): p. 1273-1282.
52. Kimura, T., et al., *Standardization of ultrasonic power for sonochemical reaction.* Ultrasonics Sonochemistry, 1996. **3**(3): p. S157-S161.
53. Dodds, J., et al., *The Effect of Ultrasound on Crystallisation-Precipitation Processes: Some Examples and a New Segregation Model.* Particle & Particle Systems Characterization, 2007. **24**(1): p. 18-28.
54. Anisi, F. and H.J.M. Kramer, *Crystallization kinetics in an airlift and a stirred draft tube crystallizer; Secondary nucleation models revisited.* Chemical Engineering Research and Design, 2018.
55. Li, M., D. Wilkinson, and K. Patchigolla, *Comparison of particle size distributions measured using different techniques.* Particulate Science and Technology, 2005. **23**(3): p. 265-284.
56. Kawashima, Y., et al., *Development of Agglomerated Crystals of Ascorbic Acid by the Spherical Crystallization Technique for Direct Tableting, and Evaluation of Their Compactibilities [Translated].* KONA Powder and Particle Journal, 2002. **20**: p. 251-262.

Chapter 6

Conclusions and Recommendations

The feasibility of the task-based design approach for crystallization processes, in which the key phenomena of crystallization are realized in separated equipment, has been developed and confirmed at Delft University of Technology by A.R. Menon and R. Lakerveld. In this thesis a number of such task-based unit operations, such as crystal growth in an airlift crystallizer, seed generation in an ultrasonic induced nucleation device and supersaturation generation in a membrane unit have been experimentally characterized and verified both as stand-alone unit operations and as integrated into a crystallization process.

- *To support the research and design of such processes, firstly, a modelling framework is developed in which crystallization kinetics are validated based on a set of seeded batch experiments in the airlift crystallizer.*
- *To facilitate the design and the integration of the membrane unit the model is further extended by adding membrane distillation section. The membrane distillation unit has been individually characterized through experiments, modelled and optimized in order to be used in the integrated system of membrane-assisted crystallization, MaC.*
- *Through several process flexibilities and manipulation possibilities continuous MaC experiments in the airlift crystallizer seem potentially to be the next area of development in the task-based design methodology. Therefore, continuous MaC experiments in the airlift crystallizer were designed using the developed model and performed which confirms the capability of the model and demonstrates the possibility of further manipulation of product quality and optimization of process performance in such a system.*
- *Since all of the mentioned experiments are seeded and seed preparation from crystal product is not the most efficient way, an ultrasound setup has been designed and used to generate seeds from a solution. Batch experiments in the airlift crystallizer using ultrasound generated seeds showed promising results for further integration of such a unit operation in a continuous crystallization process.*
- *Having shown the successful integration of task-based designed elements a necessary step is to define optimization problems to study the window of available combinations of operational parameters for stable operation.*

In Chapter 2, a dynamic parameter estimation study has been performed in order to investigate the right kinetic models in an airlift crystallizer (ALC) and to compare the kinetics with a draft tube stirred crystallizer (DTC). Low mechanical forces on the crystals and sufficient mixing in airlift crystallizer lead to crystal growth as the dominant kinetic mechanism and the secondary nucleation to be suppressed the rate of which can be estimated. The two-step model for growth which takes the hydrodynamic of the crystallizers into account found to be relevant in both types of crystallizers. The secondary nucleation in the ALC was best described by a supersaturation dependent surface nucleation, while in the DTC, this nucleation could only be described when both the surface nucleation model and the attrition model of Evans was applied. The statistical analysis of the results showed an acceptable precision in the estimated parameters. Therefore, strong suppression of attrition in the ALC compared to the DTC due to mild shear forces and the lower values of the rate constants for the surface nucleation model explain the often observed, undesired early nucleation events in DTCs.

The developed kinetic model can be used in solving optimization problems based on various process conditions in order to design new experiments and to define the window of operation for batch and continuous crystallization experiments in the airlift crystallizer.

The developed modelling framework is a generic framework where individual tasks can be considered in every processing unit. The methodology allows for formulation of a superstructure optimization problem and solving it in order to identify the optimal process flowsheet structure from the possible alternatives. Development of such a superstructure can help scaling up the process.

In chapter 3 a Liqui-Cel® Extra flow membrane module was used to concentrate a solution of L-ascorbic acid (AA) in water with the aim of supersaturation generation for crystallization processes. The results show that sweeping gas membrane distillation (SGMD) can successfully be applied for compounds with high osmotic pressures and allows for crystallization at low temperatures and forms an attractive alternative for evaporative crystallization. The application of MaC-SGMD enhances the application field for membrane-assisted crystallization considerably. A model coupling mass and heat transfer was developed to predict the membrane flux and to investigate the temperature and concentration polarization. According to the characterization experiments it has been found straightforward to manipulate the rate of solvent removal by means of changing process conditions. Feed temperature and air flow rate have been found as controlling parameters. Air flow rate has been found as the best parameter for this manipulation since it influences the flux promptly. Since the predicted membrane flux is in accordance with the results from the experiments, the model can be used for further MaC investigations.

Scale-up or scale-out of membrane unit should be studied further in order to ensure sufficient rate and level of supersaturation generation for an industrial scale crystallizer.

In chapter 4 continuous cooling crystallization experiments are performed. Application of kinetic model developed and validated for batch cooling crystallization experiments resulted in acceptable outcome for mentioned continuous experiments.

Continuous membrane-assisted crystallization experiments in the ALC have been performed for the first time and the results confirm the possibility and present the flexibility of designing such experiments.

In order to ensure process stability (reaching steady state) and stable product quality the continuous membrane-assisted crystallization experiments in the ALC should be designed and performed for a longer period (more than 4 residence times) wherefore the model can be used as a design tool.

Other model compounds can be tested to ensure the capacity of continuous membrane-assisted crystallization experiments in the airlift crystallizer to be applied for different systems.

In chapter 5 it is observed that the application of ultrasound (US) enhances the nucleation rate. Nucleation at low supersaturations, well within the MSZW, is targeted to avoid excessive nucleation leading to fines formation and hence poor size distribution. Pulsed US has been used in two configurations of inserting US horn in a vessel and using a flow-through-cell in where US probe is inserted. From the current experiments we know that the ultrasound increases the nucleation rate and the size and volume density is somehow controllable. Seeds generated by US have been applied to the ALC and a narrow crystal size distribution (CSD) has been achieved for the cooling batch experiments in ALC. However, there are rooms to improve the seeds quality and to manipulate the process to achieve the desired characteristics as well and these needs to be particularly done for every compound. Whether US seed generating unit can be an alternative for conventional seeding methods needs a more detailed study considering the mentioned aspects and only then continuous or semi-continuous ultrasound seeded crystallization experiments can be designed and optimized.

Ideally, the idea is to directly attach the US seed generator to the ALC in order to design a continuous crystallization process starting from nucleation followed by growth of the nuclei to the desired product size and CSD. However, design of the setup and the process conditions need to be initially optimized. Recommendation is to firstly extend the existing model based on the results presented here. Secondly new experiments can be designed based on the optimization of simulation results.

LIST OF PUBLICATIONS

1. Continuous Crystallization of L-ascorbic acid Using Airlift Crystallizer and Membrane Distillation
   F. Anisi, A. Potia, H.J.M. Kramer
   (in preparation)
2. Crystallization Kinetics in an Airlift and a Stirred Draft Tube Crystallizer; Secondary Nucleation Models Revisited
   F. Anisi, H.J.M. Kramer
   Chemical Engineering Research and Design; Published 2018
3. Membrane-assisted Crystallization: Membrane Characterization, Modelling and Experiments
   F. Anisi, K. Mathew Thomas, H.J.M. Kramer
   Chemical Engineering Science; Published 2017
4. Membrane Crystallization Technology and Process Intensification
   H.J.M. Kramer, **F. Anisi**, B.H. Eral, A.I. Stankiewicz
   Chapter in book: Reference Module in Chemistry, Molecular Sciences and Chemical Engineering, Published 2017
5. Applying Shear Stress to Endothelial Cells in a New Perfusion Chamber: Hydrodynamic Analysis.
   F. Anisi, N. Salehi-Nik, G. Amoabediny, B. Pouran, N. Haghighipour, B. Zandieh-Doulabi.
   Journal of Artificial Organs; Published 2014
6. The Effect of Nitric Acid, Ethylenediamine, and Diethanolamine Modified Polyaniline Nanoparticles Anode Electrode in a Microbial Fuel Cell
   M. Ghasemi, W.R. WanDaud, N. Mokhtarian, A. Mayahi, M. Ismail, **F. Anisi**, M. Sedighi, J. Alam.
   International Journal of Hydrogen Energy; Published 2013
7. Engineering Parameters in Bioreactor's Design: A ritical Aspect in Tissue Engineering
   N. Salehi-Nik, G. Amoabediny, B. Pouran, H. Tabesh, MA. Shokrgozarm, N. Haghighipour, N. Khatibi, **F. Anisi**, K. Mottaghy, B. Zandieh-Doulabi
   Biomedical Research International; Published 2013

PORTFOLIO

(Inter)national conferences

2013	R. Lakerveld, J. Van Krochten, **F. Anisi**, A.I. Stankiewicz, H.J. M. Kramer Crystallization of L-ascorbic acid in a 18-liter airlift crystallizer, AIChE (San Francisco, US)
2013	R. Lakerveld, S. F. M. Goddrie,.**F. Anisi**, A.I. Stankiewicz, H.J.M. Kramer, Membrane-Assisted Crystallization of L-ascorbic Acid, AIChE (San Francisco, US)
2014	**F. Anisi**, J.J. van Gaalen, J. J.H. van Krochten, P. Vonk, R. Lakerveld, H.J.M. Kramer, Crystallization Kinetics in an Airlift Crystallizer: A Parameter Estimation Study, AIChE (Atlanta, US)
2014	**F. Anisi** , K. Mathew Thomas, R. Lakerveld, H.J.M. Kramer, Sweeping Gas Membrane Distillation: Modelling and Experiments in Assisting Crystallization of L-ascorbic acid, BIWIC (Rouen, France)
2014	**F. Anisi**, J. van Krochten, J. Jansen van Gaalen, R. Lakerveld, H.J.M. Kramer, Kinetic Parameter Estimation for Batch Crystallization of Ascorbic Acid: A Comparison between an Airlift and Stirred Crystallizer, ISIC (Toulouse, France)
2014	**F. Anisi**, H.J. Kramer , Modelling and Optimization of Membrane-assisted Crystallization of L-ascorbic acid Using an Airlift Crystallizer, NPS (Utrecht, the Netherlands)
2014	**F. Anisi**, R. Lakerveld, H.J.M. Kramer, Kinetic Parameter Estimation for Crystallization of L-ascorbic acid: Comparison of Airlift Crystallizer with Conventional Stirred crystallizer, EYEC (Warsaw, Poland)
2014	**F. Anisi** , R. Lakerveld, H.J.M. Kramer, Application of Sweeping Gas Membrane Distillation to Assist Crystallization of L-ascorbic Acid, DECHEMA (Munster, Germany)
2015	**F. Anisi**, H.J.M. Kramer, Continuous Crystallization of L-ascorbic acid: Integration of Airlift Crystallizer with Membrane Distillation-Experiments and Results, AIChE (Salt Lake City, US)
2015	**F. Anisi**, H.J.M. Kramer, Continuous Crystallization of L-ascorbic acid: Integration of Airlift Crystallizer with Membrane Distillation-Experiments and Results, BACG (London, UK)
2015	**F. Anisi**, H.J. Kramer, Modelling and Optimization of Crystallization process of L-ascorbic acid: Integration of airlift crystallizer with Membrane distillation (Magdeburg, Germany)
2016	**F. Anisi**, H.J.M. Kramer, Continuous Crystallization of L-ascorbic Acid: Integration of Airlift Crystallizer with Membrane Distillation-Experiments and Results, AIChE (San Francisco, US)
2018	**F. Anisi**, H. Burak Eral, H.J.M. Kramer, Modelling Crystallization Kinetics in Airlift and Stirred Crystallizers; Secondary Nucleation Models Revisited, BACG (Limerick, Ireland)

ABOUT THE AUTHOR

Fatemeh Anisi was born on February 4th 1987 in Kerman, Iran. She went to University of Tehran in 2005 to study in the field of Chemical Engineering. She graduated in 2009 and started her MSc in the field of Chemical Engineering-Biotechnology in the same university. She graduated in 2011 and moved to the Netherlands to continue her studies in the PDEng program for Bioprocess Engineering in 2012 in Technical University of Delft. After completion of the first year she has got an offer for a PhD program under supervision of Dr. ir. Herman J.M. Kramer and therefore merged her PDEng second year project with the first year of her PhD. She graduated from the PDEng in 2015. Her PhD dissertation entitled “Control of the Key Phenomena in Continuous and Batch Crystallization Processes; Novel Process and Equipment Design” resulted in research publications in different scientific journals and conferences’ proceedings. She has presented her research in different national and international conferences. She partially collaborated with DSM in the Netherlands and her project was part of the European Commissions Framework 7 program through the OPTICO consortium. Since February 2017 she is working in AkzoNobel as a Development Process Engineer where she pursues her passion about design and optimization of chemical processes.

ACKNOWLEDGMENT

It is New Year 2018 and I come up with a resolution: “Shall this year be the year I finish my thesis”. It was easy said than done! Answering over and over the questions such as: “When are you finishing?”, “Do you have a draft?”, “Why don’t you tell your supervisor that you cannot work anymore?”, “Finish it faster, why does it take so long?”. Finally, I have traveled the long road of writing a thesis to completion. On the way, I have obviously experienced that writing a PhD thesis on the fringe of working life is far from easy and now I know the value of a free weekend which I experienced finally on 25th August 2018 for the first time since I have started working on 1st February 2017.

For the four year journey of my PhD and the 20 extra months of making a convincible thesis to my supervisors I do need to thank many people:

To my great supervisor, Herman Kramer: I not only learnt teaching and research from you but also patience and large-heartedness. You have been a very supportive, kind and patient supervisor to me. I have gone through many happy and sad moments in my life during these years, from my marriage to the loss of my mom, and I could feel your never-ending support and care. I appreciate the ‘believe’ you had in me as I was not able to go through all of this without you. You meant definitely more than a supervisor to me. I learnt from you that being kind and honest to people makes the life more beautiful and I see this beauty in your life. I am always grateful for this opportunity in my life to be student of you. I would like to express here how much I learnt from you and how much I enjoyed working with you and will remember you as a symbol of altruism and patience.

To my promoter Prof Andrzej Stankiewicz: The first thing I will always remember from you is your generosity. Thanks a lot for providing me with the opportunity to work in your team and enjoy your leadership attitude. You were always careful with bringing a balance to our PhD life and you have given me also the chance to sometimes play a role in our social programs. Without you it could never be possible to make such great friends and make such great memories. I appreciate your confident in me which let me grow my independence in doing research. You will remain in my heart as a symbol of generosity and liberality.

To my company advisor, Pieter Vonk: Thanks a lot for giving me the opportunity to learn from your outstanding industrial experience in DSM.

I would also like to thank Dr Behrouz for his good referencing which in the first place brought me this opportunity to be able to start my PhD.

Also I should thank Nasim for being my first-travel-to-Europe partner. We have participated in our first international biomedical (!) conference together and explored a lot together and now I am happy to have her close by living in Twente with Arman.

To my lovely mom who is not in this world anymore to see this day: My Kermani mom with her beautiful accent which I will miss for the rest of my life. Maman joon how sad it is that I am finally realizing the dream you always had for me but you are not here anymore to be proud of not me but of yourself for being such a great person. You have always said: “Because I could not continue my education due to loss of my mom, I will do whatever is necessary to see you as a doctor (in the highest levels of education)” and she did her best. I could never be able to see such a day without her efforts. She was the most altruistic benevolent person I have ever seen in my life. Thanks for being my mom for 30 years and 362 days. You left me with a “Happy Birthday 31 year old girl” three days before my birthday. May your soul be in peace. Every night I sleep I hope to see you in my dreams to moderate how much I miss you these days.

هر شب اگر بخوابم با تو قرار دارم
حسرت همیشه باقیست دیدار پشت دیدار

To my dedicated hard-working dad: Thanks for being always the best support for our little family. Your endless patience and peace especially during the time mom was under treatment taught me how to battle the toughest and melancholiest moments of this world. Your attitude of never expecting anything from anyone and never getting upset with anyone taught me to become a stronger person. You always believed in freedom and always gave me freedom to choose. I owe you my becoming an independent person. Thanks babaee joonam.

عاشقی را که چنین باده ی شبگیر دهند
کافر عشق بود گر نشود باده پرست

My little brother Mohammad: I always pulled your leg when we were kids which I am very sorry for. You did dedicated all your life and time when mom was sick and I was far. My little engineer I wish you a bright happy future from the bottom of my heart and thanks for being always online to talk even if we are still pulling each other’s leg.

کلاه سروریت کج مباد بر سر حسن
که زیب بخت و سزاوار ملک و تاج سری

When I talk about my family I cannot only talk about dad, mom and little brother. From my childhood I have seen my aunt’s family always as part of our family. I have grown up with Nahid, Homa and Hamid and I consider them as my sisters and brother. Nahid with her two beautiful girls, Yas and Rose, and her husband, Javad, is now my best daily advisor. Yas is now not even a little girl anymore but the great designer of my book cover! Homa with her little strong boy, Amid, and her husband, Mohammad, is my big sister on who I can always trust and Hamid with his two lovely kids, Arghavan and Sepehr, and his wife, Nafiseh, is as of a backup strong supporter to me. Although I have lost my aunt’s husband, Agha ame joon, in 2015, I never forget his cordiality and warmth. My tolerant indulgent aunt was always a sister to my mom and I am grateful to have her.

I believe it is not the physical distance which determines the love. My uncle David in US has always encouraged me to fight for higher and higher education in better and better places. We say the apple does not fall far from the tree. Apart from getting my PhD, I am sure I have got my love for networking from this uncle of mine.

To my office mates and friends: In the first year of my PhD I enjoyed being in one office with Mahinder, Dennis, George and Jurriaan. Marloes, Rohit and Weiwei were my officemates from the second year of my PhD. Marloes was always open to have a cup of coffee and chat. All problems with PhD, procedures, living in the Netherlands and going along with people around could be solved in a way or another when talking to her. Although we made so much fun during her PhD real presentation, I must admit she can take jokes and she has a very good sense of humor. Her game mate, Weiwei was not only my office mate in my PhD but also in my PDEng. I always admire his dedication to his work. I will never forget his cute face when drinking alcohol or when being excited about something. I wish him a very happy life together with Wenli, my chinuch friends. Last but not least was Rohit whom I have played tennis with somewhere in the end of 2012 and never imagined that he is going to be my office mate one day! Thanks to all of you for making the office a pleasant place to work in.

To my other friends in the faculty: I would like to thank Maryam for her always being ready to chat and always being kind to me.

I would like to thank Richard, Ali, Lalit, Javier, Hossein, Ahmadreza, Meng, Daniel, Guido, Karsten, Tim, Nikolaos, Noura, Vilborg, Vincent, Sergio, Gustavo, Mayra, Sathish, Uttiya, Sabrine and whoever I forgot here to mention for making such an international community and for being nice and friendly.

I should not forget to thank the staff members who are always trying to facilitate our life at university; Leslie and Helma for being very helpful and always smiling, Rob for his never ending solution findings, Michel, Jaap, Ad, Daniel, Martijn and Lennart for helping me during my experiments.

I would like to thank my students who not only worked hard and made great pieces of research for themselves but also gave me the opportunity to learn how to play the role of a coach/supervisor.

Kiran is now in Hong Kong doing his PhD. I am happy I have worked with him and we have published together. Jurian works now in Munich. Although he is originally Dutch, he was never born to live in the Netherlands. Whenever he was not to be found in the university, I could easily suspect he is now climbing in France, Switzerland or Germany. I am happy that he could finally find a job in a mountainy city of Munich. Aisa works now in Witteveen+Bos. She was a very disciplined neat one and I enjoyed working with her and wish her success in her life. Werin as my very hard-working student did almost everything to make the setup ready for continuous experiments in the time when the whole department was busy moving to the new building. He is now working in LyondellBasell and sometimes we pass each other in A4 or 15 towards Botlek. I wish him a lot of success as well. My last but not least students were Akiff and Poornima. Akiff is now working in Teva pharmaceuticals and Poornima is a colleague of Weiwei in FrieslandCampina. Both have done great job and deserve a bright future.

Beside my friends and students inside my field of study I had the chance to get to know many people in the Netherlands, not only because I love to know more people to grow my social community more and more but also because they were friendly and meaningful to me. I would like to thank Noa and Diana as now becoming almost 7 years old friends, Yasmin, Mahsa, Mar, Mahshid, Amin K, Somi and Mohi, Samira and Saleh, Samira and Mohammadali, Fahimeh and Amin, Arash, Atefeh and Alex with their little Roshanak and Parvaneh, Setareh and Michiel with their little Amber, Farzaneh, Sanaz and Shahab with their little Daniel, Zahra, Shirin and Yasser with their little Yassan and Yarin, Elnaz, Solmaz and Yashar, Shahrzad and Amir with their little Delaram, Hengameh and Hamid, Sara and Khashayar, Vincent, Robin, Janneke, Eveline, Maryam and Amin and their little Kian, Yasaman and Ashkan with their little expecting son, Sadaf, Wijbrand, Silvia and Abboy, Farnaz and Meysam and their little expecting son, Anamaria and Cristian with their little son, Erfan, Iza, Reyhaneh and Hamid, Laurens, Ana, Mark, Shadi and Danny, Katia and Barry, Parisa and Mohsen, Rudy, Anneclaire, Susana, Judith, Zohreh, Shabnam and Salar with their little Elena, Jose Francisco, Ariana, Cora, Elyas, Samir, Maryam and Hamid, Maria, Azadeh and Stefan.

And my friends in Iran, Maryam and Hamid with their little Armin, Elaheh and Payam, Noushin, Sama, Farnaz, Fatemeh, Bahareh, Shirin, Maryam, Naghmeh and many others.

I should also thank my lovely dutch teacher Jos de Neve who is now considered more as my grandmother. Zij heeft me veel geleerd en daarom praat ik tegenwoordig gewoon Nederlands op mijn werk. Ik blijf je altijd dankbaar.

My second dutch teacher, Kees van Kruining, I would like to thank you as well for teaching me a piece of your knowledge in languages. Een goed karakter en een hart van goud zijn van grote waarde. Bedankt!

Last but not least is my LOVE, Erfan. It was always my most important wish to finally meet a TRUE LOVE and I finally did. Everything has become different since we have met, 1st May 2015. Your endless support and perseverance resulted in my graduation and I am thankful for that. I love you because the reality of life is finally better than the dreams!

جز آستان توام در جهان پناهی نیست
سر مرا به جز این در حواله گاهی نیست

To anyone else, anywhere in the world, whom I might have been careless enough not to mention here, who helped me becoming a better person, A BIG THANK YOU

I'd be packing my bags when I need to stay, I'd be chasing every breeze that blows my way, I'd be building my kingdom just to watch it fade away, It's true, That's me without YOU.

از دل و جان شرف صحبت جانان غرضست
غرض اینست وگرنه دل و جان این همه نیست
پنج روزی که در این مرحله مهلت داری
خوش بیاسای زمانی که زمان این همه نیست